

Magnetic Storms in October 2003

Collaboration “Solar Extreme Events in 2003 (SEE-2003)”:

M. I. Panasyuk¹, S. N. Kuznetsov¹, L. L. Lazutin¹, S. I. Avdyushin², I. I. Alexeev¹,
P. P. Ammosov³, A. E. Antonova¹, D. G. Baishev³, E. S. Belenkaya¹, A. B. Beletsky⁴,
A. V. Belov⁵, V. V. Benghin⁶, S. Yu. Bobrovnikov¹, V. A. Bondarenko⁶, K. A. Boyarchuk⁵,
I. S. Veselovsky¹, T. Yu. Vyushkova⁷, G. A. Gavrilieva³, S. P. Gaidash⁵, E. A. Ginzburg²,
Yu. I. Denisov¹, A. V. Dmitriev¹, G. A. Zherebtsov⁴, L. M. Zelenyi⁸, G. S. Ivanov-Kholodny⁵,
V. V. Kalegaev¹, Kh. D. Kanonidi⁵, N. G. Kleimenova⁹, O. V. Kozyreva⁹, O. P. Kolomiitsev⁵,
I. A. Krashenninnikov⁵, A. A. Krivolutsky⁷, A. P. Kropotkin¹, A. A. Kuminov⁷, L. N. Leshchenko⁵,
B. V. Mar'in¹, V. G. Mitrikas⁶, A. V. Mikhalev⁴, V. A. Mullayarov³, E. A. Muravieva¹,
I. N. Myagkova¹, V. M. Petrov⁶, A. A. Petrukovich⁸, A. N. Podorolsky¹, M. I. Pudovkin^{10†},
S. N. Samsonov³, Ya. A. Sakharov¹¹, P. M. Svidsky², V. D. Sokolov³, S. I. Soloviev³,
E. N. Sosnovets^{1†}, G. V. Starkov¹¹, L. I. Starostin¹, L. V. Tverskaya¹, M. V. Teltsov¹,
O. A. Troshichev¹², V. V. Tsetlin⁶, and B. Yu. Yushkov¹

¹ Skobeltsyn Institute of Nuclear Physics, Moscow State University, Moscow, Russia

² Fedorov Institute of Applied Geophysics, Moscow, Russia

³ Shafer Institute of Cosmophysical Research and Aeronomy, Yakutian Scientific Center, Siberian Division, Russian Academy of Sciences, Russia

⁴ Institute of Solar-Terrestrial Physics, Siberian Branch of Russian Academy of Sciences, Irkutsk, Russia

⁵ Institute of Terrestrial Magnetism, Ionosphere, and Radio Wave Propagation (IZMIRAN), Troitsk, Russia

⁶ Institute of Medicobiological Problems, Moscow, Russia

⁷ Central Aerological Observatory, Dolgoprudny, Russia

⁸ Space Research Institute, Russian Academy of Sciences, Moscow, Russia

⁹ Institute of Physics of the Earth, Russian Academy of Sciences, Moscow, Russia

¹⁰ Institute of Physics, University of St. Petersburg, St. Petersburg, Russia

¹¹ Polar Geophysical Institute, Kola Science Center, Russian Academy of Sciences, Apatity, Russia

¹² Arctic and Antarctic Institute, St. Petersburg, Russia

Received May 19, 2004

Abstract—Preliminary results of an analysis of satellite and ground-based measurements during extremely strong magnetic storms at the end of October 2003 are presented, including some numerical modeling. The geosynchronous satellites *Ekspress-A2* and *Ekspress-A3*, and the low-altitude polar satellites *Coronas-F* and *Meteor-3M* carried out measurements of charged particles (electrons, protons, and ions) of solar and magnetospheric origin in a wide energy range. Disturbances of the geomagnetic field caused by extremely high activity on the Sun were studied at more than twenty magnetic stations from Lovozero (Murmansk region) to Tixie (Sakha-Yakutia). Unique data on the dynamics of the ionosphere, riometric absorption, geomagnetic pulsations, and aurora observations at mid-latitudes are obtained.

1. INTRODUCTION

Active processes on the Sun in the end of October 2003 initiated a series of magnetospheric disturbances whose investigation is of considerable interest for understanding the magnetosphere physics and solving practical problems. At the moment, experimental facilities of our country represent a large complex of ground-based and space instruments which is sufficient for a comprehensive study of the processes of solar–terrestrial activity. This paper presents an attempt to join

the efforts of Russian scientific teams in order to investigate the extreme events in October–November 2003. Therefore, the main emphasis in it is made on the comprehension of the results of measurements made by national space vehicles and ground observatories.

Magnetic storms cause a variety of processes in the magnetosphere. We consider here the basic processes: deformations of the magnetosphere structure, the boundaries of penetration of solar cosmic rays, boundaries of the auroral zone and polar cap, dynamics of the radiation belts, and the influence of substorms on evolution of the current systems of a magnetic storm. The-

[†] Deceased.

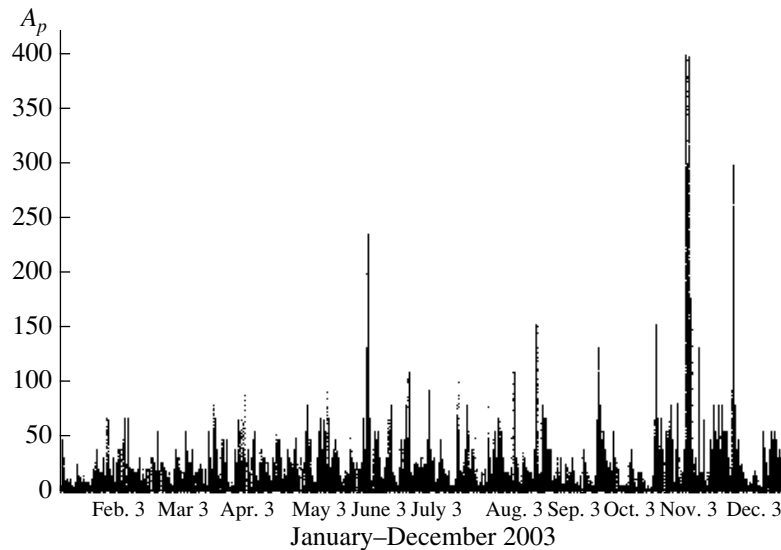


Fig. 1. Diurnal values of the A_p index of geomagnetic activity in 2003.

ory is represented by model calculations for a given particular series of global storms based on a paraboloidal model of the magnetosphere. The model results are compared with measurements. The integral pattern of a storm is modeled as a time variation of global magnetospheric current systems. These current systems are permanent and exist also in a quiescent magnetosphere. However, during storms the intensity of these current systems increases by more than an order of magnitude under the action of powerful streams of the solar plasma. The spatial structure of the magnetosphere also changes radically.

This work represents the first attempt of creating a collaboration of a large group of authors and scientific teams with the aim of a prompt analysis of events that are of exceptional interest for fundamental and applied problems of the space weather. Some nonuniformity of separate sections in dimensions and the style of presentation is inevitable in this case. A certain discrepancy in interpretations of the results of measurements is also inevitable, and we do not press only one version on the reader. Many conclusions are of a preliminary character, the majority of results are presented in a short form, and they will undoubtedly be expanded in subsequent publications.

2. GENERAL CHARACTERISTIC OF MAGNETOSPHERIC ACTIVITY

The first paper of our collaboration [1] is devoted to studying the processes on the Sun and in the heliosphere. Here we present a short compilation of solar wind parameters which determine the dynamics of magnetospheric processes in the period under investigation.

As far as geomagnetic activity is concerned, 2003 would become the most disturbed year of the 23rd cycle even without the last burst of the solar activity. All strongest interplanetary and geomagnetic disturbances in 2003 were related to the eruptive activity of the Sun. Throughout the entire year the Earth passed from one high-speed stream of the solar wind caused by a coronal hole into another stream. The magnetic storms produced by high-speed flow of the solar wind from one (the most extended) coronal hole continued for several days and sometimes for more than a week. When sporadic effects were added to the influence of coronal holes, the mean activity of the Earth's magnetic field became extremely high. This is well seen on the plot presenting the behavior of the A_p geomagnetic index in 2003 (Fig. 1). The second maximum of geomagnetic activity is observed, as a rule, on the phase of decline of the solar cycle, but in the current cycle it occurred to be considerably higher than the first maximum. The yearly averaged index A_p of geomagnetic activity is equal to 21.9 nT in 2003. This is an extremely high value which is inferior only to the years 1951, 1960, 1982, and 1991 (Fig. 2).

According to preliminary calculations, 62 magnetic storms are detected in 2003. The extremely disturbed periods October 29–31 and November 20 are among them. Three times in the period October 29–30 the maximum possible three-hour K_p index was observed, equal to 9; before this, only one such three-hour interval was recorded in the current cycle (July 2000). The last three days of October turned out to be the most disturbed three-days interval in the entire history of recording the A_p indices.

The high magnetic activity is a consequence of extremely high activity on the Sun. The first group of sunspots appeared on the eastern limb on October 17,

and an extremely rare situation arose on October 29: three huge groups of sunspots were observed on the visible solar disk simultaneously. Then, a series of flares occurred, accompanied by bursts of radio emission and ejections of matter. In this series the flare X17.2/4B beginning at 09:51 UT on October 28 and reaching its maximum at 11:10 UT stands out. It was accompanied by strong radio bursts of all types and by acceleration of charged particles to energies exceeding 7 GeV. A large, dense, and fast ejection of solar mass with a velocity of higher than 2100 km/s was observed during this flare. The interplanetary shock wave (ISW) arrived at the Earth at 06:12 UT on October 29, only in 19 h after the flare. This is the fastest arrival of an interplanetary disturbance since 1972. One more giant proton flare (X10.0/2B, S15W02) occurred in the evening of October 29, with radio bursts of the 2nd and 4th types, high flux of accelerated particles, and bright and fast (the velocity is almost 2000 km/s) mass ejection.

As a result of unique combination of the impact of two high-speed streams of the solar wind an extremely large series of magnetic storms came into existence. Unfortunately, the coronal mass ejections (CMEs) which took place during magnetic storms in October 2003 had so extreme parameters that spacecraft-based instruments for measurements of plasma characteristics in the near-Earth space turned out to be unable to work under such conditions. The powerful fluxes of particles caused malfunction in operation of the instruments for plasma measurements onboard almost all spacecraft which performed monitoring of the solar wind (*ACE*, *Geotail*, and *SOHO*). As a result, the data on the velocity and density of the solar wind during the main phase of the magnetic storms of October 28–31, 2003 are fragmentary and contradicting. Nevertheless, the data of these spacecraft presented via the Internet to the disposal of the scientific community allow one to reconstruct the time profile of the solar wind flow in the vicinity of the Earth's magnetosphere. Together with magnetic indices, they are a valuable basis for a detailed analysis of the magnetospheric processes.

Figure 3 presents the bulk velocity of the solar wind plasma derived from the spectrum of He^{++} ions measured by the SWICS instrument onboard the *ACE* spacecraft dedicated to studying the energy spectra of the solar wind ions. The velocity of the solar wind plasma was determined using the SWICS/*ACE* data, since the drift velocity of ions in crossed fields does not depend on ion mass and charge. In order to determine the density of the solar wind flow, we have used the data of the *Geotail* spacecraft (Fig. 4) which on October 28–29 was located in the solar wind, upstream of the Earth's bow shock.

Extremely powerful manifestations of the solar activity resulted in an extremely strong response of the Earth's magnetosphere, ionosphere, and atmosphere, revealing itself in impressive changes of the state of

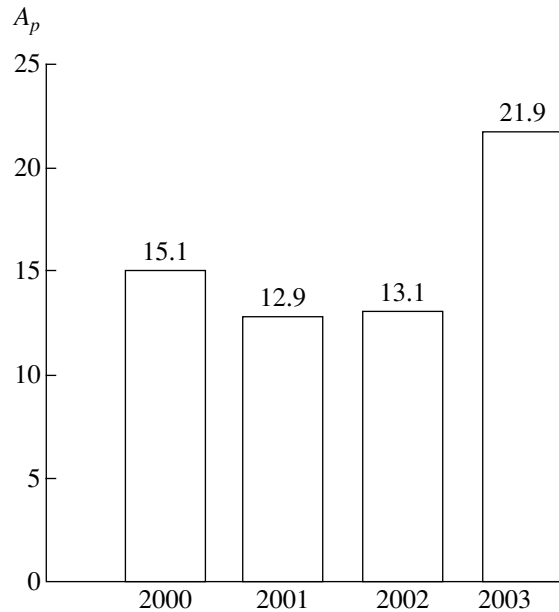


Fig. 2. Mean annual values of the A_p index of geomagnetic activity in the period from 2000 to 2003.

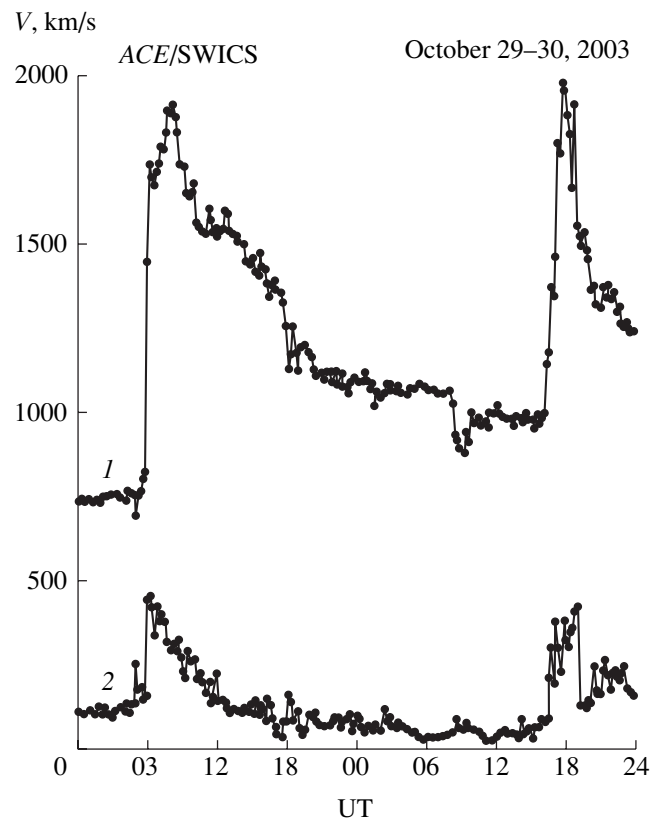


Fig. 3. The velocity of solar wind plasma derived from the spectrum of He^{++} . The data of the SWICS instrument onboard the *ACE* spacecraft placed at the point of libration. 1 and 2 correspond to the bulk velocity and thermal velocity.

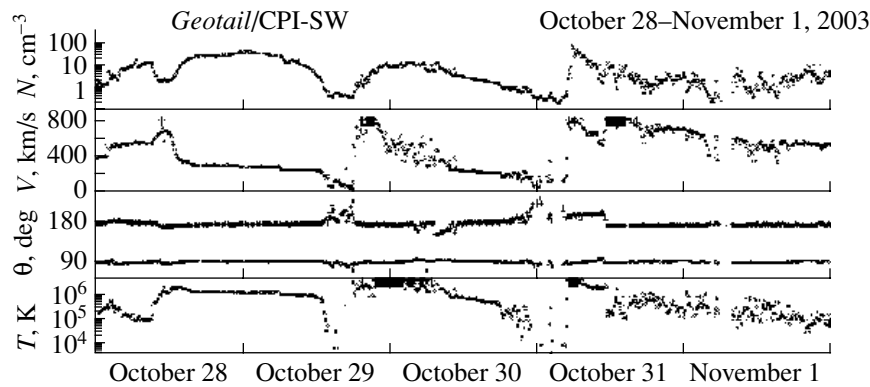


Fig. 4. The results of measurements by a plasma analyzer onboard the *Geotail* spacecraft from October 28 to November 1, 2003. From top to bottom: density, velocity, tilt angles, and temperature of plasma.

plasmas, populations of energetic charged particles, electric currents, and electromagnetic fields.

Strongly increased pressure of the solar wind and strong interplanetary magnetic field (IMF) of the geoeffective southern direction sharply changed the structure of the Earth's magnetosphere, pushing apart the boundaries of penetration of solar energetic particles deep into the magnetosphere and decreasing the size of the region, in which the trapped radiation can exist (radiation belts). According to one-minute averaged data of magnetometers of the geosynchronous satellites *GOES-10* and *GOES-12*, the B_z component of the magnetospheric magnetic field in the geosynchronous orbit was subject to strong variations on October 29 and 30, 2003, which indicates to satellite exits into the magnetosheath and magnetotail on the dayside and nightside, respectively (see Fig. 5).

The magnetic conditions were extremely disturbed throughout the entire period under consideration. A

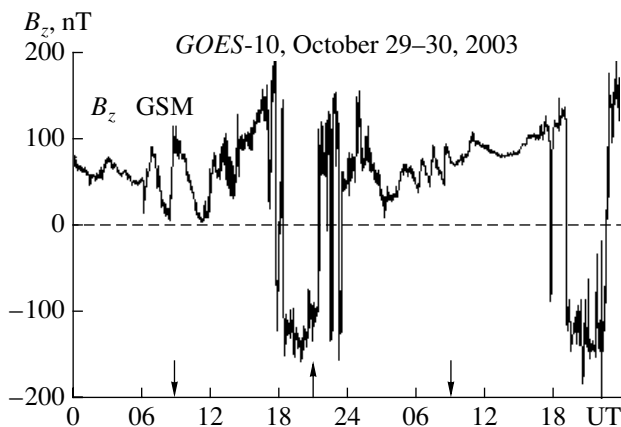


Fig. 5. The B_z component of the geomagnetic field as measured onboard the geosynchronous satellite *GOES-10* in the period October 28–31, 2003. The arrows directed up and down designate the local noon and midnight, respectively.

series of strong substorms was observed, which occurred every day, while relatively quiet periods lasted for no more than a few hours. Three magnetic storms (with sudden commencement at 06:12 UT on October 29, 2003; with gradual commencement at 12 UT on the same date; and with gradual commencement at 16–18 UT on October 30, 2003) composed a central aggregate of events which can be represented as the development of a strong magnetic storm in three stages. According to the data of the world data center C2 in Kyoto the value of the AE index reached 4000 nT, which is approximately twice higher than one usually detects during magnetic storms (~ 1500 – 2000 nT).

A detailed analysis of causes of such a high intensity and of the dynamics of auroral electrojets can be performed later, after getting the refined results of observations of various magnetospheric parameters. However, some conclusions can be made using the available preliminary data. Figure 6 presents the plots of the B_z component of the interplanetary magnetic field in the GSM coordinate system; of the electric field of the solar wind calculated according to the following formula

$$E = V\sqrt{B_z^2 + B_y^2}/2 + \alpha V^2,$$

where $\alpha = 4.4 \times 10^{-6}$ (mV/m)/(km/s)² (this combination of the solar wind parameters correlates best with the AL index, see [2]); and of the AL index (digitized from a preliminary plot). When calculating the electric field the values of the solar wind velocities presented in Fig. 3 were used.

It is the anomalously high velocity of the solar wind giving the main contribution to the electric field strength reaching 40–50 mV/m that, apparently, is the main cause of so high geomagnetic activity. Nevertheless, it should be emphasized that AL variations of such amplitudes are not unique and were detected even during not so strong magnetic storms. For example, on September 25, 1998 under a moderate electric field of the solar wind (about 12 mV/m) the stations of the CANOPUS network of magnetometers detected a deviation of the horizontal component down to values of the

order of -4000 nT, which was explained, in particular, by specific features of the substorm activity.

3. DYNAMICS OF THE MAGNETOSPHERE

Considerable changes in the structure of the magnetosphere are the main process of a magnetic storm, so that to reveal the physical nature of these changes is the main problem of studying global storms. The magnetosphere dynamics is determined both by a primary external action of a shock wave coming from the Sun and by an internal action related, for example, to the amplification of a large-scale electric field of the system “solar wind–magnetosphere.” In turn, the internal action on the structure of the magnetosphere can be divided in direct-driven and delayed (after accumulation of energy and its release by way of substorms).

An immediate result of these actions is acceleration and precipitation of particles, and other changes in the fluxes of charged particles and in the magnetosphere current systems related to them. There occur also considerable displacements of the boundaries and structures, including those located in the inner magnetosphere and fairly stable in the absence of magnetic storms. They include the approach (mentioned above) of the magnetosphere boundary on the dayside to the Earth, the motion to the Earth of the boundaries of stable trapping and radiation belts, as well as the same motion of the boundaries of quasi-trapping and, respectively, of the zone of active forms of auroras.

The processes of internal actions on the magnetosphere dynamics are reflected in ground-based observations of variations and pulsations of the magnetic field, in auroras and ionospheric disturbances. They are considered in this section. In addition, the magnetosphere dynamics is traced by measurements of distributions of energetic particles which do not change the structure of the magnetosphere by themselves, but keep tracking its changes. These measurements will be presented in the fourth section.

3.1. Substorm Activity

3.1.1. Dynamics of the auroral zone. The magnetospheric substorms accompany the global storms being their important component. The relationship of indices of substorm activity with D_{st} is well known for a long time and was confirmed in many papers. For example, Pudovkin, Zaitseva, and Sizova [3] have demonstrated the existence of a good correlation (without observable delays) between D_{st} and D_p . Similar results were obtained by some other researchers [4, 5]. This relationship indicated to the important if not decisive role of the asymmetric proton ring current arising due to injection of protons with energies 20–100 keV during substorms of the Earth’s night side. At the same time it is suggested by Iyemori [6] that the substorm onset is related with the beginning of decline of the D_{st}

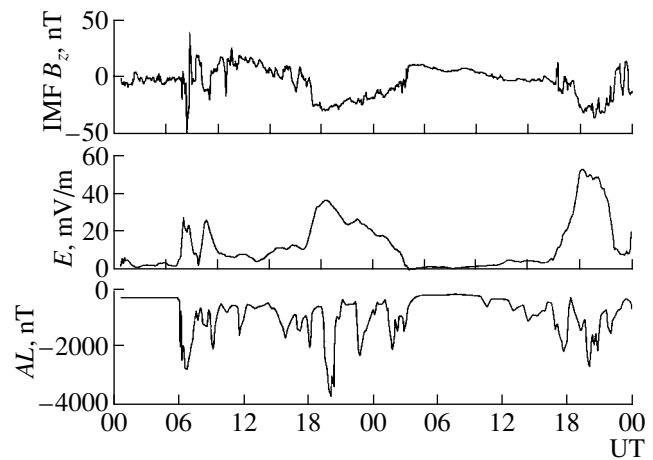


Fig. 6. The B_z component of the interplanetary magnetic field in the GSM coordinate system; the electric field of the solar wind calculated from the data of the ACE satellite properly shifted in time according to the satellite distance from the Earth; and preliminary AL index for October 29–30, 2003.

variation rather than with its amplification—the result directly opposite to the opinion commonly believed beforehand. These ideas are developed in a paper by Maltsev [7] where it is stated that substorms play no role in the development of magnetic storms. Therefore, to consider the role of substorms in a particular sequence of global storms in October–November 2003 is of great importance.

A general idea about the substorm activity is given by magnetometers of the eastern chain of stations: Tixie (TIX), Zyryanka (ZYK), and Yakutsk (YAK) (Fig. 7); and by magnetometers of the western chain: Lovozero (Fig. 8) and Moscow (Fig. 9).

Relation to D_{st} . In the bottom panel of Fig. 7 we present again the plot of the D_{st} variation as reference plot, in order to emphasize a clear coincidence of the main phases of the magnetic storm in the evening of October 29 and on October 30 with chains of bay-like disturbances. Looking at Fig. 8 we again see here the evidence of coincidence of the substorm activity with a buildup of the current system of magnetic storms. So our observations do not confirm the statements that the active phases of substorms are related to decreasing D_{st} . The traditional point of view (that ions accelerated in the course of a substorm make the main contribution to the partial ring current at the main phase of a magnetic storm) remains to be preferable.

Displacement in latitude. From the ratio of horizontal and vertical components of magnetic field variations one can determine that in most bay-shape disturbances the center of the current system was located to the south of stations of the auroral zone, i.e., the southern boundary of the auroral zone is displaced to the equator. As for the near-pole boundary, i.e., the polar cap boundary, it is displaced not so strongly as the equatorial bound-

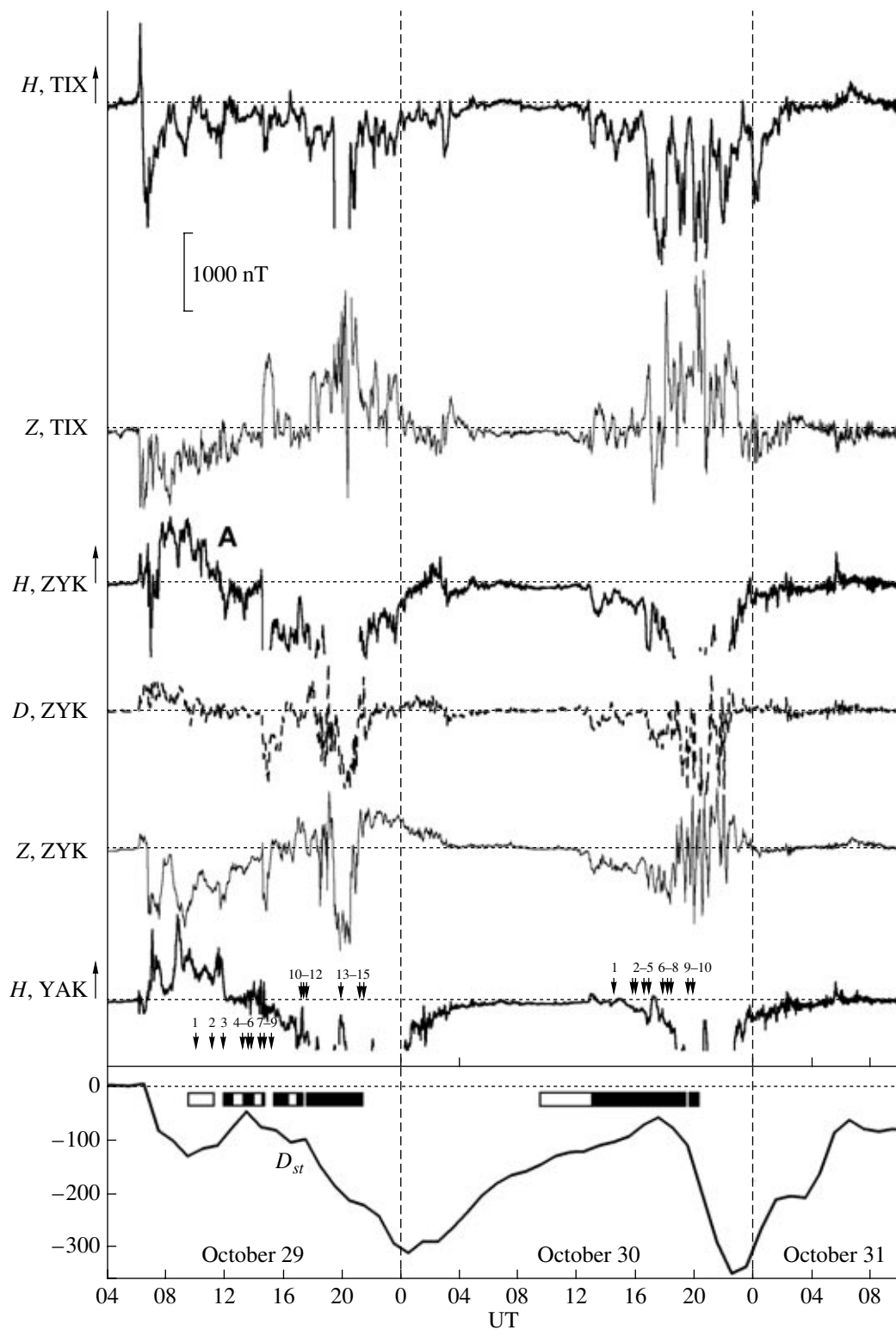


Fig. 7. Magnetograms of the eastern chain of stations (ICRA) on October 29–31, 2003. From top to bottom: Tixie (TIX), Zyryanka (ZYK), Yakutsk (YAK), and variations of the D_{st} index. Rectangles mark the intervals of all-sky survey by a TV camera at Zhygansk station (dark segments correspond to intensification of auroral activity). The figures with arrows 1–15 and 1–10 show the instants when the images of auroras on October 29–30 presented in Fig. 13 were made.

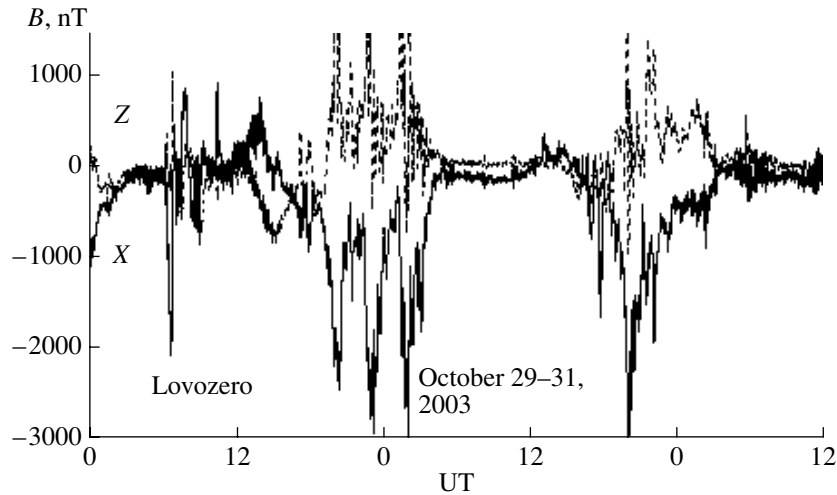


Fig. 8. Magnetogram at the Lovozero station (Polar Geophysical Institute), October 29–31, 2003.

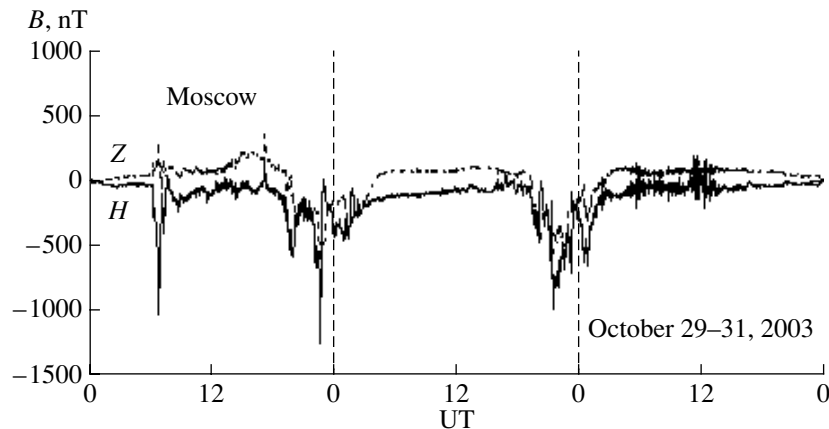


Fig. 9. Magnetogram at the Moscow station (IZMIRAN), October 29–31, 2003.

ary. The activity does not leave the traditional zone of auroras, and even if it leaves, then only for a short time. Both on October 29 and 30 we see (judging from the sign of the vertical component of the magnetic field) that the substorm originates in the south, but sometimes in the process of substorm expansion the activity slips to the pole from Lovozero and Tixie. The riometric bursts of absorption of the auroral type (one on October 29 and several on October 30, 2003) also bear witness that auroral particles were accelerated at the latitude of Tixie (Fig. 10).

Only near the maximums of D_{st} and only for a short time the auroral stations appear inside the polar cap, in particular, in the interval 22–24 UT on October 30. The small amplitude of the magnetic bay at 22 UT in Lovozero and Tixie and the low level of riometric absorption do not mean a real decrease of the substorm power: they are rather a consequence of the exit of auroral stations into the polar cap region. Figure 9 presents a magneto-

gram of Moscow station (IZMIRAN) which demonstrates a growth of disturbance amplitude in this time. This displacement of the substorm at 22 UT to the south from the auroral zone coincides with the maximum shift to the Earth of the boundary of penetration of solar cosmic rays (SCR) and of the polar cap boundary, as was measured onboard the *Coronas-F* satellite (see section 4.1). At 00:15 UT on October 31 a classic substorm of the auroral zone is observed again. The displacement of boundaries was anomalously close to the Earth, and it was not long, less than 2 h. The auroral zone remains wide in this case, i.e., between the zone of stable trapping and the magnetotail there is always a broad region of quasi-trapping.

SC on October 29. The storm sudden commencement of type SC+ is illustrated by a magnetogram of the Australian station Alice Spring (Fig. 11). It is known that SC can trigger a substorm in the auroral zone, in particular, if a growth phase is observed and energy is

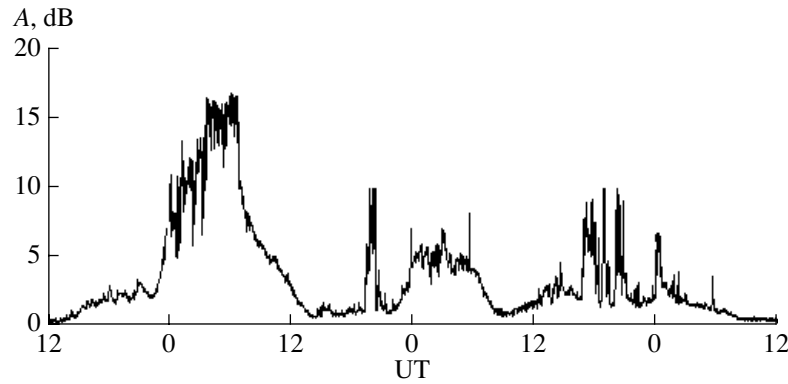


Fig. 10. Absorption of space radio noise as measured by a riometer of the Tixie station in the period from October 28 to 31, 2003.

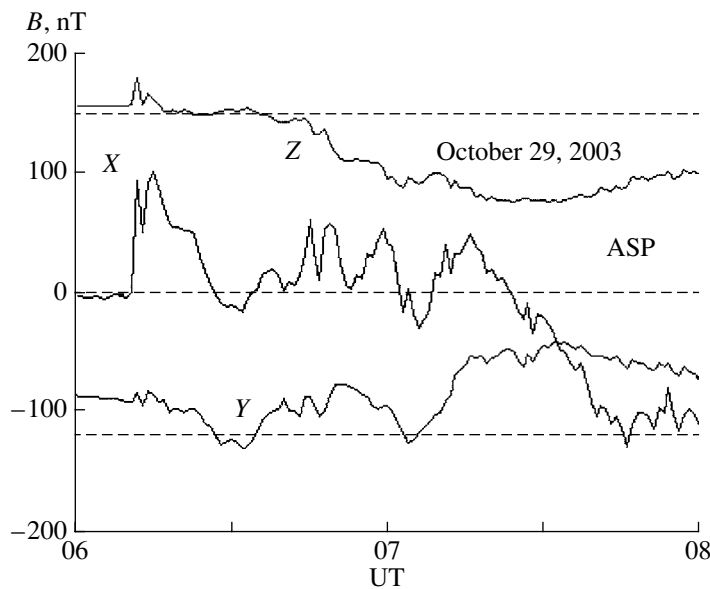


Fig. 11. An SC impulse and the onset of the main phase of the storm on October 29, 2003 at the near-equatorial station Alice Spring.

accumulated in the magnetosphere. In our case a strong substorm develops in the midnight sector, and a strong disturbance is observed both in the auroral zone and in middle latitudes (Fig. 12). Here, it is difficult to separate the substorm effect and the disturbance of the main phase of the storm, further investigations are required.

3.1.2. Mid-latitude substorms and auroras. Figure 13 presents a series of aurora images recorded at Zhigansk observatory (Institute of Cosmophysical Research and Aeronomy, ICRA) in the period from 10:02 UT to 21:14 UT on October 29, 2003 and from 14:35 UT to 19:48 UT on October 30, 2003. The instants of observations are shown by arrows in Fig. 7. The observatory is located near the southern boundary of the auroral zone, and its field of view covers disturbances both in the traditional auroral zone (for example, at 17:55 UT on October 30) and in the subauroral

zone. One can see in Fig. 13 that at 14:33 UT on October 29 a breakup of aurora of classical type was observed at the southern horizon, with a subsequent expansion to the pole (typical for substorms). A sharp commencement of a bay in the H -component was observed at Zyryanka (ZYK) located at the latitude close to that of Zhigansk (60° of corrected geomagnetic latitude), but ~ 1000 km to the east. Its amplitude was about 1000 nT (and about 600 nT at the magnetometer of the Chokurdakh station). This substorm coincided with the beginning of the main phase of the second magnetic storm, the polar cap boundary and the boundary of penetration of solar protons being located, respectively, near 60° and 53° of corrected geomagnetic latitude. Simultaneously, an enhancement of aurora was detected at the station Maymaga (ICRA).

Optical observation area of ICRA, Maymaga station. It is located 150 km to the north from Yakutsk ($\lambda =$

63° N, $\varphi = 129.5^\circ$ E). Observations were carried out using an infrared digital spectrometer designed to measure the rotational temperatures of molecules of hydroxyl and oxygen at altitudes of 87 and 94 km, respectively. A detailed description of the instrument can be found in [8]. The allowed line OI 844.6 nm of atomic oxygen typical for auroras falls within the recorded spectral region of the spectrograph. The spectrograph operates during the dark time of the day from August to May 15, and its time resolution is 10 min. On October 29 the maximum intensity of this emission reached 12 kRa (absolute calibration was performed by using records of a sensitometric setup with known color temperature). The increased intensity of OI 844.6 nm was recorded for three nights: October 29, 30, and 31. No aurora was observed in other nights, before October 29 and after October 31.

In parallel, an all-sky camera operated at Maymaga station. It was used to detect the internal gravitational waves by variations of emission of hydroxyl molecules. Because of a long exposure (150 s) almost all images in the night of October 29 turned out to be overexposed. Figure 14 presents variations of the glow intensity in the 844.6 nm line on October 29, 30, and 31, respectively. Unfortunately, at the instant of SC it was still daylight at the station, and no measurements had been started. The flash of glow at 14:30 UT during the aurora breakup described above is the largest in amplitude at Maymaga and short (less than 10 min, which corresponds to typical duration of the expansion phase of a substorm).

Among other observations on October 29, 2003, it is worthwhile to notice that the substorm beginning about 19 UT revealed itself in two bursts (Fig. 14), but in the maximum of the bay the activity sharply escaped to the north, and this strong substorm was not observed at Maymaga. Note also that the mid-latitude magnetometers of the western chain also did not observe this substorm.

On October 30 the auroras at Maymaga begin at 18:30 UT, and they give two bright bursts in the interval 19:30–21:10 UT (the same interval when a strong substorm was detected by both western and eastern chains of magnetometers, and when the displacement of the boundary of SCR penetration was observed to be closest to the Earth). Riometric observations at Maymaga confirm that the photometric observations described above belong to events of the substorm class: almost every luminosity enhancement has corresponding burst of riometric absorption of a typical substorm structure which indicates to precipitation of auroral electrons with energies of 10 keV and higher. Note also that in the evening of October 30 a photo of aurora was taken at Troitsk, near Moscow (see the site of IZMIRAN). It is a radiant arc with a red lower side (type B aurora), precisely the type that is usually associated with the active phase of a substorm [9].

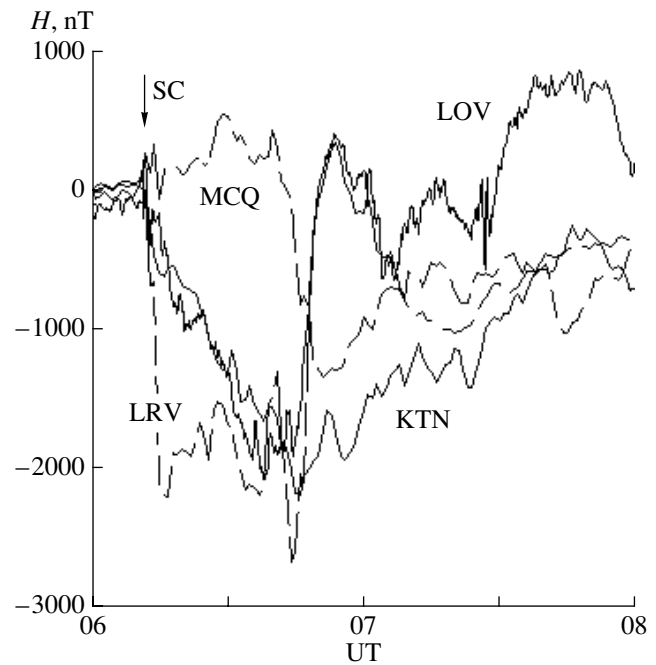


Fig. 12. Variations of H-components of magnetometers at the observatories Lovozero, Kotelnyi, Leirvoygur, and Mcquery on October 29, 2003 during a substorm triggered by SC.

Geophysical observatory of ISTP SB RAS. The geophysical observatory of ISTP (the Institute of Solar–Terrestrial Physics) of Siberian Branch of Russian Academy of Sciences is located at 52° N and 103° E. Observations were carried out using zenith photometers with interference tilting optical filter ($\Delta\lambda_{1/2} \sim 1\text{--}2$ nm) in emission lines 558 and 630 nm. The emissions in the near infrared (720–830 nm) and ultraviolet (360–410 nm) spectral ranges isolated by absorption optical filters were also observed. The angular fields of view were equal to 4°–5° for each channel of the photometer.

The optical observations on October 29–31, 2003 were carried out under conditions of continuous cloudiness. This circumstance could result in two effects. First, due to absorption by clouds the luminosities of atmospheric emissions detected near the ground surface should be lower than the luminosities at the altitudes where they are emitted. Second, because of large-angle scattering of radiation by the cloudiness the effective field of view of the photometer channels could be of much higher value. Hence, this could lead to detection of the emission from regions with higher latitudes relative to the station location ($>1^\circ\text{--}2^\circ$). In this connection, the absorption of the detected emission by clouds was preliminary taken into account, and the data were reduced to the clear sky conditions.

On October 29–30, 2003 the mid-latitude auroras were detected at the geophysical observatory of ISTP SB RAS, in which the dominant emission was concentrated in the line 630 nm of atomic oxygen. Figure 15

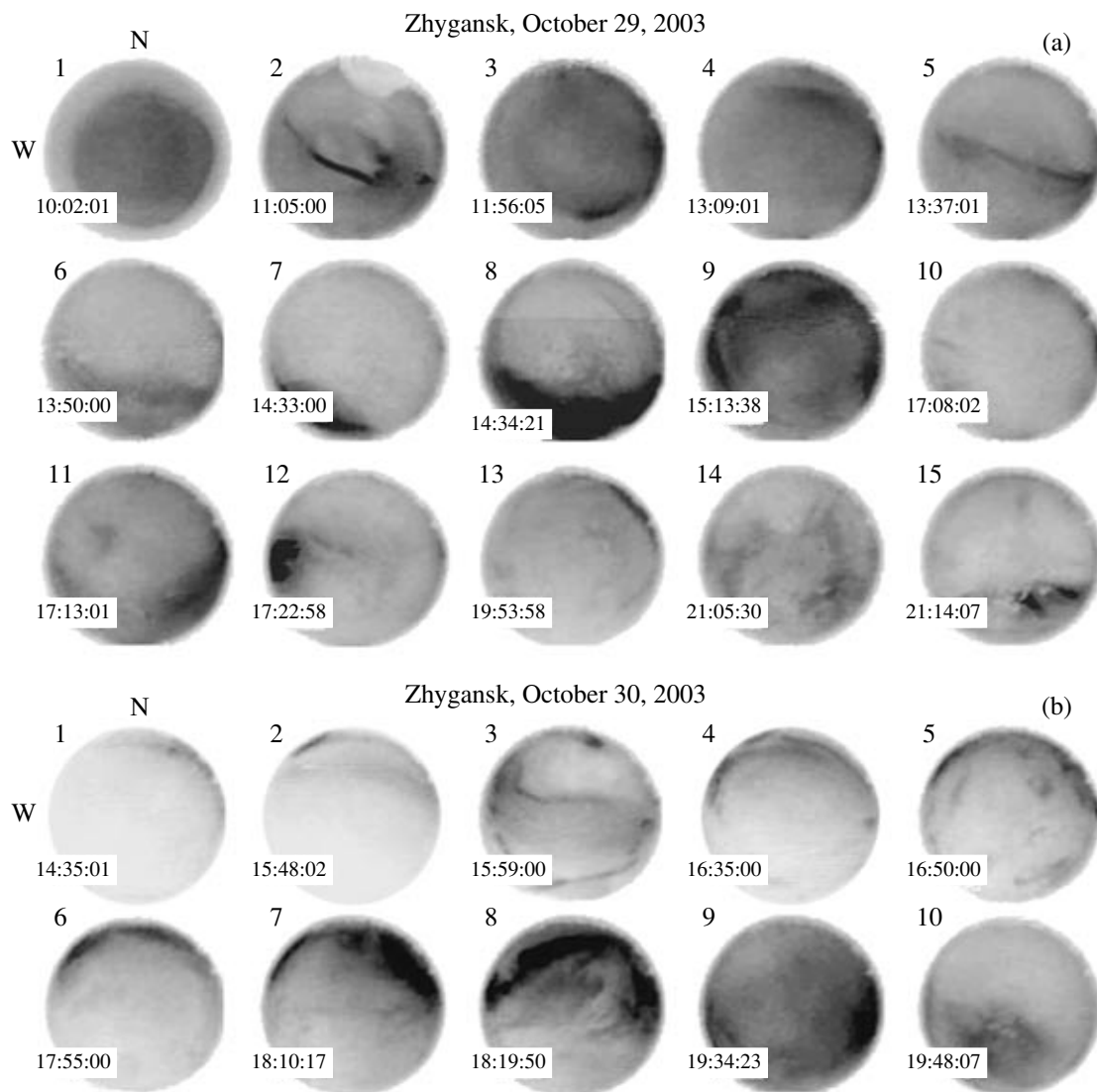


Fig. 13. The images of auroras at the Zhygansk station (ICRA) on October 29–30, 2003.

presents the distributions of D_{st} and K_p indices and the behavior of atmospheric 630 nm emission for three nights on October 29–30, 2003. For the detected mid-latitude auroras the beginning of growth of the intensity of 630 nm emission (J_{630}) and maximum J_{630} values correspond to the main phases of magnetic storms. For mid-latitude auroras under consideration the maximum values of J_{630} are observed in the second half of the night, which is typical for considered latitude zone [10]. The maximum intensities J_{630} detected during the mid-latitude aurora on October 30 and reduced to the clear sky conditions (~ 4.3 kRa and ~ 6 – 10 kRa, respectively) had the largest values over the entire period of performing optical observations in the geophysical observatory (1989–1993 and 1997–2003), which allows one to classify the mid-latitude auroras of October 29–30, 2003 as extreme events for observations both at the place of location of the geophysical obser-

vatory of ISTP SB RAS and at other mid-latitude zones. The mid-latitude aurora on November 20, 2003 is an exception giving still larger intensity: the maximum value of J_{630} exceeded 19 kRa in this case.

The continuous cloudiness during auroras does not allow one to determine precisely the shape and type of auroras. When a glow region moves to middle latitudes, most frequently, the diffuse auroras with dominant 630 nm emission are observed, which are projected into the plasmapause region and can trace the plasma boundaries at altitudes of the upper atmosphere and their natural projections into the magnetosphere: night sky glow – the plasmasphere, the equatorial boundary of weak diffuse auroral emission – the plasmapause, diffuse auroral zone – the plasma sheet and the ring current region [11]. At the same time, the southern edge of the zone of active auroras can also in extreme cases reach middle latitudes, but in order to make the right

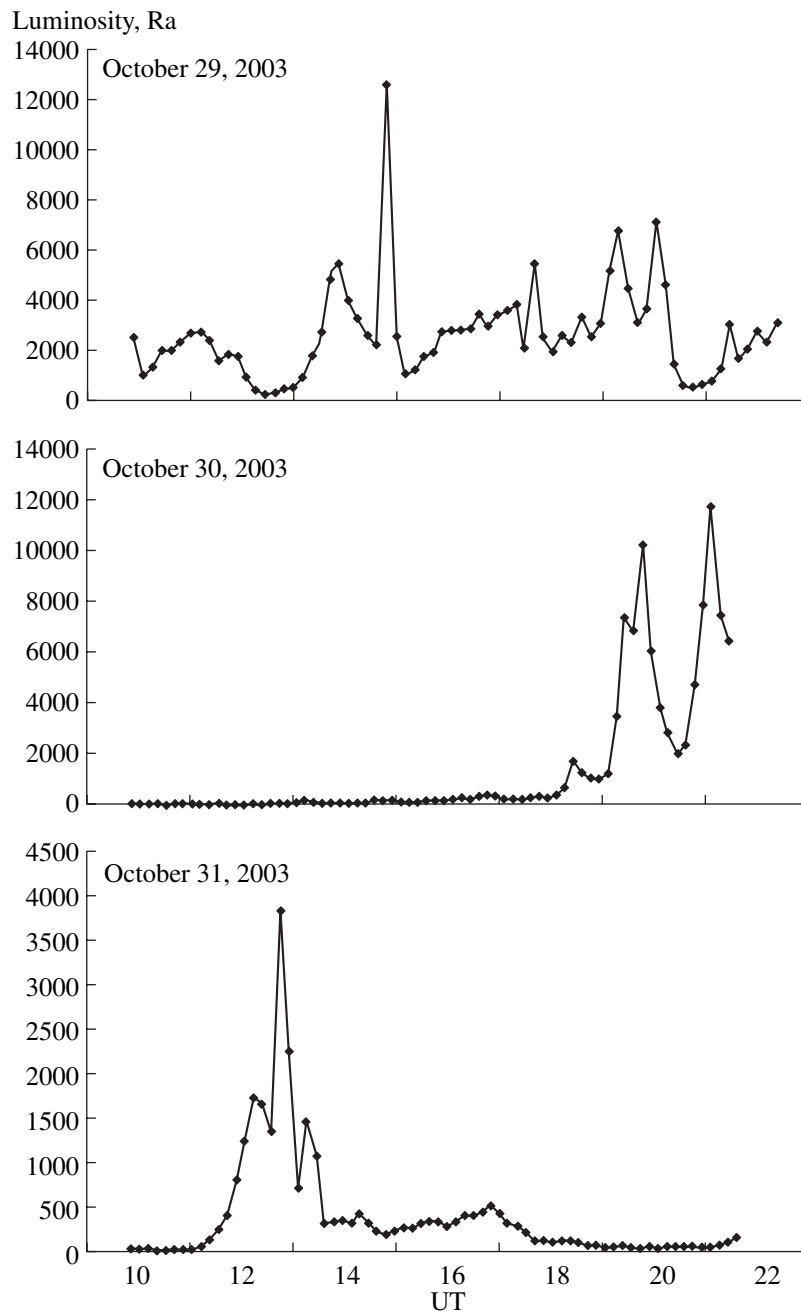


Fig. 14. Variations of aurora luminosity (atomic oxygen line OI 844.6 nm) at Maymaga station, from top to bottom: October 29, 30, and 31, 2003.

choice it is necessary to perform additional investigations.

3.1.3. Ionospheric effects above Moscow. Below, we present the results of a preliminary analysis of the data on vertical sounding of the ionosphere in the period of ionospheric–magnetospheric disturbance on October 29–31, 2003. According to the data of the IZMIRAN center of forecasting the geophysical conditions (see the website <http://www.izmiran.rssi.ru>) and the data of vertical sounding of the ionosphere at the

IZMIRAN laboratory (55° N, 37° E), a strongest ionosphere–magnetosphere storm was observed in this period. Vertical sounding of the ionosphere was carried out using the PARUS ionosonde. A description of this ionosonde is presented at the website <http://www.izmiran.rssi.ru/parus/>. When analyzing the data of vertical sounding of the ionosphere we used the data on D_{st} variations (see figures of the preceding sections). The results of analysis of half-hour data of vertical sounding of the ionosphere are shown for the storm of October 29

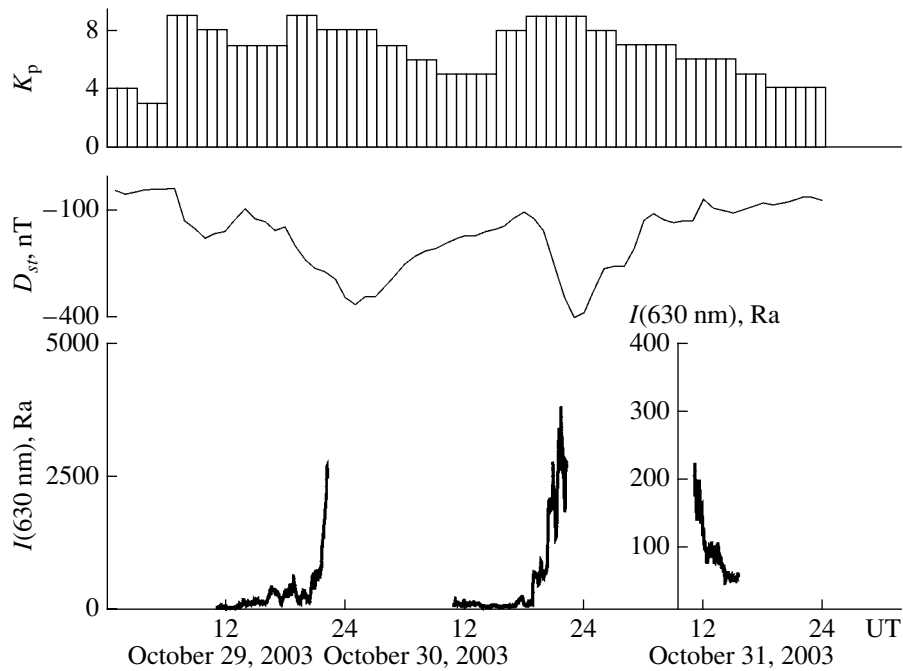


Fig. 15. Distribution of D_{st} and K_p indices and the behavior of atmospheric emission 630 nm during mid-latitude auroras at the south of Eastern Siberia on October 29–30, 2003.

in Table 1 and in Fig. 16, where some typical ionograms for this storm are presented.

Table 1 presents the date, time (h, min, LT), and the geomagnetic activity index according to the data of the magnetic observatory of IZMIRAN. In order to describe the state of the F -region of the ionosphere we have used estimating and describing letters, as is usual practice in interpretation and processing of ionograms [12]. The letters substitute numerical values of the reflected signal parameters in the case when their determination is difficult or even impossible: A means partial or complete shielding of the F -region by sporadic structures of lower lying E -region; B corresponds to complete absorption of reflected signals; and F corresponds to strong scattering of reflected signals. “No peculiarities” means that the usual ionogram (see ionogram 1 in Fig. 16) is observed, typical for given LT and season. The local time is connected to universal time by the following relation: $LT = UT + 2$ h.

The type E_s of the sporadic layer is given in the column for the E -region. The beginning of a strong disturbance during the storm of October 29 is recorded at 07:30 UT. The disturbance was observed until 08:00 UT on November 1. There were no traces of reflected signals on most ionograms in this time interval, which is indicative of the total absorption of signals developed in the ionosphere (ionogram 3). At some instants the scattered traces of the auroral sporadic E_s layer appeared with the types a (the layer strongly scattered in altitude, ionogram 2) or s (the skew E_s layer whose altitude uniformly increases with increasing frequency

of emission, ionogram 4). All observed E_s had a clearly cut lower boundary of reflections. The limiting (critical) frequency of reflections from the sporadic layer was equal to 4–8 mHz. Usually, the observed E_s fully screened the F -region. A sharp increase of the minimum acting height of the layer $F - h'F$ and a sharp decrease of the layer critical frequency f_oF2 are characteristic for the beginning of the disturbance, with subsequent development of either full screening or complete absorption. This was typical for all three storms at the maximum of D_{st} . Thus, we have all characteristic features of the high-latitude ionosphere [13, 14].

Of interest is the fact that “an attempt” of recovery of the vertical structure of the F -region in the period of development of the described disturbance revealed itself on the background of different phases of the magnetic storms. The first recovery was observed near the minimum of D_{st} of the first storm, the second took place near the minimum of D_{st} of the second storm, the third one was recorded at the recovery phase of the second storm, and so on (see Table 1).

In [15] the dynamics of the main trough of electron density N_e and of the maximum of the latitude behavior of electron temperature T_e was considered as a function of geomagnetic activity. Direct measurements of T_e onboard the *Kosmos-378* satellite and the vertical sounding of the ionosphere at 11 observatories in the period of December 10–20, 1970 were used as initial data of this analysis.

It was found that at the main phase of the storm a sharp displacement to the equator of the T_e maximum

and N_e trough occurred during several hours, then they gradually returned to the initial position for several days. The displacement of the trough reached $L \sim 2$, in this case T_e was equal to ~ 5000 K at the altitudes of maximum of the F -layer. Similar variations of D_{st} were observed earlier in September 1957 [14].

The events in the magnetosphere and ionosphere caused by the outstanding activity of the Sun in October 2003 showed similar evolution, though they were considerably more complicated. As was shown above, at middle latitudes such disturbances of the upper atmosphere and ionosphere were observed that usually take place only in the auroral zones of Arctic and Antarctica.

This analysis of the ionosphere state should be supplemented by the fact that during the described intervals of ionosphere-magnetosphere disturbances, during the night from October 30 to 31, auroras were observed above Troitsk in the northern sector of the sky: a rayed arc with a red bottom edge (<http://www.izmiran.rssi.ru>).

3.1.4. Precipitation of auroral electrons. The satellite Meteor-3M. When the substorm activity is displaced to the equator, one can expect that corresponding displacements of the inner boundary of the plasma sheet and of the region of precipitation of auroral electrons will also take place. The measurements on the polar satellite *Meteor-3M* give a possibility to study dynamics of auroral precipitation. Below, we present some results of measuring auroral electrons by the spectrometer MSGI-5EI. (See description of the instrumentation and some other results of measurements onboard the *Meteor* satellite in section 4.)

The dynamics of the regions of precipitation of low-energy electrons causing the glow of auroras were studied in many papers (see, for example, [16, 17] and references therein). Of special interest are the data on very strong magnetic storms. In the last 40 years only four storms have been detected with D_{st} lower than -400 nT, two of them in October–November 2003.

Figures 17 and 18 present the intensity profiles for electrons with $E_e = 10$ keV, measured during passages of the *Meteor-3M* satellite through the same regions of the magnetosphere in the southern hemisphere. Figure 17 represents comparatively quiet geomagnetic conditions on October 27, 2003, while Fig. 18 corresponds to ~ 1 h before the maximum of the storm on October 30, 2003. A large contribution to the counting rate of the spectrometer on October 27 made electrons of the outer radiation belt with energies > 2 MeV (see two peaks of the counting rate in evening and afternoon hours of local time at $L \sim 3.3$). One can reliably identify only “auroral” peaks of intensity on the dayside at $L \sim 8$ with a counting rate of 3×10^2 s $^{-1}$. The maximum counting rate in the entire passage comprised 3×10^3 s $^{-1}$.

The picture has radically changed during the passage on October 30, 2003 (Fig. 18). The maximum of electron precipitation on the dusk and day side was shifted to $L \sim 2.8$ and $L \sim 4$, respectively, while the

Table 1. Preliminary results of analysis of the data on vertical sounding of the ionosphere over Moscow during the ionosphere storm on October 29–31, 2003. The properties of reflected signals

Date (h, min, LT)	K_p index	F region	E region, type E_s
October 29, 2003			
08:00	4	Without peculiarities	–
08:30	9	$f_oF2 \sim 5.8$ mHz, $h'F \sim 260$ km	f
09:00	9	$f_oF2 \sim 4.5$ mHz, $h'F \sim 470$ km	–
09:30–10:30	9	B	–
11:00–18:00	6	Without peculiarities	–
18:30–19:30	7	F	–
20:00–21:30	9	A	s
22:00–22:30	9	B	–
23:00	9	A	a
23:30	9	B	–
October 30, 2003			
00:00	9	A	f
00:30–01:00	9	B	–
01:30	9	A	s
02:00	8	F	s
02:30	8	$f_oF2 \sim 2.5$ mHz, $h'F \sim 530$ km	–
03:00	8	$f_oF2 \sim 3.5$ mHz, $h'F \sim 500$ km	–
03:30–04:00	8	B	–
04:30	8	$f_oF2 \sim 2.3$ mHz, $h'F \sim 500$ km	–
05:00–07:30	5	Without peculiarities	–
08:00	4	$f_oF2 \sim 2.3$ mHz, $h'F \sim 300$	–
08:30	4	B	–
09:00	4	Without peculiarities	–
09:30–12:00	4	B	–
12:30–20:00	4	Without peculiarities	–
20:30–22:30	9	F	–
23:00	9	A	a
23:30	9	B	–
October 31, 2003			
00:00	9	F	s
00:30–01:30	9	A	s
02:00	9	F	–
02:30–04:00	9	B	–
04:30	9	$f_oF2 \sim 2$ mHz, $h'F \sim 510$ km	–
05:00	7	Without peculiarities	–

Note: The peak values of D_{st} were observed in the observation interval from 11:00 to 18:00 LT: $D_{st} = -180$ nT at 12:00 and $D_{st} = -98$ nT at 16:00 LT.

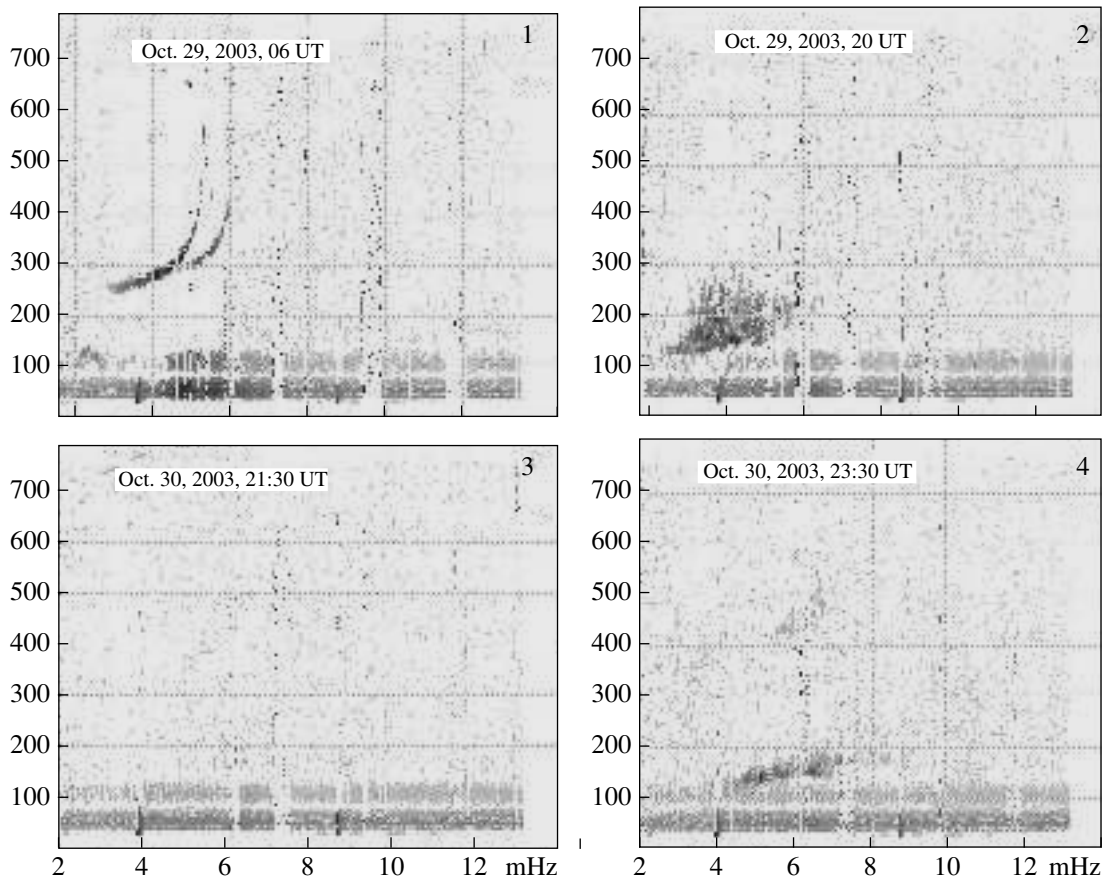


Fig. 16. Ionograms of the Moscow station (IZMIRAN) on October 29–30, 2003.

counting rate in maximums increased by more than order of magnitude. Figure 19 presents the electron spectrum in the energy range of 0.1–15 keV which was measured in the precipitation maximum ($L \sim 2.8$) on the dusk side during the passage shown in Fig. 18. The spectrum has a maximum at energies of ~ 1 keV, which is typical for spectra of auroral electrons in the structures of the “inverted V” type. The main phase of the superstorm on October 30, 2003 developed very quickly, strong substorms followed one after another. The preliminary analysis of geomagnetic data of SAMNET and IZMIRAN shows that at the end of the main phase of the storm the center of the western electrojet was displaced at least to the zenith of Borok station ($L \sim 2.9$). At the Moscow station ($L \sim 2.6$) the Z-component of the magnetic field (Fig. 10) remained negative all this time (electrojet to the north of Moscow).

3.2. Long-Periodic Geomagnetic Pulsations

3.2.1. Daytime pulsations of Pc5 range. The excitation during daytime on October 29 and 31 of geomagnetic pulsations Pc5 was one of bright manifestations of the strong magnetic storm in October 2003. These pulsations were characterized by unusually large amplitude (up to 600 nT) with a maximum in the frequency

band 2.5–5.0 mHz (periods of order of 3–6 min). Let us consider the properties of these pulsations and dynamics of their evolution in more detail. We have used in our analysis the 1-min data of the global network of 80 ground-based observatories INTERMAGNET, Scandinavian profile IMAGE (19 stations), and European network SAMNET (7 stations including the Russian station Borok). Figures 20 and 21 present magnetograms for October 29 and 31, respectively. They were recorded at several observatories of the dayside sector covering the latitudes from polar caps to the equator and plotted in one and the same scale. Triangles on the plots show the location of the local magnetic noon. International codes of observatories and their geomagnetic latitudes are given on the right scale. One can see that in both cases well-pronounced long-term monochromatic oscillations are observed in the dayside of the magnetosphere. The spectral analysis showed the existence of a clearly cut maximum in the frequency band 2.5–5.0 mHz.

In order to study their spatial-temporal properties, the maps of isolines of the integral intensity (nT/mHz) of geomagnetic pulsations in the frequency band 2.5–5.0 mHz (spectral maximum) were constructed using the programs developed in the Institute of Physics of

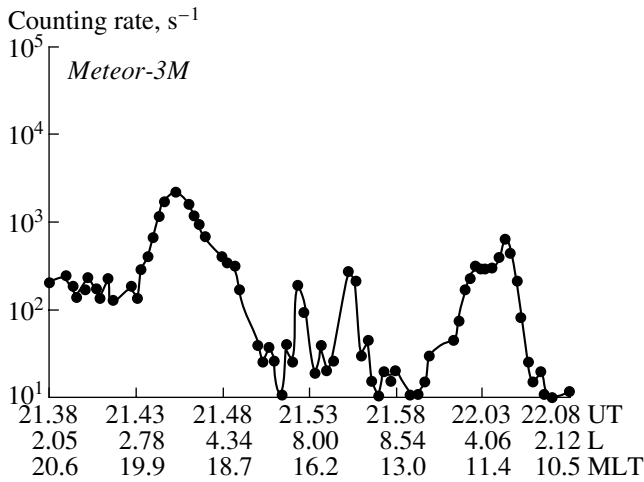


Fig. 17. The profile of the counting rate of electrons with $E_e = 10$ keV detected during a passage of the *Meteor-3M* satellite in the southern hemisphere on October 27, 2003.

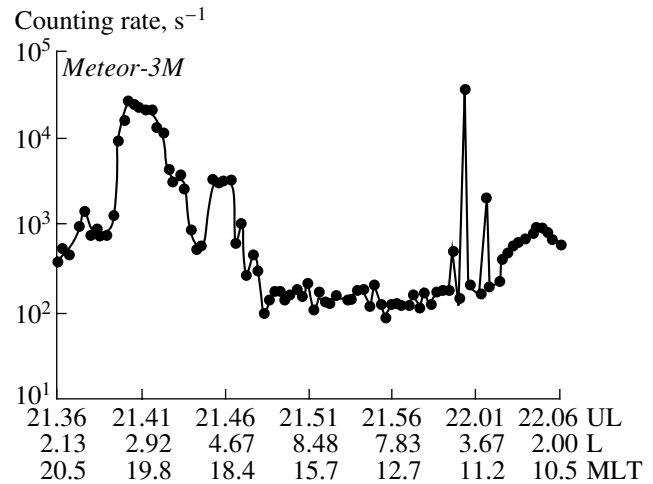


Fig. 18. The same as in Fig. 17, but for a passage on October 30, 2003.

the Earth (IPE). The coordinates of these maps are the corrected geomagnetic latitude – local magnetic time. The UT interval, for which the calculations were made, is shown at the top of each map, and the locations of observatories are shown by asterisks with corresponding international codes. For each day the maps are in one scale (it is different for different days).

Figure 22 presents two maps constructed using hourly averaged data for two time intervals, 12–13 UT and 13–14 UT, on October 29, 2003. It is seen that the strongest activity of pulsations was recorded in two space regions divided by a clearly cut minimum: in post-midnight and afternoon sectors of the auroral zone. In this case, rather unusual spatial–temporal dynamics of the amplitude of oscillations is observed. In the hour interval from 12–13 UT to 13–14 UT the maximum of intensity of post-midnight Pc5 has increased and been displaced in longitude to the midnight side (from 04 MLT to 02 MLT) and in latitude to the higher geomagnetic latitudes (from 63.5° to 64.7°). The maximum of afternoon Pc5 also was slightly displaced in longitude to the west, while in latitude it was displaced to the opposite direction, i.e., to lower latitudes (from 62.5° to 58.5°). Simultaneously, a small maximum has appeared about noon hours in polar latitudes (cusp?).

Figure 23 gives two maps of the spatial distribution of Pc5 amplitudes on October 31. One can see that on this day, as opposed to the preceding case (October 29), the spatial-temporal distribution and dynamics of Pc5 were quite different. Pulsations were observed only in near-noon and afternoon sector. One could isolate two latitude zones. At 11–12 UT the most intensive high-latitude (65° – 70°) zone was extended far into the morning sector (almost up to 04 MLT). No pulsations were observed in this morning time in the low-latitude zone (52° – 57°). In an hour the longitude extension of both

zones became similar, and the amplitudes of pulsations decreased. The maximum of Pc5 intensity in the high-latitude zone was displaced from 66° – 69° to 62° – 66° , while in the low-latitude zone the displacement from 55° to 51° took place.

One can assume that sources and mechanisms of generation of Pc5 oscillations were different on October 29 and 31. The pulsations Pc5 observed in the afternoon of October 29 have morphological characteristics that allow one to classify them with Alfvénic resonance oscillations widely discussed in the literature (see, for example, [18]). However, the pulsations in the morning sector of the same day and pulsations on October 31

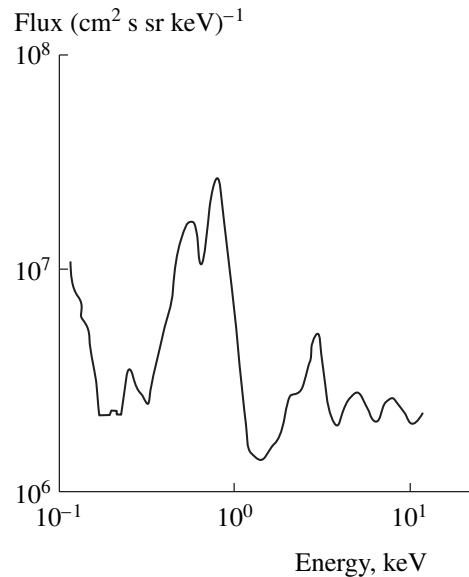


Fig. 19. Spectrum of electrons at the maximum of intensity ($L \sim 2.8$) in evening hours (MLT) of October 30, 2003.

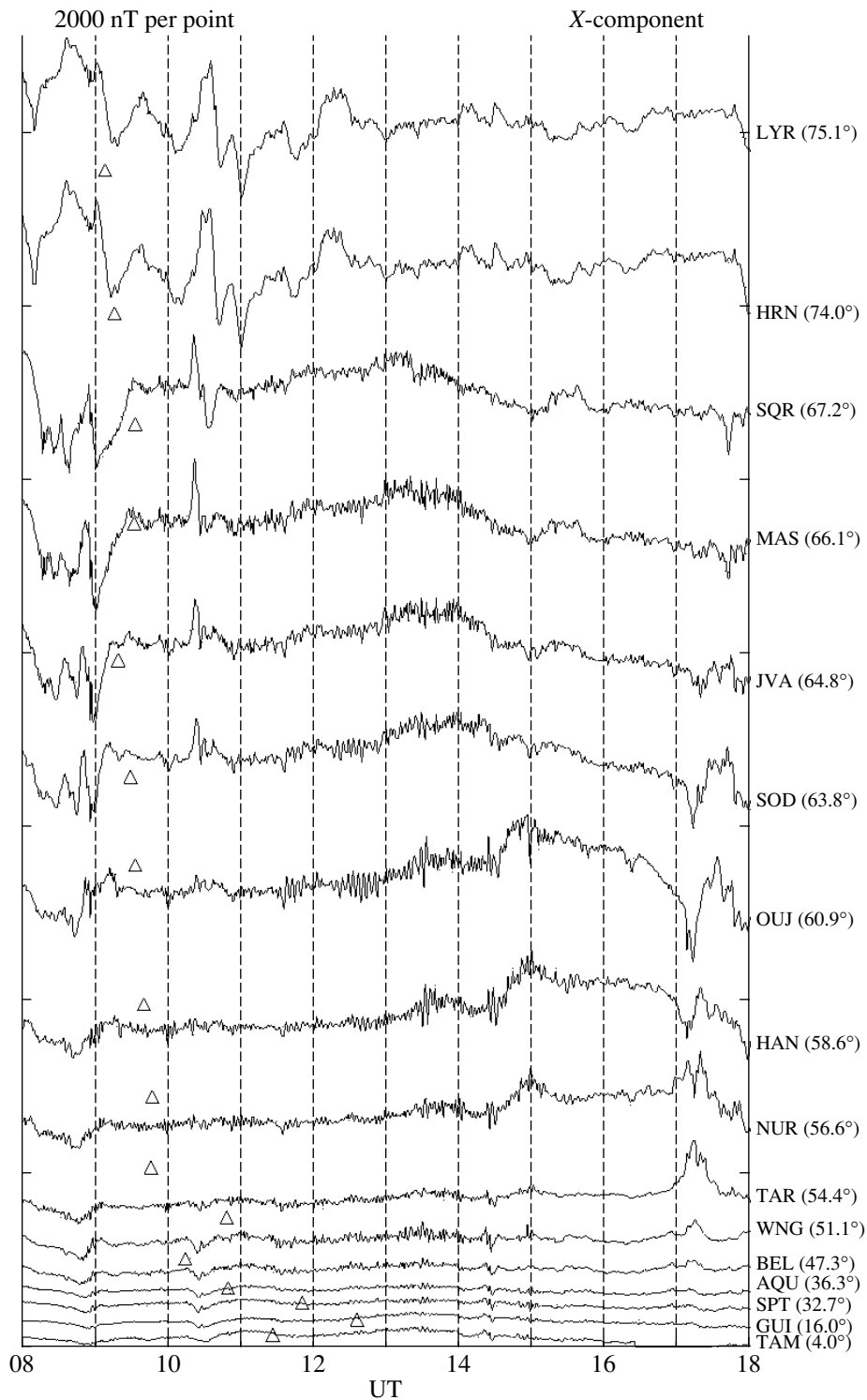


Fig. 20. Magnetograms on the Scandinavian profile of observatories (noon sector) on October 29, 2003, at latitudes from the polar cap to the equator.

cannot be explained by this mechanism. In the pulsations observed there was no change of the sign of oscillation polarization in the passage through the maximum of amplitudes, which is characteristic of resonance

waves. It is also improbable that the global magnetospheric mode (cavity mode) would be the source of these oscillations (as it was the case during the strong magnetic storm on March 24, 1991 [19] and during the

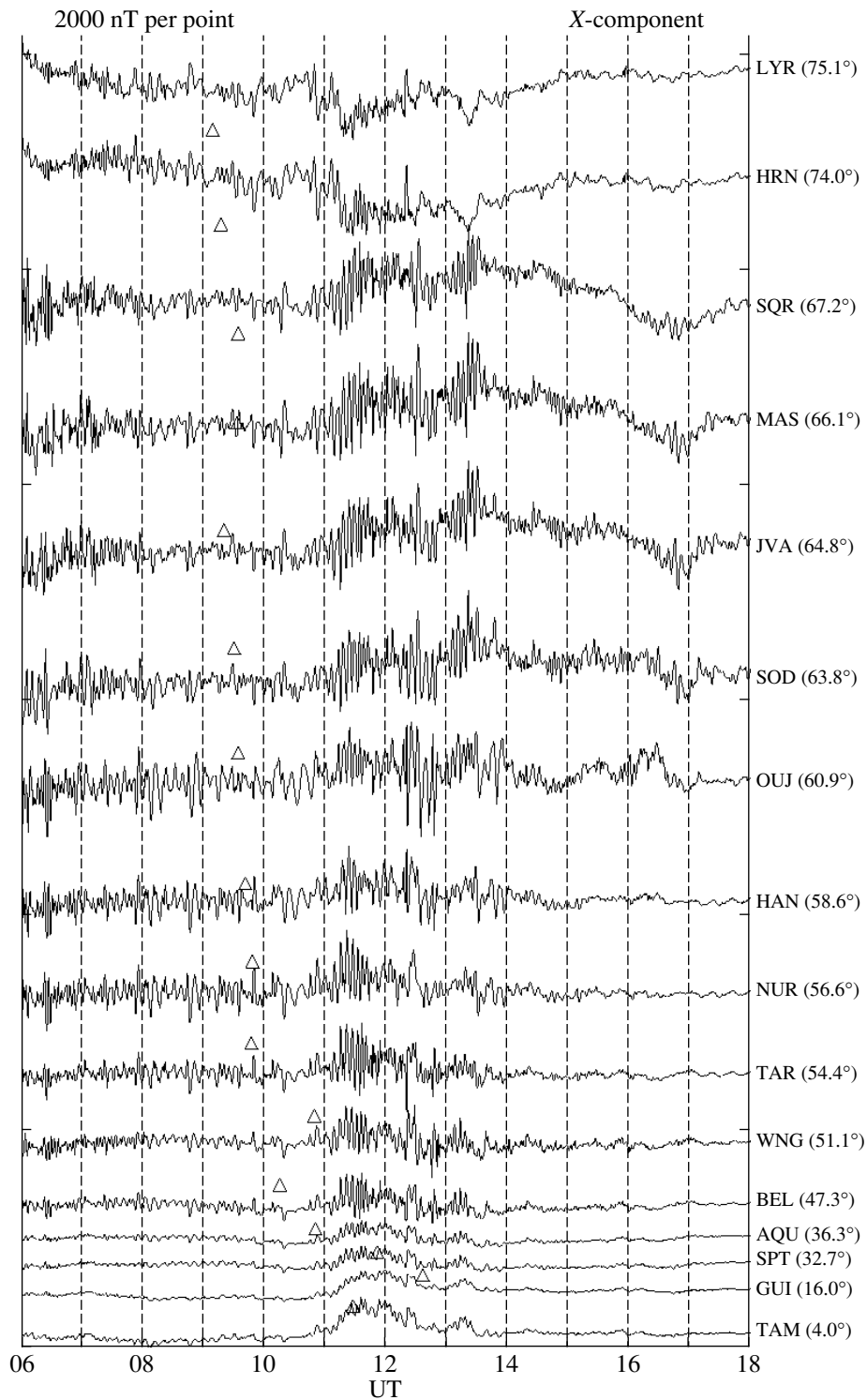


Fig. 21. Magnetograms similar to those in Fig. 20, but on October 31, 2003.

storm on February 21, 1994 [20]), since the frequencies of observed Pc5 pulsations are significantly higher than the frequencies typical for the global mode.

Fluctuations of field-aligned electric currents and corresponding precipitation of energetic electrons can

serve as a source of post-midnight irregular oscillations observed at auroral latitudes at 12–14 UT on October 29, as it was discussed in [21, 22]. One can suggest, as it was done in [22], that generation of daytime Pc5 pulsations is related to the intrusion into the ionosphere of

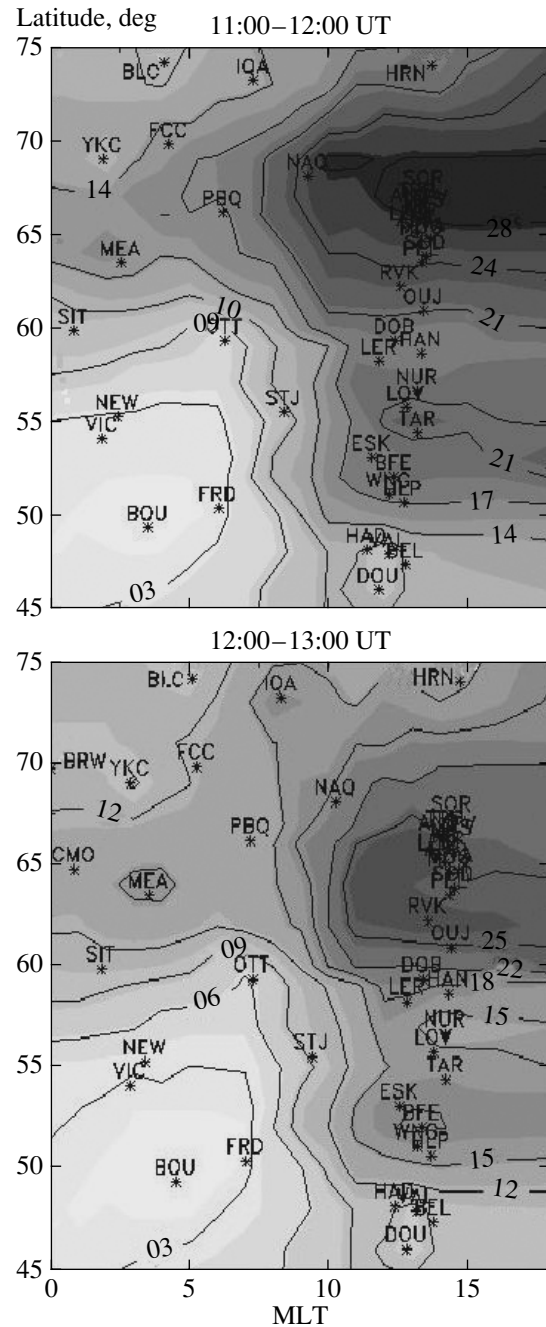
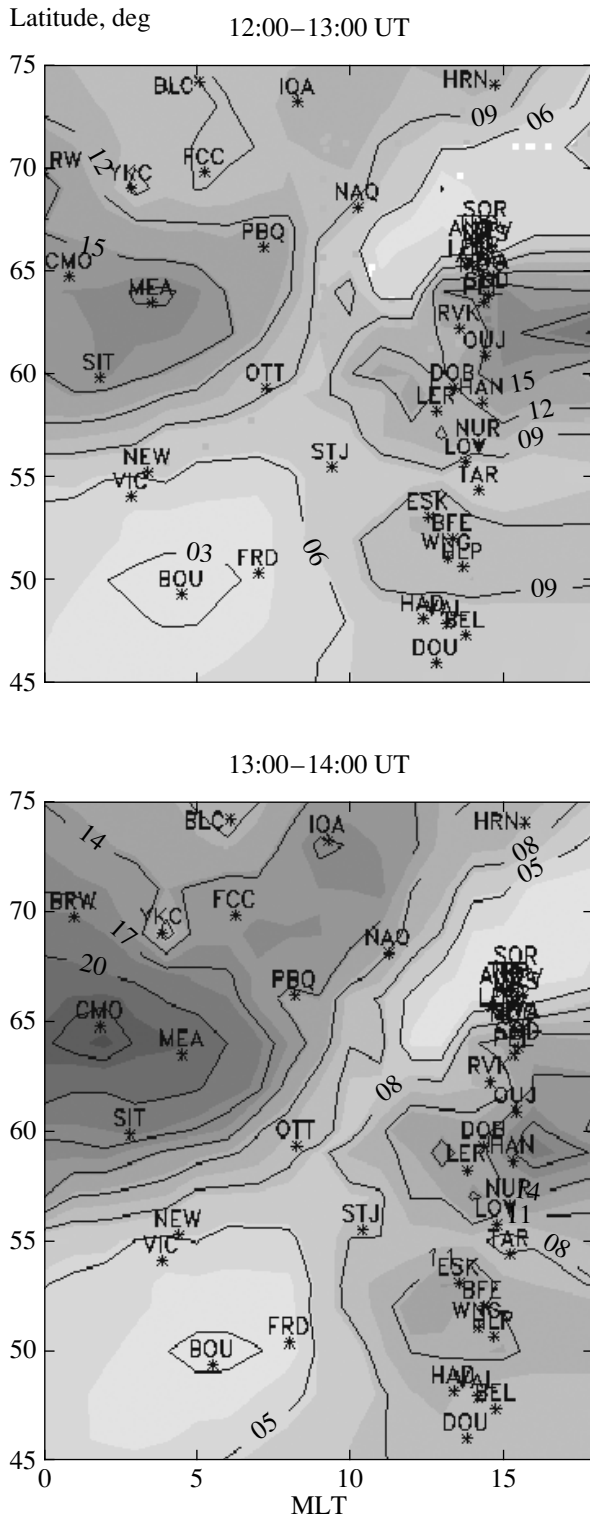


Fig. 23. The same as in Fig. 22, but on October 31, 2003.

Fig. 22. Maps of distribution of the integral intensity (nT/mHz) of geomagnetic pulsations in the frequency band 2.5–5 mHz (spectral maximum) on October 29, 2003 in the coordinates “corrected geomagnetic latitude–local magnetic time.” Interval UT is shown at the top of each map, the observatories are shown by asterisks together with their international codes.

protons of the ring current. However, such a hypothesis needs experimental confirmation. In addition, there are a number of questions that still have no answers. Here are some of them.

- What is the source of the beginning of a sharp increase in the amplitude of pulsations?
- Why do the pulsations end so abruptly?
- What does determine the latitude dimensions of the region of enhanced amplitudes of Pc5?

—What has resulted in the appearance of two latitude zones of afternoon Pc5?

—Why is the longitude asymmetry (relative to noon) of Pc5 observed?

3.2.2. Night geomagnetic pulsations Pi2–3 during substorm. The most intensive substorms were observed at the main phase of the magnetic storm of October 30 at 18–22 UT. Figures 24a and 24b present the magnetograms (*X*- and *Z*-components, respectively) of some observatories of the night sector (diamonds mark the local geomagnetic noon). Near 20 UT a very strong (almost 3000 nT) substorm was observed which included two intensifications: one a few minutes before 20 UT, and second, stronger one, after 20 UT. From the ratio of *X* and *Z* components it is seen that the center of electrojet for the above time interval has moved stepwise from the geomagnetic latitude $\sim 65.5^\circ$ to the latitude $\sim 61^\circ$. One more, less intense substorm was observed between 21 and 22 UT at geomagnetic latitudes $\sim 55^\circ$ – 62° .

All substorms considered above were accompanied by bursts of riometric absorption and by geomagnetic pulsations in the frequency band 1–15 mHz, i.e., in the range of Pi3 and Pi2. In addition to traditional amplifications of variations in the frequency band 1–2 mHz, which can be considered as high-frequency continuation of substorm current variations DP2, in the spectrum of oscillations the amplitude maximums were observed in the band 3.5–5 mHz (periods of order of 4–5 min, the range Pi3) and in the band ~ 6 –15 mHz (periods of order of 60–150 s, the range Pi2).

In order to study spatial-temporal variations of the intensity of these pulsations, the maps of isolines of the integral intensity of oscillations (nT/mHz) were constructed in the coordinates the corrected geomagnetic latitude – local geomagnetic time. These maps turned out to be almost identical for Pi2 and Pi3 oscillations, which indicates to their common origin. Figure 25 presents the maps of isolines of Pi2 intensity for three time intervals including two intensifications of the first substorm (19–20 UT and 20–21 UT) and the subsequent substorm at 21–21 UT.

As a rule, the region of appearance of irregular geomagnetic pulsations on the ground surface and the region of development of an auroral electrojet coincide. One can see from the maps in Fig. 25 that at the beginning, during the first intensification of the substorm activity the pulsations were observed in a relatively small interval of geomagnetic latitudes, higher than 65° . Then, the amplitude of Pi2 pulsations increased sharply, and the region of its maximum values became very narrow ($\lambda = 62^\circ$ – 63°) and displaced to the southeast. During the substorm of the maximum of the main phase of the magnetic storm (21–22 UT) the Pi2 pulsations were observed in a large area of space at unusually low geomagnetic latitudes (from 60° down to 50° and lower) with a maximum at a latitude of approximately 58° . Apparently, the auroral electrojet had the same spatial-temporal dynamics.

3.3. ULF Emission at Yakutsk

The ULF emission was detected at the Yakutsk station (ICRA) at 11 discrete frequencies from 0.47 to 8.7 kHz. Figures 26–29 present the results of measuring the ULF emission on October 28–31, 2003. The measurements carried out at several frequency channels are placed from top to bottom with increasing frequency, and the amplitude of variation is given in arbitrary units on the logarithmic scale.

The date of October 28, 2003 is a day with ULF disturbances. The bursts of ULF emission were observed mainly at frequencies below 6.7 kHz (up to the channel 6.7 kHz of the ULF detector). The beginning of basic variations of October 28, 2003 is due to magnetospheric processes (small D_{st} variations), since the outer radiation belt (with which usually the excitation of ULF emissions is associated) was formed (the maximum of intensity of electron fluxes in the outer radiation belt was at $L = 3.3$, see section 4). The subsequent bursts of ULF emission are, probably, related already to intensification of the fluxes of energetic electrons, as was measured, in particular, by the *Coronas-F* satellite. At the end of the day a new ULF disturbance developed with a broadening of the spectrum to the higher frequencies. It continued until October 29, 2003.

Apparently, this disturbance resulted in a partial depletion of the belt discussed in section 4.1. At a weak source of particles (weak injection into the inner magnetosphere), 4 h before the SC this began to manifest itself in a transition from a quasi-constant level of ULF emission to almost spiking mode. At the instants of quasi-periodic variations of ULF emission the mean interval between peaks was equal to 2–6 min. A sudden impulse of SC at 06:12 UT had appeared in a broad pulse of ULF emission (the upper frequency higher than 10 kHz) of considerable amplitude, after which a suppression of ULF emission oscillations occurred in the entire range of frequencies.

The recovery occurred only at 10 UT: separate bursts of emission corresponding to positive variations of the D_{st} field were detected. However, the next strong magnetic disturbance manifested itself in the ULF emission only on the next day, October 30, 2003, i.e., on the recovery phase of the magnetic storm. In this case, the record character is opposite to that observed in the beginning of the preceding day, which indicates to an increase of the source power of energetic electrons. Predominant values of the time spans between peaks in the periods of quasi-periodic modulation of ULF emission are within the same limits as on October 29, 2003.

Then, following the same scenario, in the second half of the day October 30, 2003 there were practically no bursts of ULF emission at the main phase of the next storm, while on the recovery phase a strong ULF disturbance began at 22 UT that was accompanied by a deep (up to 100%) modulation of the amplitude with the same periods 2–6 min. The modulation continued throughout the first half of the day October 31, 2003.

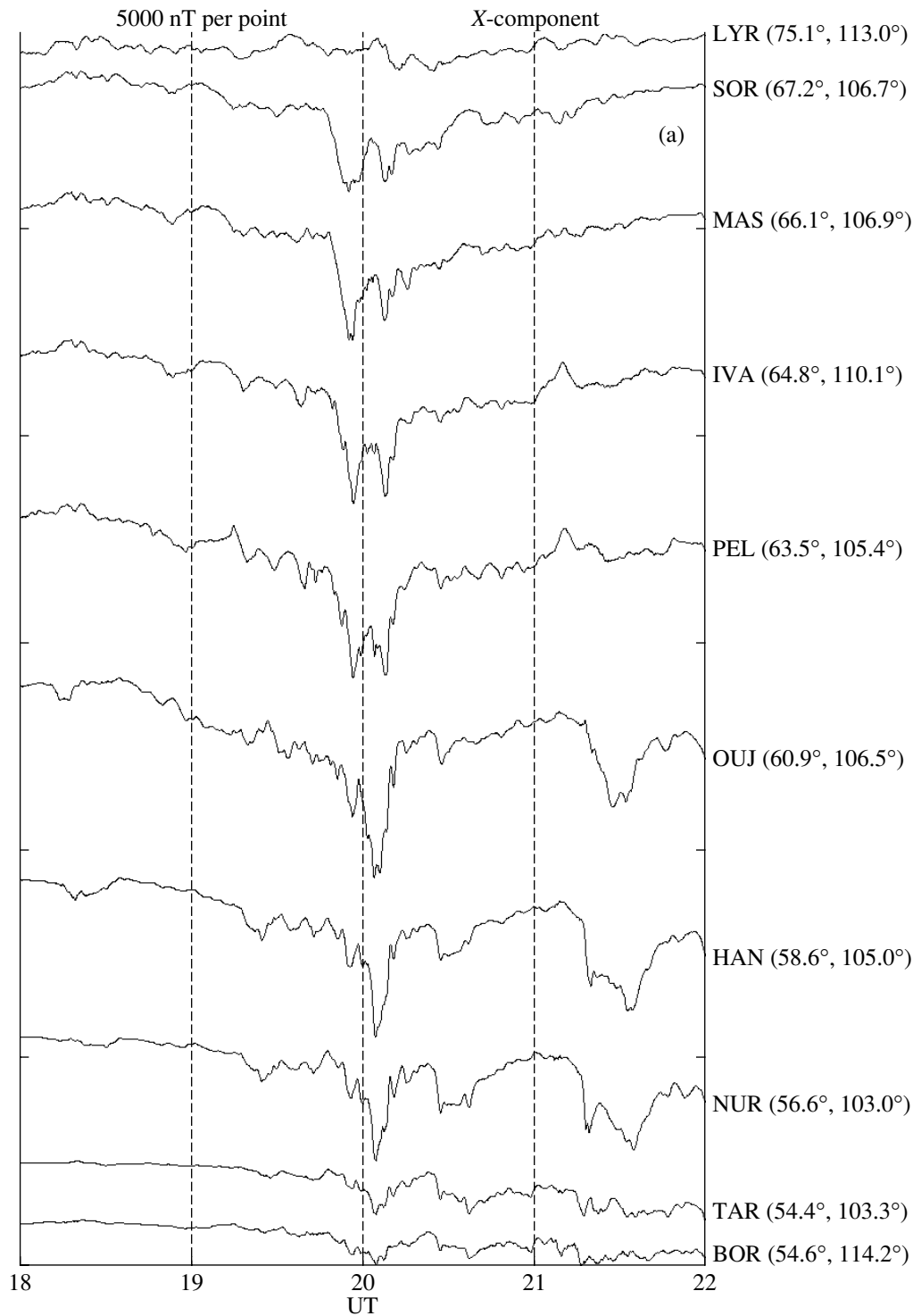


Fig. 24. Magnetograms of the night sector on October 30, 2003: (a) X-component and (b) Z-component of the field. The codes of observatories and their geomagnetic latitudes and longitudes are given on the right.

This range of periods of peaks observed in ULF emission at the Yakutsk station for three days (in the first half of each UT day and in daytime hours) corresponds to the period of geomagnetic pulsations Pc5. In this connec-

tion, it is interesting to consider pulsations Pc5 detected in the period of magnetic storms and discussed in the preceding section. The coincidence of periods of peaks with the periods of geomagnetic pulsations Pc5 and

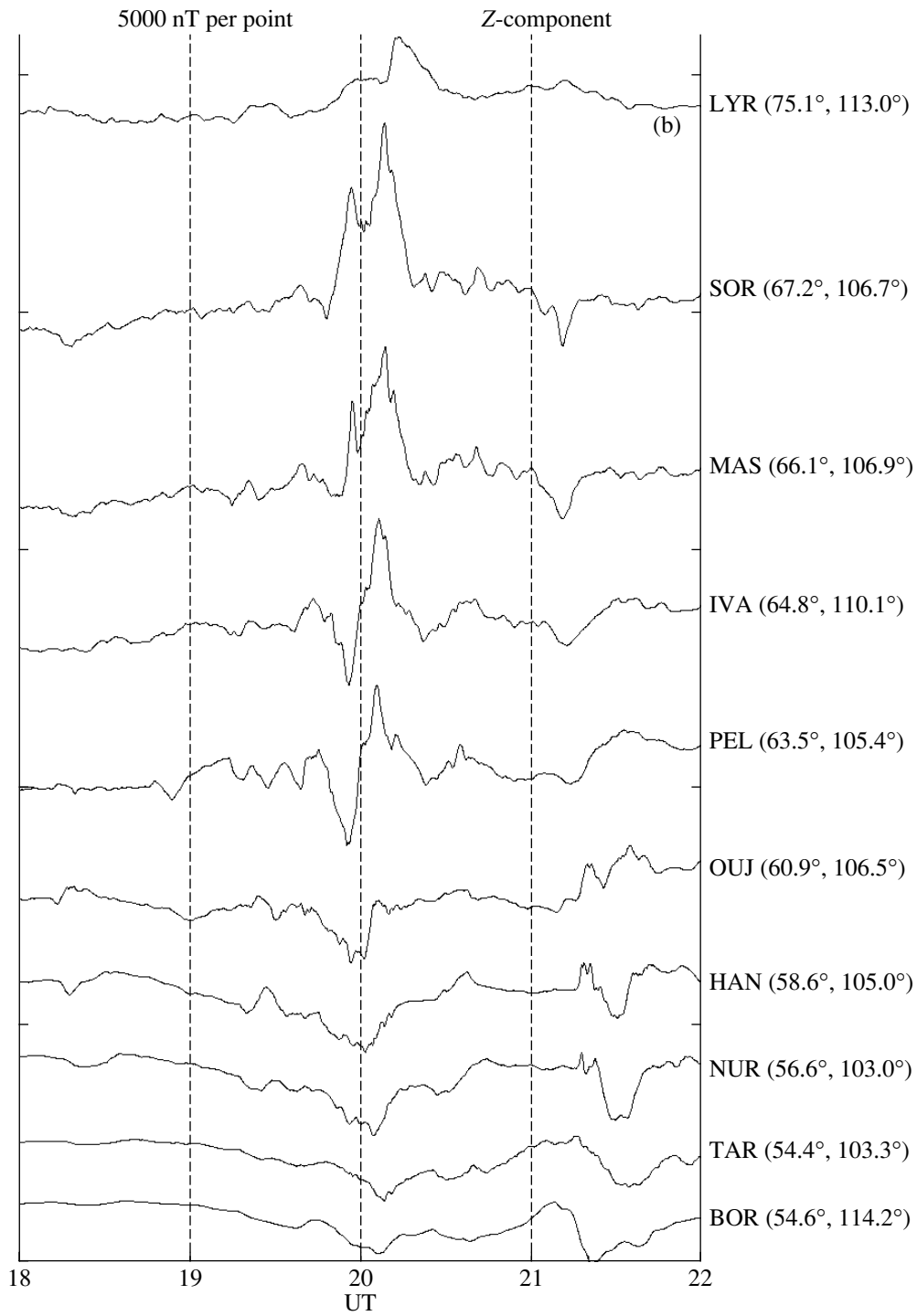


Fig. 24. (Contd.)

insignificant dispersion in peaks of ULF emission allow one to say that the pulsations facilitated the modulation of ULF emission. At the same time, as follows from magnetic data of the Yakutsk station, no Pc5 pulsations were detected until the SC instant on October 29, 2003.

3.4. Magnetic Field Dynamics: Model Calculations

The data on the solar wind in the vicinity of the Earth allow one to determine basic parameters of the magnetosphere. Five such parameters are used in the paraboloidal model [23]. First of all, this is the tilt angle

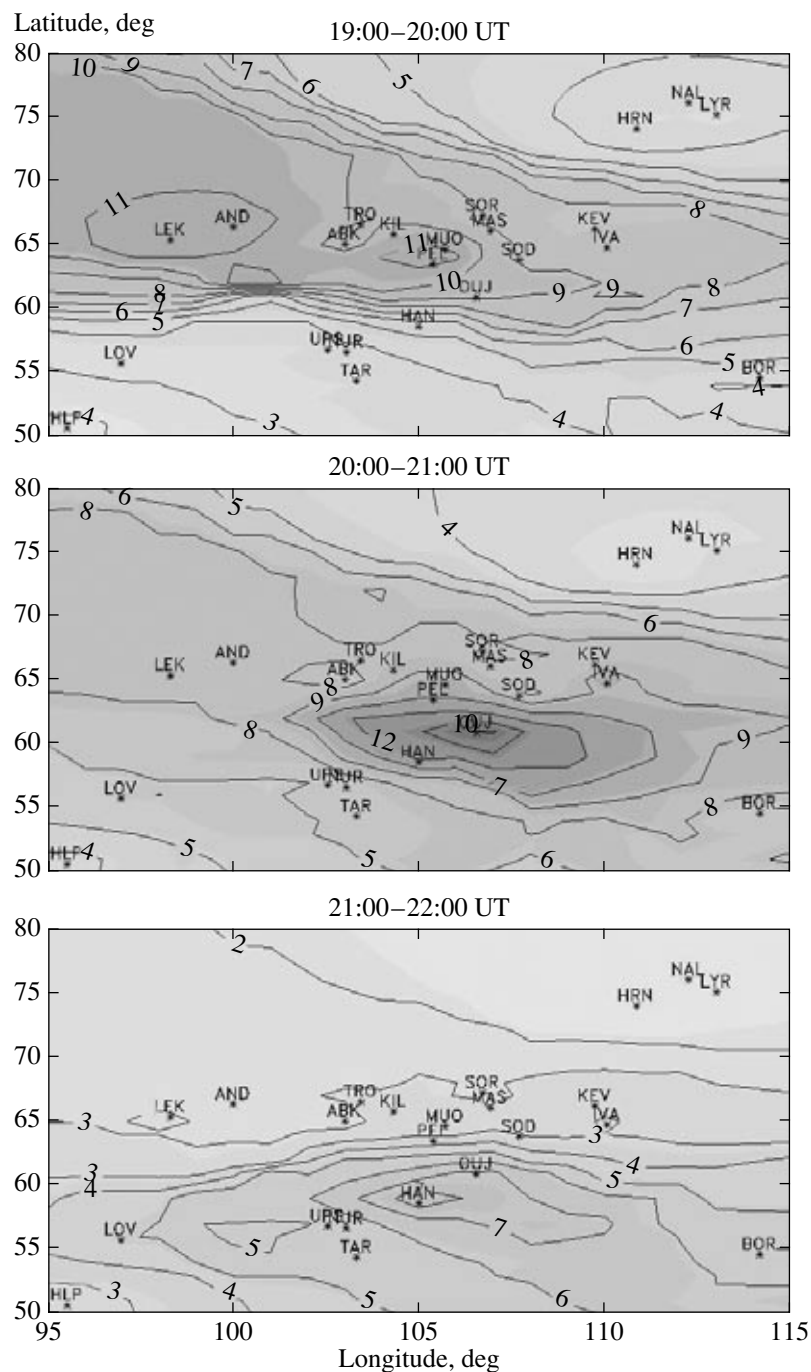


Fig. 25. The maps of isolines of the integral intensity (nT/mHz) of geomagnetic pulsations Pi2 for three discussed time intervals of October 30, 2003: (a) 19:00–20:00 UT, (b) 20:00–21:00 UT, and (c) 21:00–22:00.

ψ of the geomagnetic dipole to the Z axis of the solar-magnetospheric coordinate system. It is determined unambiguously by the date and universal time, and seasonal and diurnal variations of the magnetospheric field are characterized by it.

The magnetic flux in the lobes of the magnetotail (or flux in the polar cap) Φ_8 is another important parameter

of the magnetosphere. When carrying out model calculations, we used for Φ_8 the following expression

$$\Phi_8 = \Phi_0 + \Phi_s,$$

where Φ_0 is the magnetic flux in the magnetotail lobes during quiet periods, and Φ_s is the magnetic flux due to intensification of the current system of the magnetotail

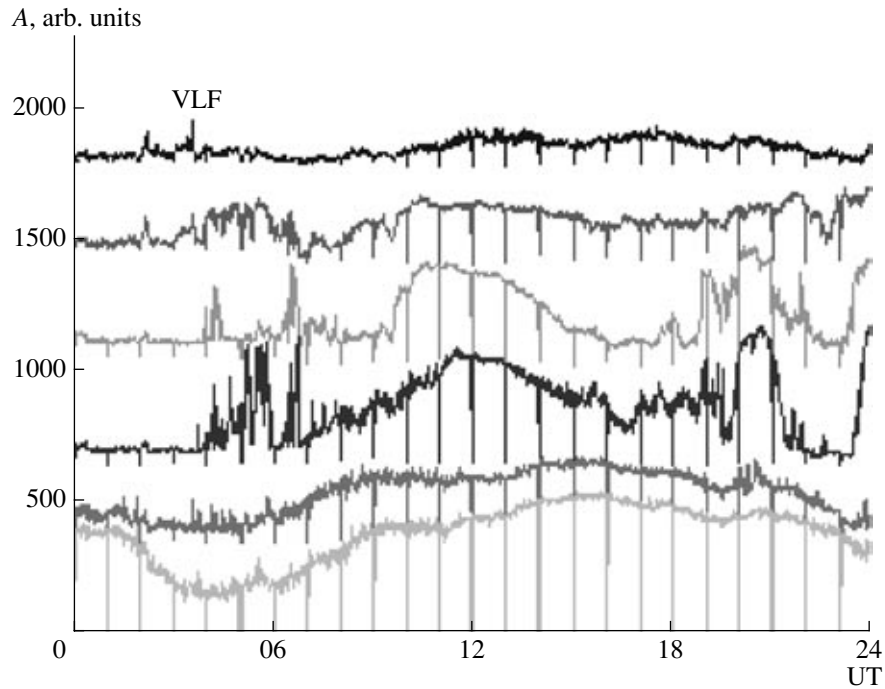


Fig. 26. The intensity of ULF emission according to measurements on October 28, 2003 at frequencies 0.47, 0.73, 1.6, 3.1, 5.6, and 8.7 kHz.

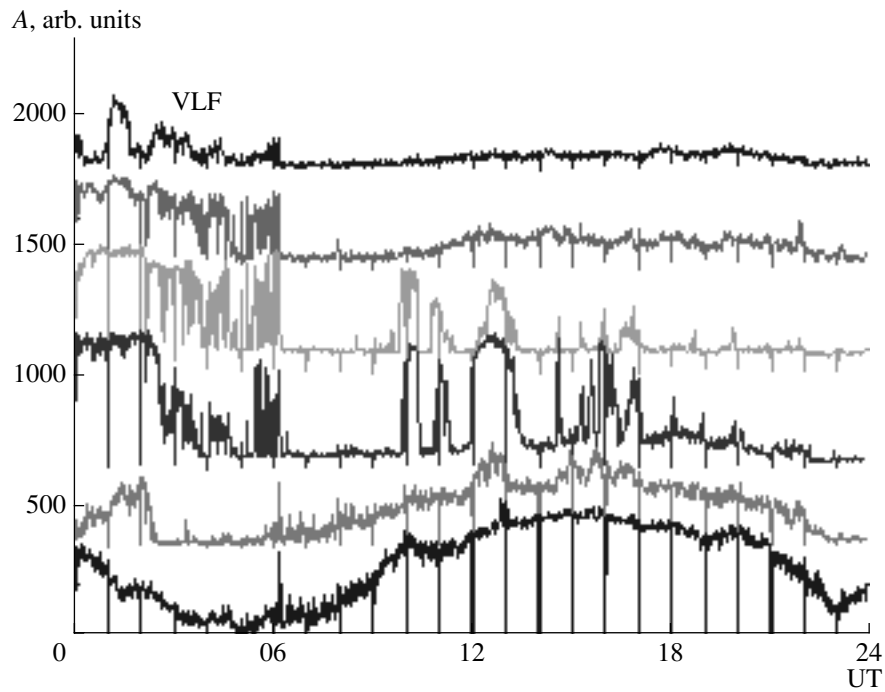


Fig. 27. The same as in Fig. 26, but on October 29, 2003.

during substorm disturbances:

$$\Phi_0 = 3.7 \times 10^8 \text{ Wb},$$

$$\Phi_8 = -AL \frac{\pi R_1^2}{14} \sqrt{\frac{2R_2}{R_1} + 1}.$$

The AL index was obtained by digitizing the preliminary data presented in the graphic form on the website of the World Data Center (WDC) C2 in Kyoto, R_1 and R_2 are the distances to the subsolar point on the magnetopause and to the leading edge of the current sheet of

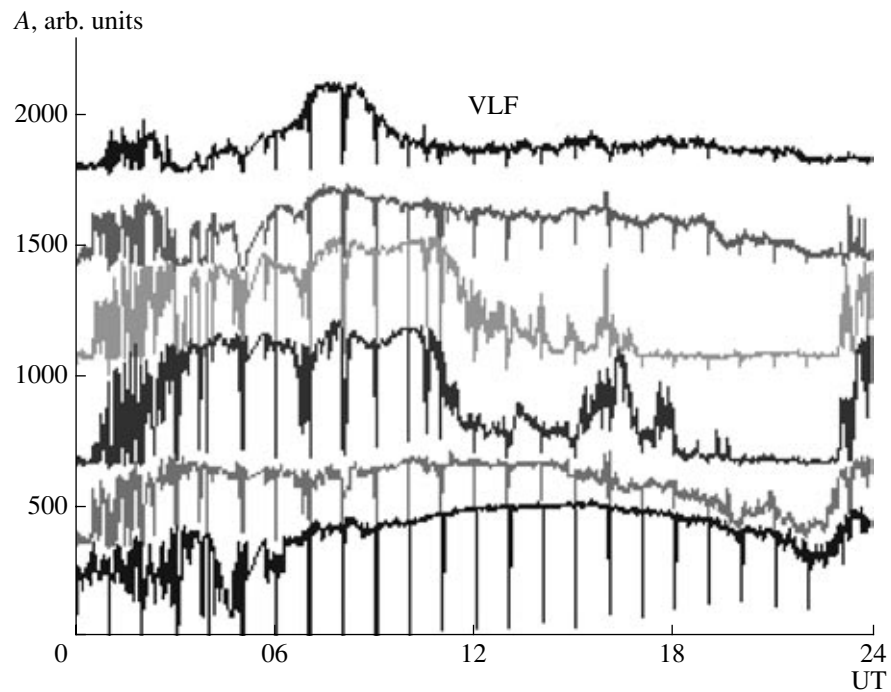


Fig. 28. The same as in Fig. 26, but on October 30, 2003.

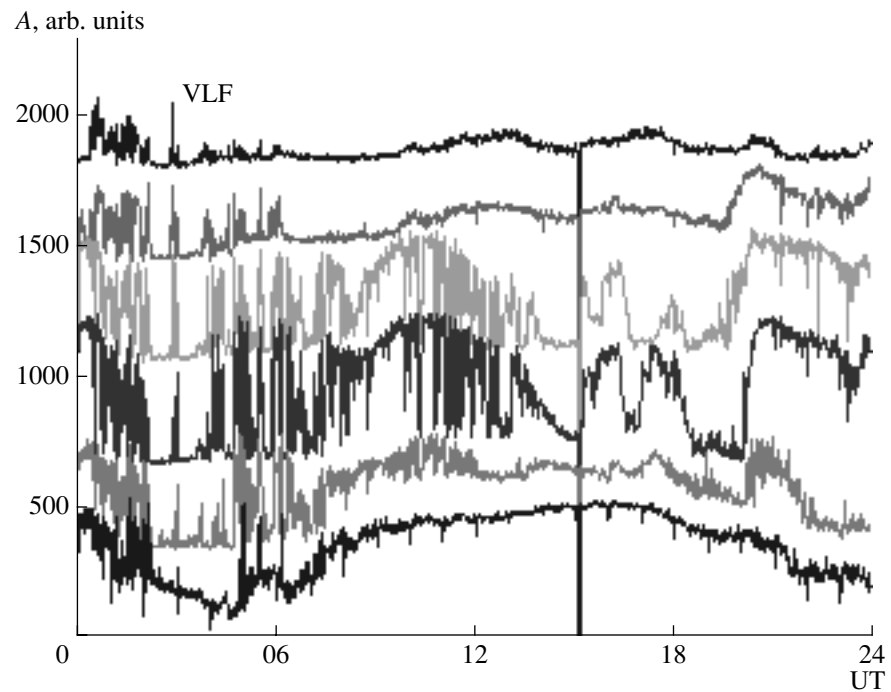


Fig. 29. The same as in Fig. 26, but on October 31, 2003.

the magnetotail, respectively. The distance R_1 was determined according to model [24] from the data of measurements in the solar wind of the plasma velocity and density, and of the B_z component of the IMF. The

distance R_2 was determined by projecting the equatorial boundary of the auroral oval. This boundary was found by a formula of [25] using the preliminary data about the D_{st} index, also taken from the WDC C2.

The magnetic field b_r of the ring current in the center of the Earth is the fifth parameter of the magnetosphere model. In accordance with the equation of Dessler–Parker–Scopce this parameter is proportional to the total energy of trapped particles in the ring current region. This parameter characterizes the intensity of the ring current during a magnetic storm and can be determined from the Burton equation that describes the ring current dynamics during magnetic storms as a superposition of two processes: the injection of plasma from the magnetotail region and the ring current decay [26]. In more detail the model parameters of the magnetosphere and the technique of calculations are described in [23]. A set of empirical data necessary for determination of the magnetosphere parameters ψ , Φ_8 , R_1 , R_2 , and b_r includes the indices D_{st} and AL , as well as the B_z component of the IMF, and the velocity and density of the solar wind.

The data of a proton monitor installed onboard the *SOHO* spacecraft were used in the calculations. Though the rate data are not very accurate, these measurements are the most complete among all currently available in the world network, which allows us to perform the analysis of magnetic field dynamics over the entire period October 28–31, 2003.

The initial parameters of the solar wind: the B_z component of the IMF (according to *ACE* data), density N and velocity V (data of the *SOHO* proton monitor) are shown in Fig. 30, as well as geomagnetic indices D_{st} and AL taken from Kyoto. The mean hourly data are presented. The data of *ACE* and *SOHO* are given with accounting for propagation time from the libration point to the Earth.

Using the data of measurements presented in Fig. 30 we have calculated the time profiles of the magnetosphere parameters. Figure 31 presents the parameters ψ , Φ_8 , R_1 , R_2 , and b_r of the magnetosphere model. It is noticeable that in the period October 29–30 the frontal magnetopause several times occurred to be closer to the Earth than the distance of 6.6 Earth's radii. The magnetic field of the Earth's magnetosphere is calculated in the paraboloidal model as the following sum

$$\mathbf{B}_2 = \mathbf{B}_{sd}(\psi, R_1) + \mathbf{B}_r(\psi, R_1, R_2, \Phi_\infty) + \mathbf{B}_r(\psi, b_r) + \mathbf{B}_{sr}(\psi, R_1, b_r).$$

Subtracting the quiet day variation, which was calculated for the quiescent conditions in the solar wind ($V = 400$ km/s, $N = 5$ cm $^{-3}$, $B_z = 0$ nT, $D_{st} = -5$, and $AL = 0$), from the field of magnetospheric sources, and taking into account the contribution of terrestrial diamagnetic currents that prevent the magnetospheric magnetic field from penetrating inside the Earth (30% of variation), we get

$$D_{st} = DCF + DT + DR.$$

Figure 32 presents the contributions to D_{st} of currents on the magnetopause (a), of the ring current (b), and of the current sheet of the magnetotail (c). A comparison of measured and calculated D_{st} for the interval October 28–31, 2003 is shown in Fig. 32d. The root mean square deviation is equal to 45 nT, which comprises a value of order of 11% of the maximum D_{st} . The largest discrepancy is observed during the main phase of the last storm at midnight of October 30, which can be connected with insufficient reliability of determination of the solar wind parameters by the *SOHO* proton monitor.

Summarizing, one can say that the magnetic storm in October 2003 belongs to the strongest geomagnetic disturbances in the current cycle of solar activity. The model of the magnetosphere describing the dynamics of global magnetospheric current systems during magnetic storms [23] allows one to predict sufficiently accurately the behavior of the D_{st} variation using the interplanetary medium parameters.

The authors of this section of the paper believe that the results of model calculations demonstrate the substantial role played by the current sheet of the magnetotail in the formation of the D_{st} variation at various phases of storms. Recent publications of the Los-Alamos group [27] contain experimental evidence of a dominant role of the current sheet of the magnetotail in formation of the geomagnetic field depression until the maximum of the main phase (D_{st} to -350 nT) of the magnetic storm on March 31, 2001. The relevant prediction (about the substantial role of the current sheet during magnetic storms) was made by Russian researchers (Yu.P. Maltsev, Ya.I. Feldshtein, and scientists from Institute of Nuclear Physics of Moscow University I.I. Alexeev, V.V. Kalegaev, and E.S. Belenkaya) even in 1993–1996 [28, 29]. (This concept of the magnetosphere geometry during storms is not shared by all members of the collaboration, and it is developed in more detail in a separate paper of this issue).

During the fall of a coronal mass ejection onto the magnetosphere on October 28–31, 2003 three successive injections of energetic particles into the ring current zone were observed. In essence, we are dealing with three sequential storms overlapped on each other. During the first storm the contribution of the current sheet was prevalent. Geomagnetic activity was directly controlled by the solar wind. The role of energy accumulation in the inner magnetosphere was relatively small. Two subsequent disturbances were related to the formation and decay of the ring current.

Another unique property of strong magnetic storms associated with dense coronal mass ejections moving from the Sun with high velocity is a strong compression of the magnetosphere. The dynamic pressure of the solar

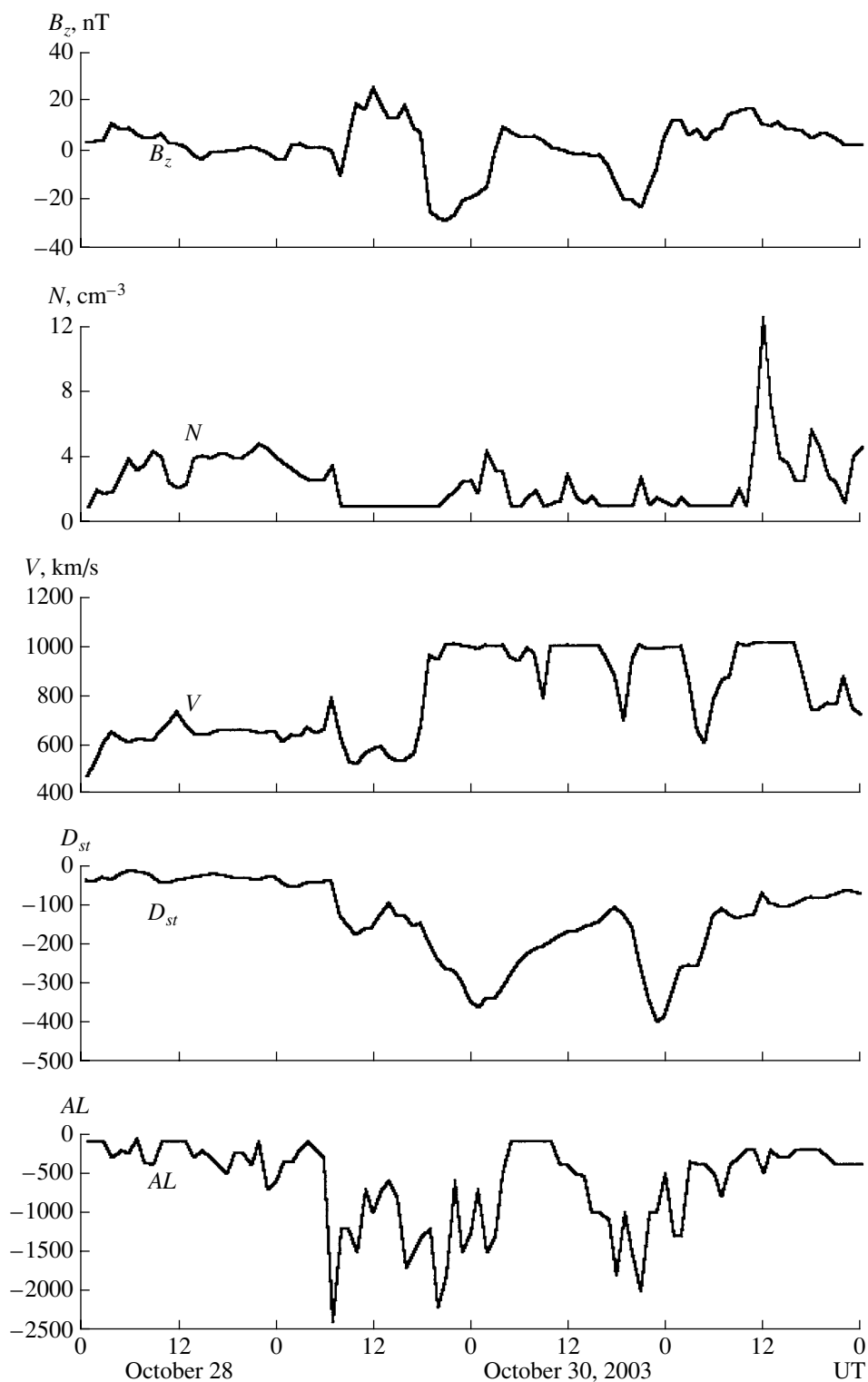


Fig. 30. Original data about parameters of the interplanetary medium and geomagnetic activity during the storm of October 28–31, 2003.

wind inside the coronal ejection was so high that the magnetopause multiply crossed the geosynchronous orbit. During the main phase of the storm of October 29, 2003 the magnetometers of geosynchronous satellites for 6 h

recorded the field of the southern direction (opposite to the terrestrial field) about 150 nT. This implies that the spacecraft were located behind the magnetopause in the magnetosheath and, probably, even beyond it in the solar wind.

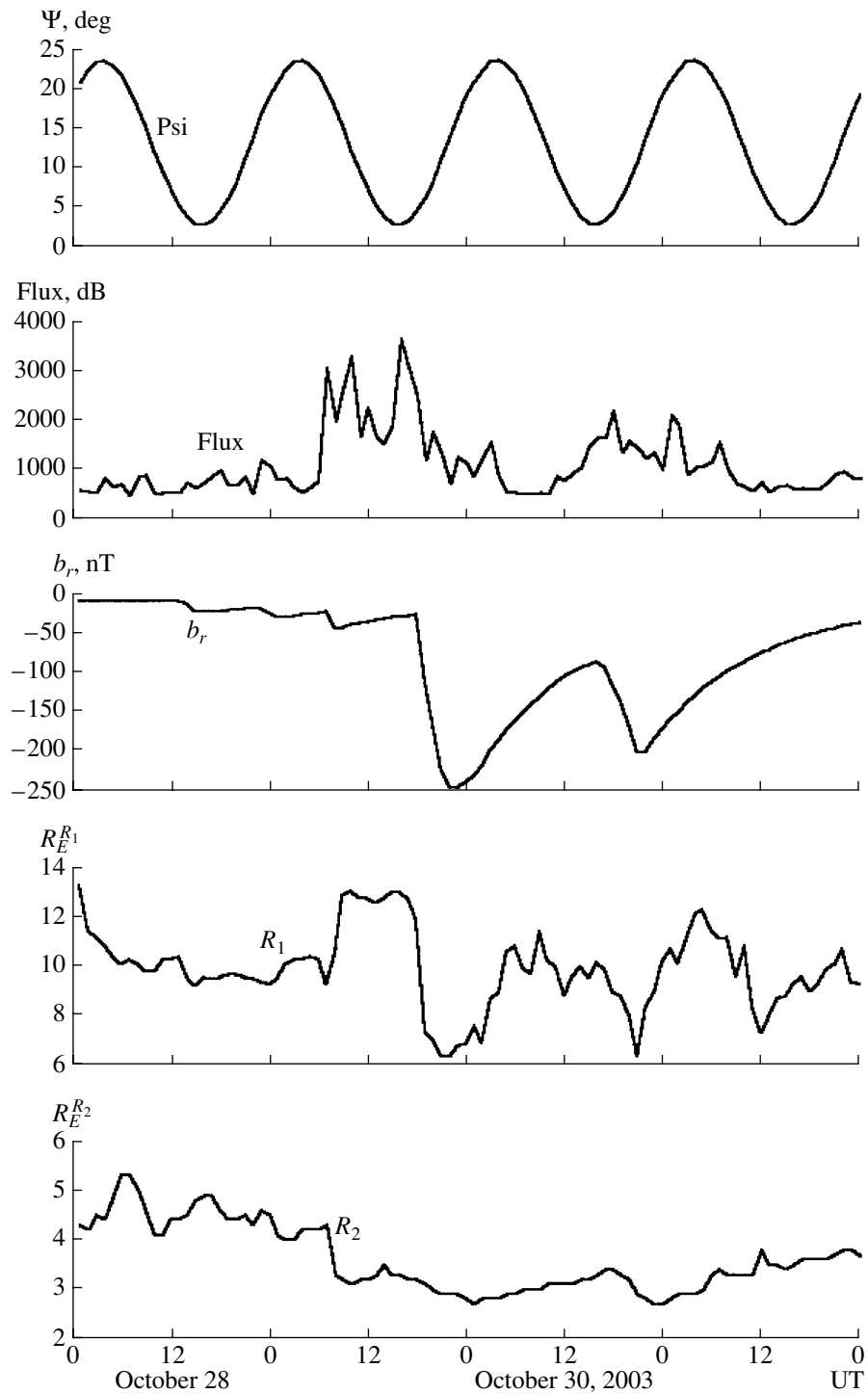


Fig. 31. The key parameters of the magnetosphere during the storm of October 28–31, 2003 calculated from the experimental data.

4. DYNAMICS OF ENERGETIC PARTICLES IN THE MAGNETOSPHERE

4.1. Solar Cosmic Rays (SCR) in the Earth's Magnetosphere

A transfer of active processes into the inner magnetosphere is one of the main features of magnetic

storms. On the dayside the magnetosphere boundary is displaced to the Earth from 10 down to 6 R_E and deeper, as a result of which geosynchronous satellites for some time turn out to be outside the magnetosphere. On the night side the boundaries of the auroral oval are displaced to the Earth to 50° (equatorial boundary) and 60° (polar boundary) [16]. The radiation belts of the

tude and the indices of geomagnetic activity were studied in great detail using a large data set for protons with $E_p > 1$ MeV measured onboard satellites of the *Kosmos* series in 1972–1977 [35]. The boundaries of SCR penetration are discussed in more detail in section 4.1.4.

The SCR measurements in October 2003 on the satellites *Coronas-F*, *Meteor-3M*, and *Ekspress* allowed one to get valuable data on (1) fluxes of solar protons, electrons, and nuclei in the polar cap, (2) fluxes of solar protons on the geosynchronous orbit, (3) dynamics of the polar cap boundary from measurements of energetic electrons of solar origin, and (4) dynamics of the boundaries of penetration of solar protons into the quasi-trapping region. Below, we present the results of a preliminary analysis of these measurements sequentially.

4.1.1. The fluxes of SCR in the polar cap. The low-altitude satellite *Coronas-F* with a polar orbit ($h \sim 500$ km, $i = 82.5^\circ$, $T_{\text{rev}} = 94.5$ min) was equipped with particle detectors MKL and SKI described in [37]. *Coronas-F* passes through the polar cap where field lines go into the magnetotail and are practically open for SCR penetration, therefore, no significant difference exists there with the temporal behavior of solar particles in the interplanetary space. The quasi-trapping zone is partially open, and the depth of penetration depends on energy (rigidity) of particles and their type. Figure 33 presents the time behavior of the fluxes of protons and electrons for one passage of the satellite through the polar cap on October 30, 2003 in the maximum of the main phase of the magnetic storm. In the magnetosphere there are protons and electrons of solar origin with energies from one to a few hundred MeV, they fill homogeneously the polar cap and (partially) the outer part of the radiation belt, i.e., the zone of quasi-trapping. The boundaries of penetrations for electrons and protons are shown by arrows. The projection of the background boundary of SCR penetration coincides with the location of the maximum for electrons of disturbed outer belt, which is also characteristic of quiescent periods. Solar electrons do not penetrate into the quasi-trapping zone.

Figures 34–36 presents combined plots for the fluxes of protons, electrons, and heavy nuclei of solar origin in several energy channels of the *Coronas-F* detectors in the northern and southern polar caps.

The profiles of SCR intensity in the period from October 26 to November 4, 2003 are determined by the conditions of motion in the interplanetary space of particles generated on the Sun during the flares on October 26, 28, and 29, and on November 2 and 4. Trapping and acceleration of SCR particles by interplanetary shock waves (ISW) and other features of propagation in the disturbed interplanetary space are an additional source of intensity variation, especially in the low energy region. A delay of the intensity decay and an increase related to ISW, becoming steeper while it approaches, and changing energy spectrum indices

are caused by the arrival of ISW and CME particles. In more detail the time behavior of SCR particles is considered in paper [1] dealing with solar and heliospheric phenomena.

4.1.2. Fluxes of solar protons at the geosynchronous orbit. In the period under consideration the geosynchronous satellites *Ekspress-A2* and *Ekspress-A3* operated at longitudes 80° E and 14° W, respectively. Energetic particles were detected on these satellites by identical instruments DIERA developed in INP MSU for monitoring the radiation environment at high-apogee navigation, communication, and TV satellites [38, 39]. The *Ekspress-A2* and *Ekspress-A3* satellites had a fixed orientation in space with respect to the axis X passing through the Earth's center.

Figure 37 presents the counting rates (counts per second) of semiconductor detectors having Si sensitive layer with a thickness of ~ 1 mm. Electrons with energies $E_e = 0.8$ – 1.0 MeV and protons with $E_p = 12$ – 50 MeV were detected within the cone with an opening angle of $\sim 20^\circ$ oriented to the Earth along the X axis of the satellite. The acceptance factor for detecting particles of such energies was $G \sim 10^{-3}$ cm² sr. The time of data averaging in each cycle of measurements was 6 min.

Beyond the angle of the acceptance cone the detectors are surrounded by a passive shield through which electrons with energies $E_e \sim 10$ MeV and protons with $E_p \sim 80$ MeV can penetrate. The acceptance factor for detection of particles of such energies within the angle $\sim 2\pi$ comprised $G \sim 5$ cm² sr.

In the period from 06 UT on October 28, 2003 to 06 UT on October 31, 2003, when the hardest spectrum of SCR was observed, high energy protons could contribute to the instrument counting rate passing through the lateral surface of the passive shield. A comparison with the above measurements onboard *Coronas-F* showed that variations of the flux of solar protons at the geosynchronous orbit almost coincide with variations of the flux in the polar cap (and, hence, in the interplanetary space). This result indicates that the boundary between the magnetotail and quasi-trapping region (i.e., the polar cap boundary in projection onto the ionosphere) during the entire disturbed period was located near the geosynchronous orbit or closer to the Earth.

4.1.3. The boundary of penetration of solar electrons. Figure 38 shows the time dependence of the invariant latitude of the boundary of the region of penetration of solar origin electrons from the morning and evening sides (empty and solid circles, respectively) on October 29 and 30. Also shown are the B_z component of the magnetic field according to the data of the *GOES-10* satellite and the quantity H_{sym} (minute analog of the D_{st} variation). The boundary of penetration of solar protons traces the polar cap boundary and field lines stretched into the magnetotail. Its approach to the Earth on evening hours of October 29 and 30 corresponds to

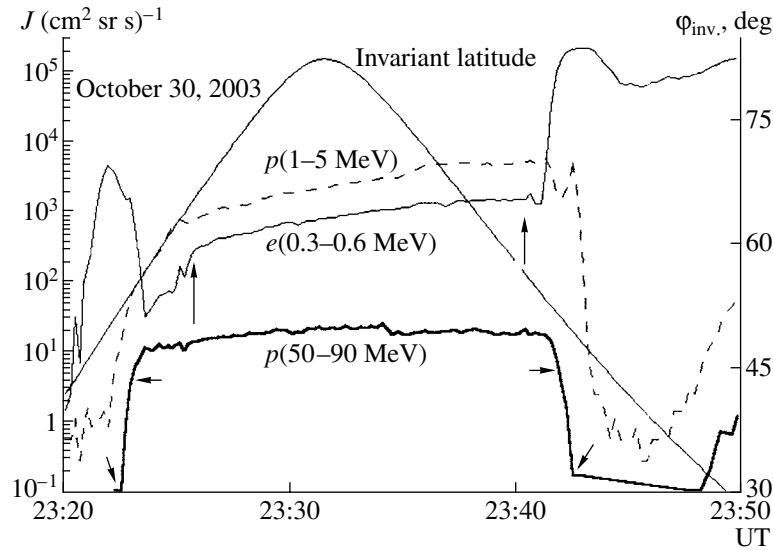


Fig. 33. An example of measurements of the fluxes of energetic particles on the *Coronas-F* satellite during its passage through radiation belts, auroral zone, and polar cap on October 30, 2003.

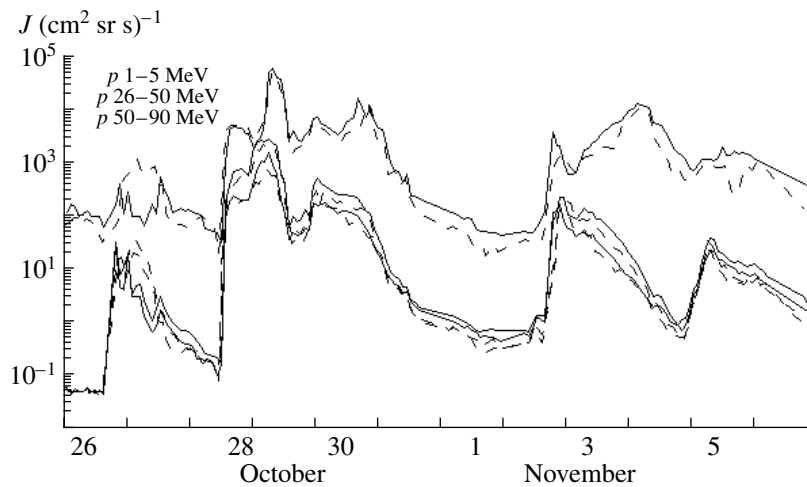


Fig. 34. Proton fluxes in the polar cap in the period October 26–November 4, 2003 as measured by the *Coronas-F* satellite. The southern polar cap is shown by a dashed line.

measurements onboard geosynchronous satellite. The satellite *LANL91* that was located at a longitude close to that of *GOES-10* observed a sharp reduction of the flux of electrons with $E_e \sim 135$ keV on October 29 and 30 in evening UT hours near the local noon because the satellite turned out to be outside the magnetosphere. The satellite *LANL97* at 06 UT on October 29 after the SC was near the local noon ~ 12 MLT and also detected a sharp decrease of the flux of electrons with $E_e \sim 135$ keV, but, apparently, the satellite did not leave the region of the magnetosphere. As one can see from Fig. 38, the boundary of penetration of solar electrons on the morning side at the end of main phases of the magnetic storms of October 29 and 30 was displaced to $\sim 58^\circ$.

Earlier, the strongest displacement to the equator of the dayside boundary of penetration of solar electrons ($\sim 61^\circ$) was detected by the *Kosmos-900* satellite during a magnetic storm with the amplitude $D_{st} \sim 200$ nT [32].

4.1.4. The boundary of penetration of solar protons. Unlike electrons, solar protons fill not only the tail of the magnetosphere, but penetrate to the quasi-trapping region as well. With the development of the main phase of the storm, the penetration boundary is displaced to the Earth.

In the preceding works of INP MSU this problem was studied in some detail [30–35, 40–41]. In particular, it was demonstrated that the displacement value

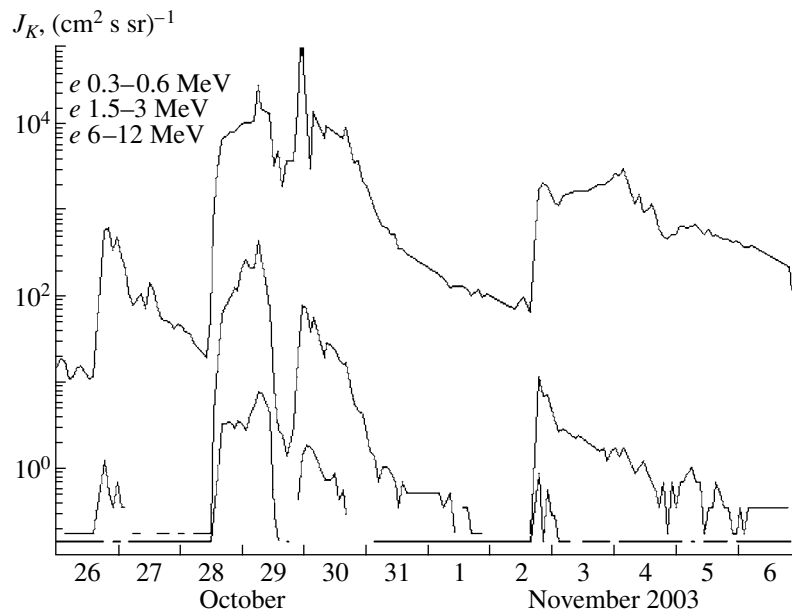


Fig. 35. Electron fluxes in the polar cap in the period October 26–November 4, 2003 as measured by the *Coronas-F* satellite.

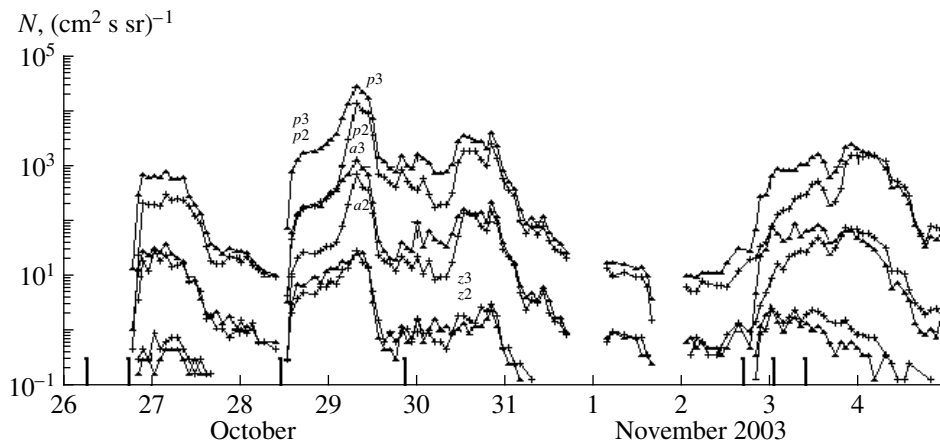


Fig. 36. The fluxes of SCR nuclei in the southern polar cap in October–November 2003. *p2* and *p3* are the fluxes of protons with energies in the ranges 2.3–4.2 MeV per nucleon and 4.4–19 MeV per nucleon, respectively. Similarly, *a2* and *a3* represent helium nuclei of the same energies. *z2* and *z3* are the nuclei of C, N, O group with energies 4–8 MeV per nucleon and 8–40 MeV per nucleon, respectively.

correlates with the magnetic activity indices D_{st} and AE . The joint influence of the ring current and auroral activity was studied in [35], and it was found that for protons with energies $E_p > 1$ MeV the penetration boundary best correlated with the parameter AD representing the following combination of AE and D_{st}

$$AD = (D_{st}^2 + 0.02AE^2)^{1/2}.$$

Apart from the indices characterizing the evolution of processes inside the magnetosphere, a correlation to

the solar wind pressure was investigated, taking it into account by the distance to the subsolar point of the magnetosphere. The latter is determined by the formula

$$X_0 = \frac{8.51}{P^{0.19}} + \frac{3.45}{P^{0.22}} \exp\left(-\frac{(|B_z| - B_z)^2}{200P^{0.15}}\right).$$

Where the pressure P of the solar wind plasma and the magnetic field are measured in nPa and nT, respectively [40]. The statistical analysis of several events has

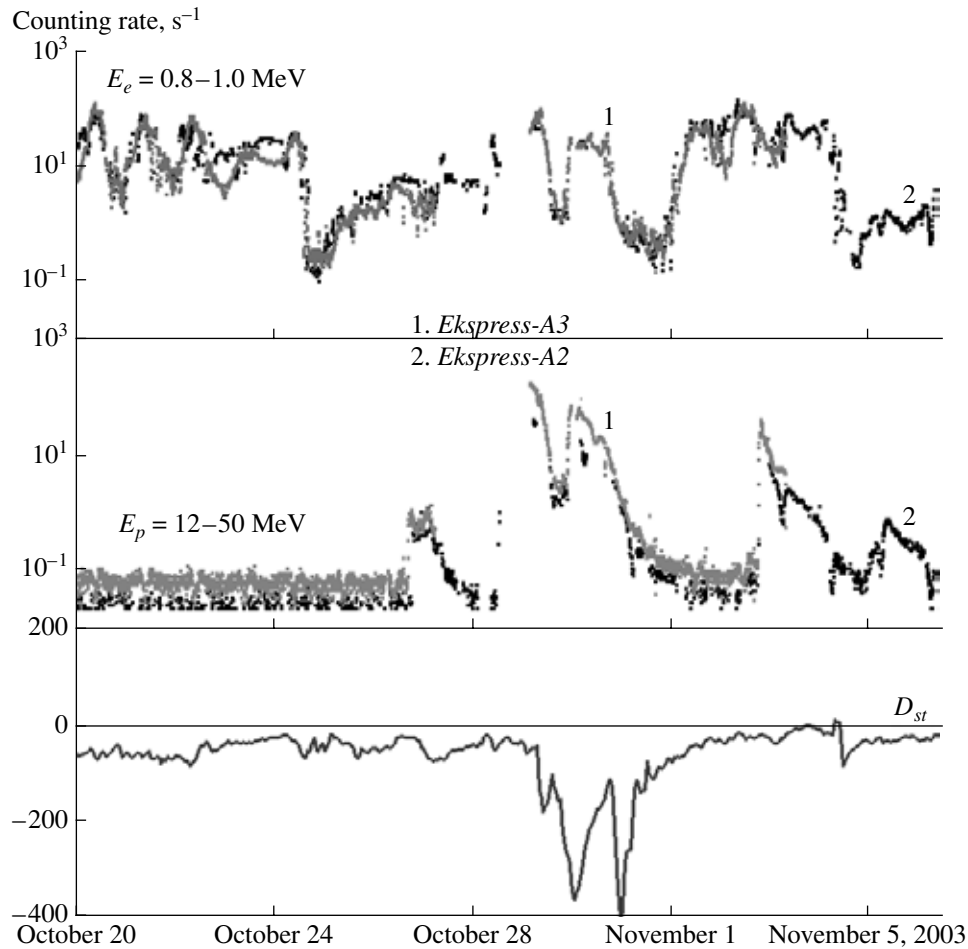


Fig. 37. Charged particles detected by the geosynchronous satellites *Ekspress-A2* and *Ekspress-A3* in the period from October 20 to November 11, 2003. The upper and middle curves represent, respectively, the fluxes of electrons with $E_e = 0.8\text{--}1.0$ MeV and the fluxes of protons with $E_p = 12\text{--}50$ MeV.

shown that the boundary of penetration of solar electrons is controlled by the substorm index of auroral activity AE and (to the lesser extent) by X_0 . For solar protons the X_0 and AD indices are equally significant [41].

A series of magnetic storms on October 29–30, caused by coronal mass ejections during the solar flares on October 28 and 29 is all-time strong both in the D_{st} value (down to -400 nT) and in the depth of penetration of energetic solar particles, as well as in the decrease of the region in which trapped radiation can exist (radiation belts). In late evening hours (in universal time) on October 29 and 30, according to data of the *GOES-10* satellite (LT = UT – 9 h for *GOES-10*) the magnetopause at the main phase of the magnetic storms was located at $R < 6.6 R_E$ (see Fig. 5).

When approaching the Earth, the flux of solar protons does not fall down instantaneously, so one can define the outer boundary as the place where the flux begins to decrease (for certainty, we have chosen the distance at which the proton flux drops twice). The

background boundary passes where the proton flux falls down by two orders of magnitude in comparison to the polar cap flux. In order to determine dynamics of the boundary we had at our disposal the data of measurements of several detectors onboard two satellites passing through both southern and northern polar caps. Only the data of *Meteor-3M* satellite (the channel with energy $E_p > 90$ MeV) and of the *Coronas-F* satellite (the channels detecting solar protons with $E_p = 1\text{--}5$ and $50\text{--}90$ MeV) were used for the analysis.

Meteor-3M: orbit and instrumentation. The satellite *Meteor-3M* was launched on December 10, 2001 into a near-polar circular solar-synchronous orbit with an altitude of ~ 1000 km, inclination 99.6° , and period of revolution 105 min. The onboard instrumentation for observing the flux variations of charged particles includes the complex of geophysical measurements KGI-4S (Institute of Applied Geophysics) and multi-channel spectrometer of geoactive radiations MSGI-5EI (INP MSU and NTs OMZ). In the KGI-4S instrument 8 particle counters used as detectors: two scintil-

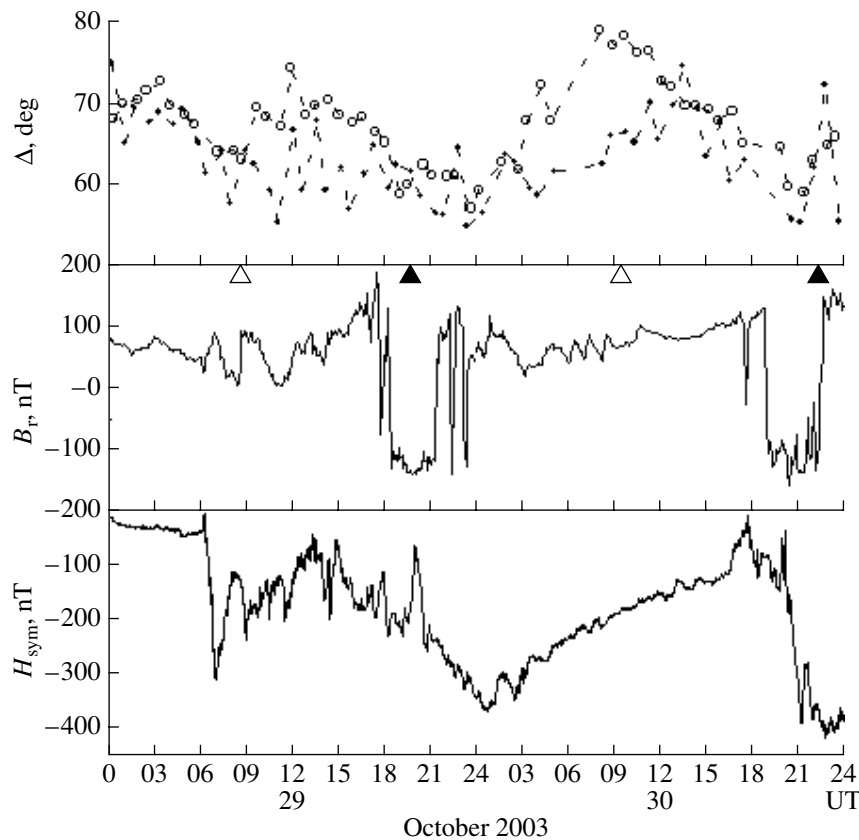


Fig. 38. Dynamics of the boundary of penetration of SCR electrons with energies $E_e = 0.3\text{--}0.6$ MeV according to the *Coronas-F* satellite data (upper panel) in comparison with variations of the magnetic field B_z component according to the *GOES-10* data (middle panel) and variations of H_{sym} (lower panel). Empty and solid circles designate the boundaries in the morning and evening sectors, respectively. Triangles mark the time of passage of the *Coronas-F* satellite through the regions of trapped radiation (see Fig. 44).

lation counters, one Cherenkov counter, and five Geiger counters. Design and electric parameters of the scintillation counters provide for detection of the fluxes of protons with threshold energies 90 MeV (high threshold) and 30 MeV (low threshold), the electron signals being suppressed. The Cherenkov counter detects the fluxes of protons with energies above 600 MeV and electrons with energies above 8 MeV. The Geiger detectors with various shields measure the total fluxes of protons and electrons. The shield thicknesses are chosen so as to provide for different threshold energies for protons in the range 5–40 MeV and for electrons in the range 0.15–3 MeV. These data are supplemented by measurements with the Geiger detector incorporated into the MSGI-5EI instrumentation with threshold energies 1 MeV (protons) and 40 keV (electrons).

The spectrometer MSGI-5EI is designed to measure differential spectra of both electron and ion (proton) components of geoeffective corpuscular radiations. Detection of low-energy particles, and their separation in charge and energy are performed by two types of spectrometric modules consisting of cylindrical electrostatic analyzers, secondary electron multipliers of the type VEU-6 (module of low sensitivity) and VEU-7

(high-sensitivity module), charge-sensitive amplifiers, and shapers of normalized pulses. These spectrometric modules allow one to measure differential energy spectra of low-energy ions (protons) and electrons in the energy range 0.1–15 keV. The energy spectra of electrons and ions (protons) can be measured in two modes:

- (i) the mode of studying spatial–temporal variations in the periods of heliogeomagnetic disturbances (mode 1): in this case the total time of measuring one energy spectrum is 2 s, while the number of energy steps is 10;
- (ii) the mode of diagnostics (mode 2): the total time of measuring one spectrum is 10 s, and the number of energy steps is 50.

The modes of operation are determined by specific conditions of measurements and are held by external commands.

Meteor-3M. Measurements. Figure 39 presents variations of the invariant latitude Λ_b of the boundary of penetration of solar protons as measured by *Meteor-3M* in the evening-midnight sector of the magnetosphere at the end of October 2003. The location of boundaries was determined according to the instant when the intensity of high-energy protons with $E_p > 90$ MeV fell down

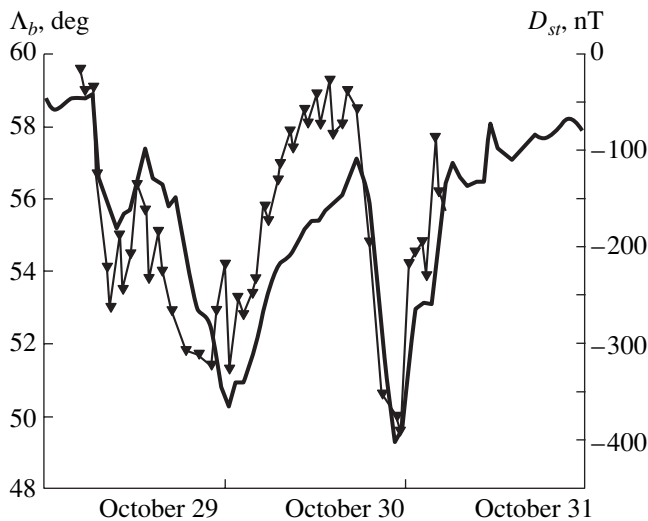


Fig. 39. Variations of the position of the boundary of penetration of solar protons with energies $E_p > 90$ MeV in the evening–midnight sector of the magnetosphere (dark triangles) during a series of strong magnetic storms on October 29–31, 2003. Thick solid curve represents the D_{st} variation.

by a factor of two with respect to its mean value on the polar plateau. One can see that the lowest latitude position of the boundaries well corresponds to the instants of maximum amplitudes of D_{st} variation during the superstorms on October 29 and 30. The minimum invariant latitude of the boundary ($\Lambda_b \sim 49^\circ$) was reached at the maximum of the superstorm of October 30. The boundaries well trace the D_{st} value during the main phase of this storm. However, during the first and second storms the behavior of the boundaries is significantly different from that of D_{st} . It is clear that the location of the SCR boundaries depends on the solar wind parameters and substorm activity in a more complicated way.

Coronas-F. The plots of motion of the background boundary of protons with an energy of 60 MeV on October 29 and 30, 2003 are presented in Fig. 40 together with the plot of D_{st} . As it could be expected, this boundary is located closer to the equator than the boundary shown in Fig. 39. In the evening of October 30 it reached a latitude of 45° , i.e., $L = 2$. Generally, here there is also a good coincidence of the boundary motion with D_{st} , as was demonstrated above using *Meteor* data. A good correlation takes place on the phase of recovery, when the penetration boundary retreats to the poles. At the same time, the picture at the main phase is more complicated. In the beginning of the first storm the displacement of boundaries proceeds fast, almost stepwise. At the main phase of the second storm the boundary displacement is also fast, much faster than the decrease of D_{st} .

In order to explain the fast and sudden changes of the penetration boundary, found independently in the

data of two satellites, one can suggest a contribution of the processes having different characteristic time scale and related to the substorm activation, namely, to a fast reconstruction of configuration of the magnetosphere. Indeed, as was demonstrated in the preceding section, an unusually strong substorm was triggered by a sudden commencement at 06 UT on October 29. The second rapid displacement of the boundary at 19–20 UT also coincided with a strong substorm in the midnight sector.

At the same time the direct impact of the solar wind on the structure of the magnetosphere must be also taken into account: the moments under consideration coincide with a compression of the magnetosphere near the bow shock and with a sharp intensification of the large-scale electric field (see Fig. 6).

4.1.5. The motion of the penetration boundary before the storm onset. Solar cosmic rays exist in the polar caps since October 26, which allows one to trace the motion of their penetration boundary before the onset of the magnetic storms of October 29–30 and further, until the phase of their decay. Figure 41 presents the time behavior of the latitude of the background penetration boundary for protons with energy 1–5 MeV on October 26–28. One can see from the figure that substantial variations of the penetration boundary position were observed not only during magnetic storms. In the first half of October 26, 2003 the boundary moved to the poles up to $\lambda = 68^\circ$, then in the evening of October 26 and in the early morning of October 27 it deviated to the equator down to 56° of invariant latitude. Then, almost all the day of October 27 and until 02 UT of October 28 the boundary moved to the poles and again to the equator, which is accompanied by strong variations of this latitude.

One can assume with a large certainty that the approach of the boundary to the Earth in the second half of October 26, 2003 is due to enhanced substorm activity, while the boundary motion away from the Earth is caused by a decrease of this activity.

The analysis of magnetograms of the Lovozero observatory presented in Fig. 42 confirms this hypothesis. At the same time, we did not succeed in finding a similar chain of substorms for the next equally deep displacements of the boundary on October 28, 2003. The magnetic conditions were quiet throughout the first half of the day when the boundary displacement was observed. It is probable that the solution to this enigma should be found in the solar wind behavior. According to the data of the *Wind* and *Geotail* spacecraft the solar wind density increased ten times since 02 UT to 04–06 UT, from 1 to 10 particles per cubic centimeter. The velocity grew substantially, from 480 to 600 km/s. In addition, a discontinuity with sharp changes of density and temperature is observed about 09 UT, probably related to a passage of the front of a shock wave. It is this fact that can explain the scatter in the location of SCR penetration boundaries observed

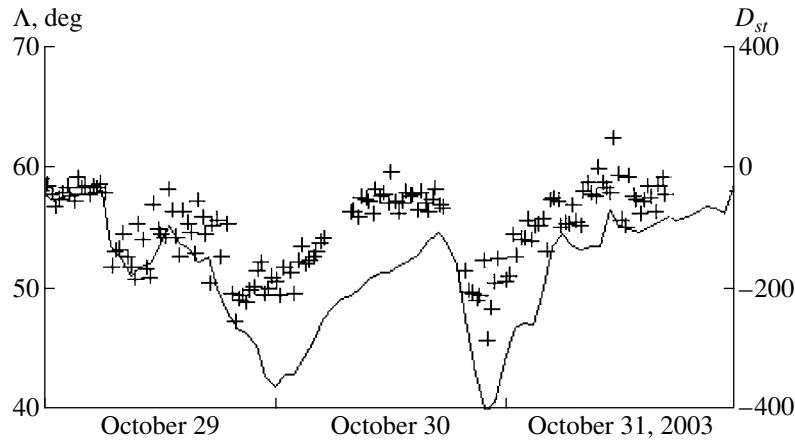


Fig. 40. The motion of the background penetration boundary for solar protons with $E_p = 60\text{--}90$ MeV on October 29–30, 2003 according to *Coronas-F* data.

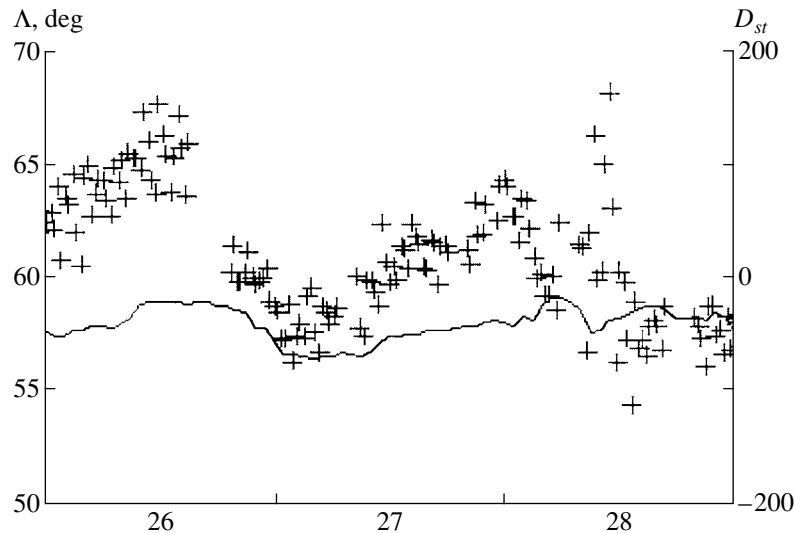


Fig. 41. The motion of the background penetration boundary for solar protons with $E_p = 1\text{--}5$ MeV in comparison with D_{st} in the period October 26–28, 2003 (before the beginning of magnetic storms) according to *Coronas-F* data.

during daytime and night passages at these hours. Thus, it is discovered that the boundary of SCR penetration always “breathes” moving to the Earth and back with an amplitude of more than 10 degrees of invariant latitude (from 68° to 58° in our case) even when there are no magnetic storms.

4.2. Dynamics of the Radiation Belts

The radiation belts are a main source of radiation hazard in the near-Earth space, and their variations during magnetic storms attract the attention of researchers for a long time [42–45]. These variations are strong and cannot be described in some simple model. Quick particle losses and even total disappearance of the outer belt give way to the formation of a new belt (sometimes, two or three), the radial displacement to the

Earth, and acceleration of particles. The dynamics of the radiation belts during storms depends on particle energy, charge, and nuclear composition. At the main phase of storms the variations proceed on the time spans shorter than the time of satellite revolution, therefore, it is impossible to trace this process in detail. Moreover, it is correct to compare measurements during a given passage only with measurements at the same region and at the same local time; as a result, only the total variation for a day can be established reliably. Taking the said above into account, it is not surprising that still there are so many unclear details in the dynamics of the radiation belts during global storms. In addition, it is obvious that any sufficiently detailed analysis of a particular event requires a special investigation: within the limits of a general paper we can only present some results specific for a given series of superstorms.

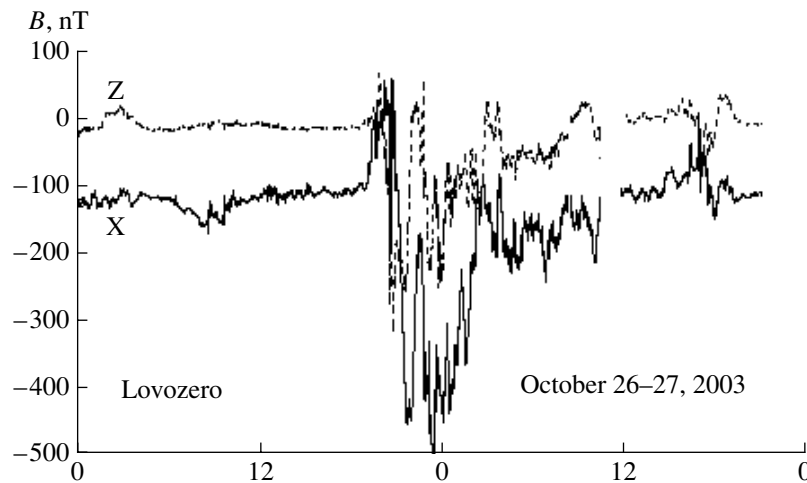


Fig. 42. Magnetogram of the Lovozero observatory on October 26–27, 2003.

4.2.1. Dynamics of the outer belt of electrons: Meteor-3M satellite. This paper presents preliminary results of studying the dynamics of the radiation belts of relativistic electrons with energies E_e higher than 8 MeV. Measurements of electrons of such energies are scarce and, hence, they are most interesting.

The time variations of the flux profile for electrons with energies above 8 MeV were recorded by the Cherenkov detector at various passages through the outer belt and are presented in Fig. 43. The instants of satellite passages are shown on the plot of D_{st} variation in the lower panel of the figure. On October 27, 2003 the maximum of the outer radiation belt was observed at $L \sim 3.3$. On the phase of recovery of the first superstorm it was displaced to $L \sim 2.6$; an increase of the counting rate in the region $L > 3$ during this passage is due to solar protons with energies higher than 600 MeV detected here by the Cherenkov counter. To the end of the recovery phase of the second superstorm (November 2, 2003) some additional displacement of the belt to the Earth occurred ($L_{\max} \sim 2.5$) and the intensity increased (the passages with close values of the magnetic field strength B were selected).

Thus, as a result of several strong magnetic storms, the maximum of the outer radiation belt of relativistic electrons with $E_e > 8$ MeV was displaced to the L -shells of the inner belt. We observed a similar effect in the data of the *Meteor* satellite during the storm of March 24–25, 1991 [46]. The maximum of a belt of electrons with $E_e > 8$ MeV, which had been formed as a result of a shock injection during a powerful storm sudden commencement, in the course of a subsequent superstorm ($|D_{st}|_{\max} \sim 300$ nT) was displaced from $L \sim 2.8$ to $L \sim 2.3$. On the recovery phase of this storm a new belt of electrons of lower energies (0.7–3 MeV) appeared with the maximum at $L \sim 3$. This value of L_{\max} is in a good agreement with the dependence of the maximum's location of the belt of relativistic electrons injected dur-

ing magnetic storms on the amplitude of D_{st} variation [47]. At the recovery phase of the superstorm on October 31, 2003 a new belt of electrons with $E_e > 0.7$ MeV also was formed (with a maximum at $L \sim 2.9$), and at the end of the recovery phase (November 1–2) one more additional maximum appeared on the profile of the outer belt at $L \sim 4.5$ (for electrons of all energies).

4.2.2. Dynamics of radiation belts: Coronas-F satellite. The data on the particle fluxes in the polar caps and radiation belts are obtained by the *Coronas-F* satellite. The satellite altitude was about 500 km; therefore, we could detect trapped radiation only in the region of the South-Atlantic magnetic anomaly. In Fig. 38 the time of detection of trapped particles in morning hours (~ 9 MLT) and evening hours (~ 21 MLT) is shown by empty and solid triangles, respectively.

In order to get information about the outer and inner belts, one needs to compare the data of two-three passages through the region of the anomaly. The data about radiation belts on October 28 can serve as a characteristic of the belt before magnetic storms. The left part of Fig. 44 presents the data on the structure of the fluxes of electrons with energies 0.3–0.6 and 1.5–3 MeV on the morning side, while the structure of the fluxes of protons with energies 1–5 and 14–26 MeV is shown on the right. The right part of the figure has similar structure for the analysis of particle fluxes detected on the evening side of the Earth. From the morning side the data are obtained in a relatively quiet time (excluding October 29). Thus, on October 30 and 31, 2003 we observe the results of impact of the storms of October 29 and 30, 2003. On October 29 the data on the outer radiation belt were obtained at $\sim 08:39$ UT at $D_{st} = -150$ nT ($H_{\text{sym}} = -120$ nT). One can see that the size of the outer belt was strongly diminished. At the preceding passage through the outer belt (at $\sim 07:03$ UT) the belt was not virtually changed in comparison with October 28 (see Fig. 45), though $H_{\text{sym}} = -300$ nT. The belt of protons

with energies 1–5 MeV in October 2003 had an additional maximum at $L \sim 3$. At 08:39 UT on October 29 the penetration boundary for protons of solar origin was located at $L \sim 3$. In the evening hours of October 29 and 30 the belt was detected on the main phases of the magnetic storms.

On October 29 the electron belt was not yet formed completely. At $L > 3$ the flux of electrons with energies 0.3–0.6 MeV was considerably less than before the magnetic storm. At $L < 2.7$ the flux of trapped electrons with energies 1.5–3 MeV was higher than before the storm. The maximum of the main phase was detected some minutes past twelve on October 30, and one might expect an increase in the electron flux after 01 UT on October 30. At 09:28 UT on October 30 the outer belt was detected with a maximum at $L \sim 2.5$. The belt of protons with energies 1–5 MeV was also formed here. At 22:10 UT on October 30, near the maximum of the main phase, the maximum of the outer belt was displaced to $L \sim 2$, and its boundary was detected at $L \sim 3$. The boundary of penetration for solar protons with energies 1–5 MeV was detected at $L \sim 2$. At 08:43 UT on October 31 the outer radiation belt had the boundary at $L \sim 6$, and the maximum of electron belt was at $L \sim 2.2$.

We have also detected a flux increase of protons with energies 1–5 and 14–26 MeV at $L \sim 2$ –2.2. On October 31 we had no data at 22–23 UT, therefore, we presented the evening data for October 1. One can see an extension of the outer belts of electrons and a considerable increase of the flux of electrons with energies 1.5–3 MeV. The peaks of intensity of protons with energies 1–5 and 14–26 MeV survived. The structure of the belts varied slightly in the period from October 1 to 5, 2003. The maximum of electron fluxes was detected at $L \sim 2.5$. The peaks of protons with $E_p = 1$ –5 and 14–26 MeV continued to be observed. The peak of protons with energies 14–26 MeV was observed at $L \sim 2.7$ –2.9, and the peak of protons 1–5 MeV was at $L \sim 2$.

One can see from the data presented above that during the main phases of magnetic storms the boundary of the region of penetration of solar electrons was displaced to invariant latitude of 50° ($L = 2.5$) and 55° ($L = 3.1$) on the evening and morning sides, respectively. This can explain the formation of the outer radiation belt at $L \sim 2.5$. Protons of solar cosmic rays penetrated to $L = 2$ during the main phases of magnetic storms. Additional belts of protons with energies $E_p = 1$ –5 and 14–26 MeV originated at $L > 2$. No such an effect was observed for protons with energies 26–50 MeV.

4.2.3. Post-storm increase of electron flux: Satellites *Ekspress A-2* and *Ekspress A-3*. In the data of the electron channel of *Ekspress* satellites (upper panel of Fig. 37) the diurnal variation of fluxes at the geosynchronous orbit is readily seen. Sharp drops of the intensity of electrons with $E_e = 0.8$ –1 MeV that took place on October 24 and November 4, 2003 engage our attention. These variations are related to intensification of

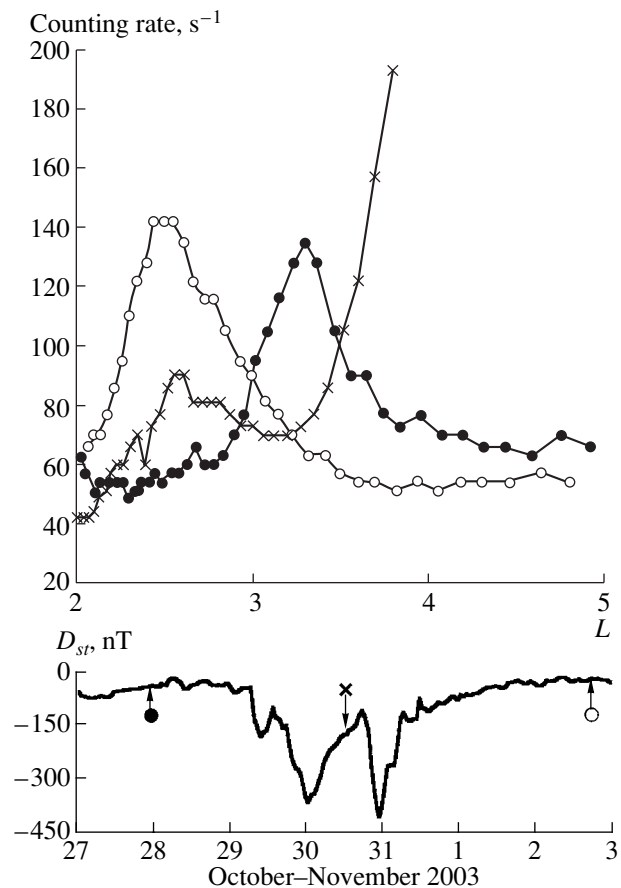


Fig. 43. Profiles of the radiation belt of electrons with $E_e > 8$ MeV observed in the period October 28–November 2, 2003. The instants of passages of the *Meteor-3M* satellite through the radiation belt are shown by arrows on the plot of D_{st} variation.

geomagnetic disturbances during weak magnetic storms (see D_{st} variation in the lower panel). After the drop of electron intensity on October 24, 2003, it was permanently increasing for approximately three days. However, in the beginning of solar proton events the level of electron intensity still was an order of magnitude lower than before the storms. During a strong enhancement of energetic solar protons on October 28–30, 2003 the counting rate of the detector was provided by protons with energies of tens of MeV.

The intensity of electrons began to increase on November 1, 2003, and in ~ 10 h it reached the level exceeding that before the storm by an order of magnitude. Thus, the electrons that appeared at the geosynchronous orbit were accelerated on the phase of recovery of the last superstorm whose maximum amplitude of the D_{st} variation (~ 400 nT) was detected at 23 UT on October 30, 2003. In this case, acceleration of electrons by substorm impulses could play an important role [48].

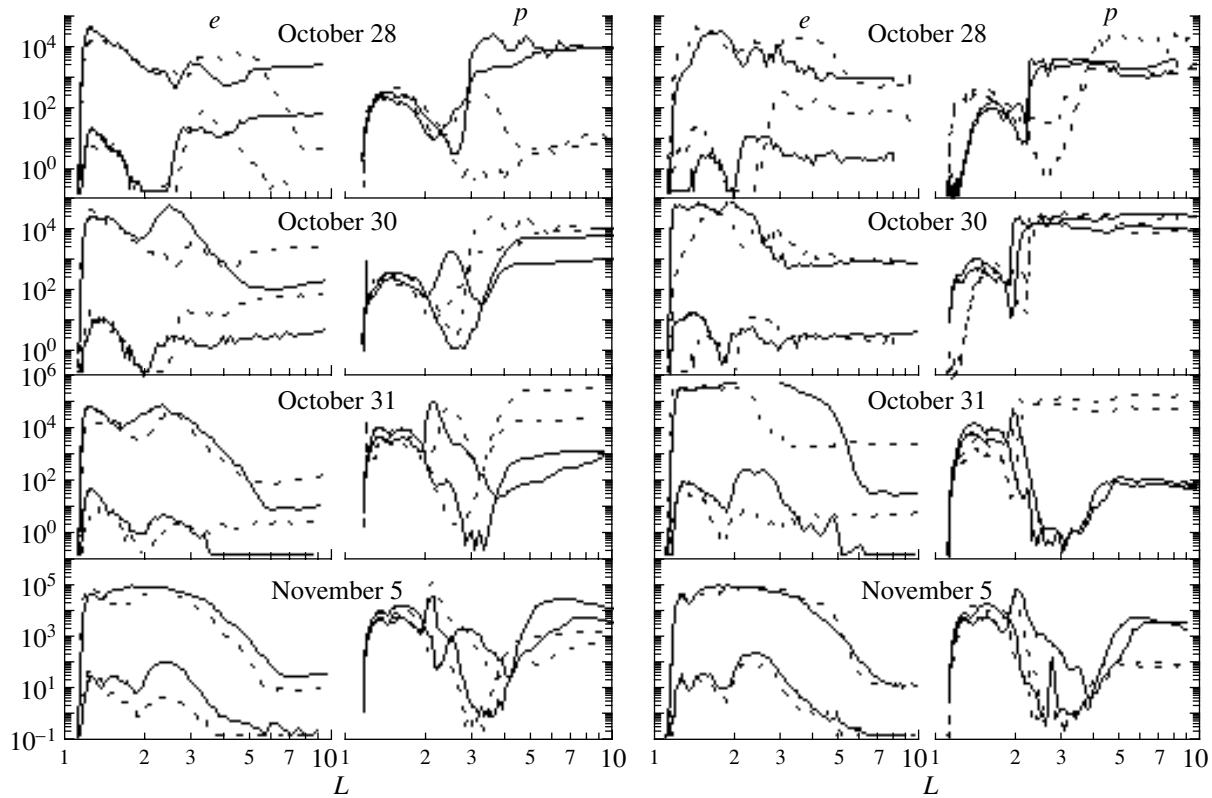


Fig. 44. A comparison of the profiles of particle fluxes in radiation belts measured by the *Coronas-F* satellite from October 28 to November 5, 2003. In the left and right parts presented the data obtained at 07–09 UT and 19–23 UT, respectively. In the left part of each plot the data on fluxes of electrons with $E_e = 0.3\text{--}0.6$ MeV (thin line) and $E_e = 1.5\text{--}3$ MeV (thick line) are presented. The right parts represent the fluxes of protons with $E_p = 1\text{--}5$ MeV and $14\text{--}26$ MeV, respectively. For comparison, the dashed lines show the data related to the preceding panel. The dashed lines in the top panel demonstrate the data for October 28.

4.3. Radiation Conditions on the International Space Station

During the events in the end of October and beginning of November 2003 a system of radiation control (SRK) was operating on the Russian service unit of the *ISS*. It was designed for determination of the level of radiation impact on the *ISS* crew. The sensitive elements of this system were placed in the blocks DB-8 and dosimeter R-16. All four blocks DB-8 are identical. Each of them included two fully independent channels consisting of a silicon semiconductor detector 300 μm thick and a subsequent circuit of processing the signal. One of two detectors incorporated in each DB-8 block was shielded by a lead layer with a thickness of 2.5 mm. Two ionization chambers, one of which has additional plexiglass shield 3 cm thick, are sensitive elements of the R-16 dosimeter.

When organizing the radiation control it was essential that onboard the station the DB-8 block were installed inside a hermetically sealed compartment. The points of arrangement were chosen in such a manner that different conditions of screening of the SRK detectors by the station equipment would be realized. It was necessary, in order to determine the curve of dose atten-

uation after the analysis of results. Then, this curve can be used for calculations of the absorbed doses at any place of the Russian segment of the *ISS*.

Figure 46 presents the dynamics of dose accumulation according to the data of unshielded detectors of the least protected block DB-8 no. 1 and the most protected block no. 4. The detector records at 00 UT of October 21, 2003 were used as the initial level. Here and below, the universal time is used.

As one could expect, it is well seen that during the solar proton events under consideration a considerable change of the dose was observed in the station compartments. Three periods of a substantially increased rate of dose accumulation were observed onboard the station.

The first period started at 15:25 UT on October 28, after the appearance of high-energy SCR protons in the near-Earth space. At this time the trajectory of *ISS* flight passed through the zone of penetration of high-energy charged particles above the southern part of the Indian Ocean. To the instant of 19 UT on October 28 the *ISS* trajectory stopped going through the high-latitude zones of penetration of energetic charged particles. Therefore, the rate of dose accumulation onboard the station became corresponding to the usual level before

08 UT on October 29, despite the fact that precisely in this period the maximum proton flux was observed.

The second period started at 08:15 UT on October 29, when the trajectory of *ISS* flight again became passing through the zones of penetration of energetic charged particles. The second period finished at 12:15 UT on October 29 after passing the zone above the north of Canada, due to a reduction of SCR proton fluxes.

The third period was caused by a new solar flare that occurred at 20:40 UT on October 29. However, the enhanced rate of dose accumulation onboard the *ISS* was observed in the period from 07 to 13 UT on October 30, which was caused by the next passage of the *ISS* through the zones of penetration of energetic charged particles.

A hard spectrum of protons hitting the Earth's magnetosphere was characteristic for the first period, as well as a low level of geomagnetic disturbance. The second period, having the largest accumulated dose, was characterized by a softer spectrum of protons and a modest level of geomagnetic disturbance. The third period proceeded on the background of the strongest geomagnetic storm. Therefore, in spite of the fact that proton fluxes were considerably lower than in the preceding SCR enhancement, the values of absorbed doses onboard the station turned out to be lower only slightly.

Figure 47 presents similar results derived from the data of the R-16 instrument. Unfortunately, the channel D2 of the R-16 instrument stopped operating normally on October 25. The ionization chamber of this channel has no additional plexiglass shield, therefore, it is more sensitive to changes in the radiation environment. Standard functioning of the channel D2 was restored only after 20 UT on October 28, therefore, the first part of the enhancement turned out to be missed in the data of this channel (a horizontal segment in Fig. 47). Nevertheless, the data of other detectors allowed us to control the radiation conditions onboard the *ISS* reliably during the entire disturbed period.

No significant influence of other solar proton events in the end of October and beginning of November 2003 on the radiation conditions onboard the *ISS* was discovered. One can indicate to a small increase of the mean daily dose after October 30.

Figure 48 presents the plot of the dose rate detected on October 31, 2003 by an unshielded detector of the DB-8 block no. 1 on a descending part of the trajectory passing through the zone of the South-Atlantic Anomaly (SAA). The existence of the second maximum of the dose rate after passing through the SAA zone is well seen. This illustrates the influence of unsteady processes in the Earth's radiation belts on the radiation conditions onboard the *ISS*.

Notice that the absorbed doses onboard the *ISS* caused by solar proton events of October 2003 turned out to be substantially less than the doses detected onboard the *Mir* station in October 1989, though the values of proton fluxes were of the same order in these

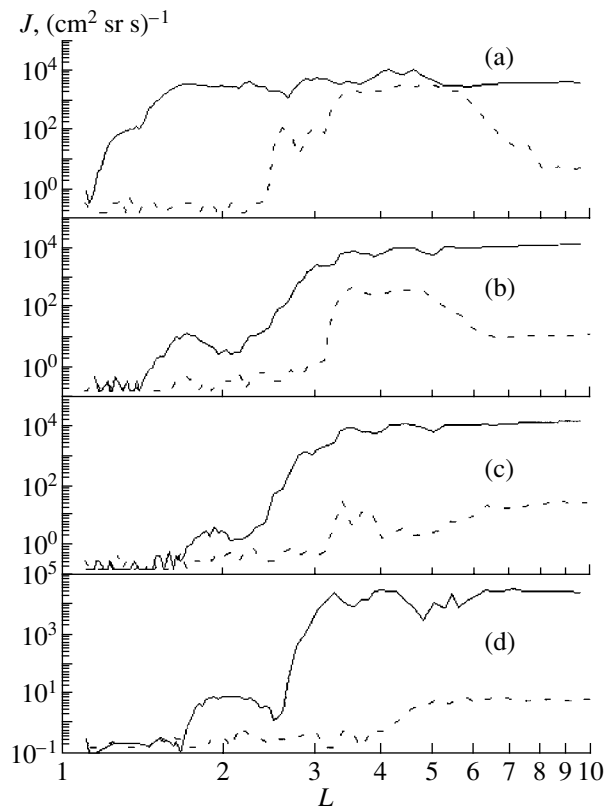


Fig. 45. A comparison of the structure of the outer belt at ~07:03 UT on October 29, 2003 (solid lines) and at ~04:43 UT on October 28, 2003 (dashed lines). From top to bottom: the fluxes of electrons with $E_e = 0.3\text{--}0.6$ MeV (a) and $E_e = 0.6\text{--}1.5$ MeV (b), and the fluxes of protons with $E_p = 1\text{--}5$ MeV (c) and $14\text{--}26$ MeV (d). Measurements onboard the *Coronas-F* satellite.

two cases. The unique dose enhancement aboard the *Mir* station on October 20, 1989 was caused by the time coincidence of the peak intensity of solar protons and of the reduction of latitude of their geomagnetic cutoff during strong geomagnetic disturbances, which increased substantially the time of station staying at latitudes of the polar plateau of solar protons [49, 50]. A detailed analysis of causes of the difference between two superstorms was made in paper [51]. Let us present here the basic results of this work.

Table 2 gives the integral characteristics of solar proton events (SPEs) in October 1989 and October 2003. One can see from the table that the SPEs under consideration are indeed comparable in the values of proton fluxes. However, the conditions of penetration of protons to the orbit of a manned station (the *Mir* orbital complex in October 1989 and the *ISS* in 2003) were radically different. For further analysis we have used the program developed in the Institute of Medical and Biological Problems. This program calculates radiation doses onboard *Mir* and *ISS* stations depending on the location in orbit and the intensity of basic radiation sources: galactic and solar cosmic rays, and the Earth's

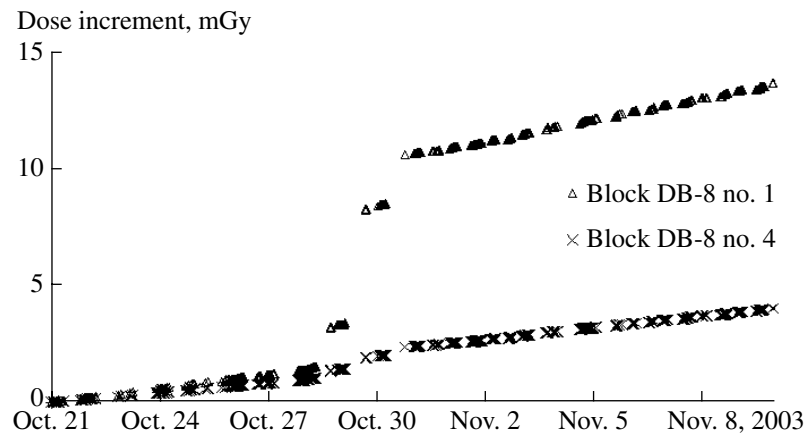


Fig. 46. Dynamics of dose accumulation according to the data of unshielded detectors of the blocks DB-8 no. 1 and no. 4.

radiation belts. Figures 49 and 50 give the dynamics of orbit values of the absorbed dose for the channel D2 of the radiometer R-16 on the *Mir* and *ISS* stations calculated using the functions of shielding from [52] and [53] for October 1989 flare and for a series of flares in October 2003.

For solar proton events of October 19, 1989 the maximum proton flux on October 20, 1989 coincided in time with a minimum of D_{st} variation. Precisely at this time the *Mir* complex was passing the polar cap regions, through which protons of solar flares could penetrate to the trajectory of the station flight. The dose contribution of SPE protons is shown in Figs. 49 and 50 by dark areas. The dose contribution of the constant sources is shown by the solid line.

In 2003 the picture of propagation of SPE protons to the *ISS* orbit was substantially different from the 1989 situation. In the period of maximum of the October 28, 2003 flare the ring current amplitude was positive, and at this time the orbital station executed its flight in the most protected (by the Earth's magnetic field) orbits. Because of this, the contribution to the absorbed dose

was significantly less than on October 20, 1989. Comparing the values presented in Table 2 one can estimate the total dose value in the channel D2 of the R-16 instrument. Based on the values of the shielded channel of the DB-8 block no. 2 (the closest in rate) one can estimate the total dose in channel D2 of the R-16 instrument recorded on the *Mir* station in October 1989 was 30.7 mGy (3070 mrad) [54]. So strong difference of doses at close parameters of the fluxes and spectra of SCR protons is caused by the difference in conditions of penetration to the trajectories of station flights, and by higher degree of protection of the instrument R-16 on the *ISS* as compared to the *Mir* station.

In conclusion we emphasize that the operation of SRK on the Russian unit of the *ISS* allowed the radiation conditions to be reliably controlled in the period of strong solar proton events of October 2003. The contribution of solar cosmic rays to the absorbed dose for 2 days of flight from 15 h of October 28 to 15 h of October 30 was in the range from 0.85 mGy (85 mrad) to

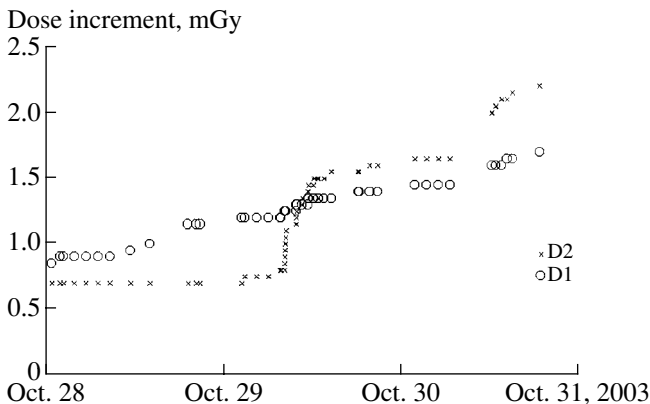


Fig. 47. Dynamics of dose accumulation according to the data of the dosimeter R-16.

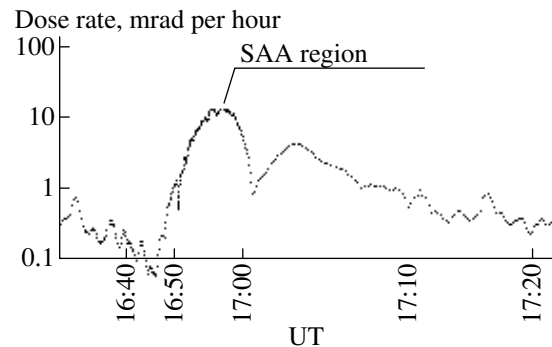


Fig. 48. The dose rate recorded on October 31, 2003 by an unshielded detector of the block DB-8 no. 1 on the descending leg of the trajectory. The time scale is nonuniform.

Table 2. Integral characteristics of SPEs in October 1989 and October 2003

Date of SPE onset	Characteristics	Date of SPE onset	Characteristics
October 19, 1989	$J(>30 \text{ MeV}) = 2.25 \times 10^9$ $R_o = 103.6 \text{ MV}$ $\gamma = 1.59$ $D_{st} = -127.4 \text{ nT}$	October 26, 2003	$J(>30 \text{ MeV}) = 1.92 \times 10^7$ $R_o = 47.6 \text{ MV}$ $\gamma = 3.42$ $D_{st} = 8.6 \text{ nT}$
October 22, 1989	$J(>30 \text{ MeV}) = 9.77 \times 10^8$ $R_o = 109.6 \text{ MV}$ $\gamma = 1.72$ $D_{st} = -74.7 \text{ nT}$	October 28, 2003	$J(>30 \text{ MeV}) = 2.52 \times 10^9$ $R_o = 64.9 \text{ MV}$ $\gamma = 2.79$ $D_{st} = -28.2 \text{ nT}$
October 24, 1989	$J(>30 \text{ MeV}) = 5.14 \times 10^8$ $R_o = 133.5 \text{ MV}$ $\gamma = 1.28$ $D_{st} = -40.0 \text{ nT}$	October 29, 2003	$J(>30 \text{ MeV}) = 5.66 \times 10^8$ $R_o = 78.7 \text{ MV}$ $\gamma = 2.10$ $D_{st} = -125.9 \text{ nT}$
		November 02, 2003	$J(>30 \text{ MeV}) = 2.28 \times 10^8$ $R_o = 60.6 \text{ MV}$ $\gamma = 2.57$ $D_{st} = 15.3 \text{ nT}$

Note: Here, $J(>30 \text{ MeV})$ is the fluence of protons with energies above 30 MeV (30 MeV is used as the energy of protons absorbed by a shield 1 g/cm^2 thick); R_o is the characteristic rigidity of the spectrum of SPE protons for exponential representation; γ is the spectral index of SPE protons for power-law representation; and D_{st} is the mean value of the ring current amplitude during SPE.

8.65 mGy (865 mrad) at various points of the service unit of the *ISS*. These values are the largest over the entire period of dose measurements onboard the *ISS*.

The results obtained contain necessary data for verification of (i) model descriptions of the radiation conditions on the flight trajectory of the *ISS*, (ii) the techniques of calculating the shielding conditions and dose values onboard the station in the period of solar proton events.

5. EFFECTS IN THE EARTH'S OZONOSPHERE

Based on the data of *Coronas-F* and *GOES* satellites on the fluxes of solar cosmic rays observed in October–November 2003, the calculations of ionization in the high-latitude atmosphere were carried out. The results of calculations presented in Fig. 51 have shown that the maximum values of ionization by energetic solar protons for chosen latitude of 70° lie in the range 50–70 km. The strongest ionization was caused by a solar flare that took place on October 28, 2003 (the maximum of ionization values was on October 29). Assuming that each pair of ions produced by solar protons leads to formation of 1.25 molecules of nitrogen oxide (NO) and two molecules of OH radical in the Earth's atmosphere, we have carried out a numerical photochemical modeling of the response of chemical composition of the high-latitude atmosphere to additional sources of nitrogen and hydrogen oxides of cosmic origin. The results of calculations demonstrating the variation of the ozone content after the solar flare of October 28, 2003 illustrates Fig. 52. It is shown that, as a result of intensification of catalytic cycles with participation of ozone-destroying molecules NO and OH, the ozone content reduced twice at the altitudes of maximum ionization.

The obtained results of modeling based on the data of *Coronas-F* testify that after the solar flare on October 28, 2003 the impact of energetic protons on the Earth's atmosphere should lead to significant changes in contents of both ozone and some other gas components (see paper [55] in the next issue).

6. DISCUSSION AND CONCLUSIONS

Geomagnetic disturbances in October–November 2003 were a response of the Earth's magnetosphere to anomalously large number of strong coronal mass ejections, which transported to the Earth high-speed plasma streams, energetic electrons, protons and nuclei, along with a strong and long-lived interplanetary magnetic field, including that of geoeffective southward direction. In addition, these disturbances were quite specific because of overlapping of the external effects comparable in strength and following one after another. As a consequence, the response of plasma populations, radiation belts, and electromagnetic field turned out to be fairly complicated.

(1) In this paper a preliminary analysis has been made of Russian satellite and ground-based measurements during extremely strong magnetic storms in the end of October 2003. The measurements of charged particles (electrons, protons, and ions) of solar and magnetospheric origin were made on geosynchronous satellites *Ekspress-A2* and *Ekspress-A3*, and on low-altitude polar satellites *Coronas-F* and *Meteor-3M* in a wide range of energies. The magnetic field disturbances caused by extremely high solar activity were studied at more than twenty magnetic observatories from Lovozero (Murmansk region) to Tixie (Sakha-Yakutia). The unique data have been obtained on dynamics of the

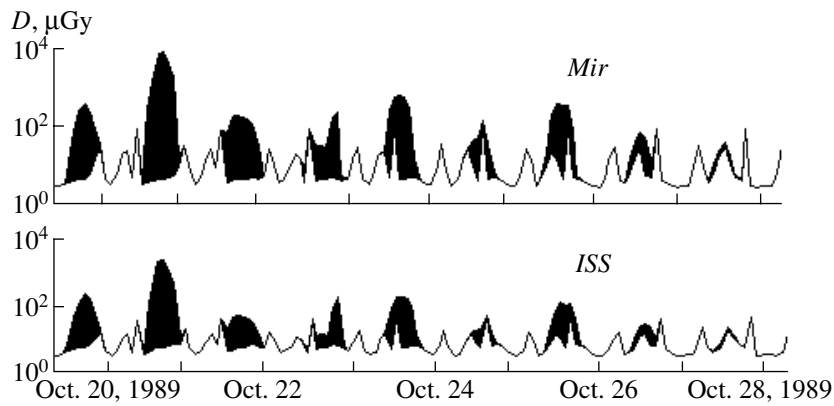


Fig. 49. Dynamics of the absorbed dose onboard the *Mir* and *ISS* stations in October 1989.

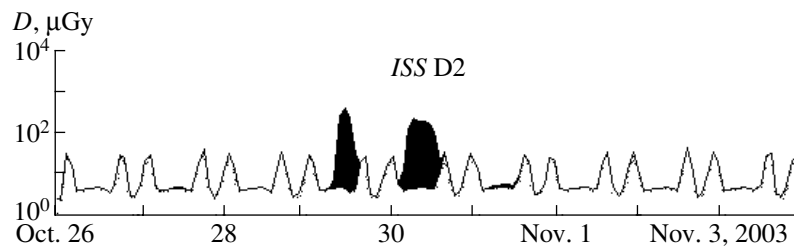


Fig. 50. The same as in Fig. 49, but on October 26–November 3, 2003.

ionosphere, riometric absorption, geomagnetic pulsations, and mid-latitude aurora observations. The collaboration of authors includes the scientists of twelve institutes and universities of the Russian Federation. In addition to the analysis of experimental data, some results of numerical modeling of the current systems and magnetic field are also presented.

(2) Concerning the processes of the Sun that caused the magnetic storms of October 29–30, 2003 and their manifestations in the Earth's magnetosphere and ionosphere, these storms can be classified as extreme phenomena of the current cycle of solar activity. The preliminary analysis of magnetospheric processes made in this paper has shown that the following phenomena were observed: the largest displacement to the equator of the projection of the boundary of penetration of solar cosmic rays, high energies of electrons accelerated in the inner magnetosphere, extremely strong substorms, and unusual (in duration and amplitude) geomagnetic pulsations.

(3) The *Ekspress* satellites detected significant variations of the intensity of relativistic electrons: sharp drops of the flux on October 24, 2003 and October 4, 2003 (associated with intensification of geomagnetic disturbances during weak magnetic storms) and its slow (for three days) recovery. Acceleration of electrons was observed on the phase of recovery of the last

superstorm, as a result, the intensity increased by an order of magnitude in 10 h.

The appearance of relativistic electrons is an immediate hazard for space instrumentation placed in high-apogee orbits; in addition, these electrons through a chain of aeronomic reactions have an effect on the ozone content in the mesosphere and further on the atmospheric circulation and weather.

(4) The satellites *Ekspress* and *Coronas-F* measured in a wide energy range the time behavior of the intensity of solar protons, electrons, and nuclei at geosynchronous orbit and in the polar cap. These data reflect the situation in the interplanetary space, and they are important for studying the problems of acceleration and propagation of solar cosmic rays, and for solving the applied problems.

(5) Considerable changes in the structure of proton and electron radiation belts were observed. The outer boundary of the electron and proton belt was displaced to $L = 3$, while the inner boundary was displaced to $L = 2.2$. As a result of impact of a series of strong magnetic storms the maximum of the outer radiation belt of electrons with energies $E_e > 8$ MeV was displaced to the region of L -shells of the inner belt ($L \sim 2.5$). The inner boundary of the plasma sheet was seen to be shifted to $L \sim 2.8$.

(6) The displacement of SCR penetration boundary is a consequence of a radical change in the structure of

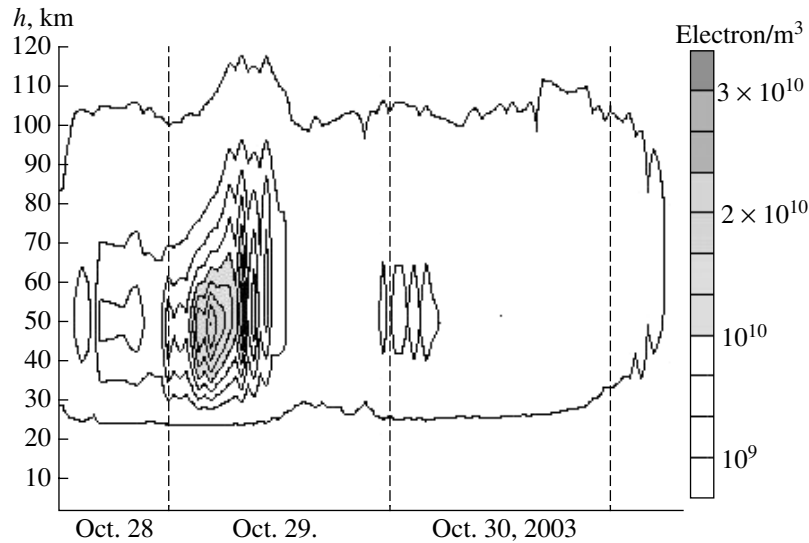


Fig. 51. Ionization rates by solar protons after the flare of October 28, 2003 in latitude 70° N (calculation based on the data of the *Coronas-F* satellite).

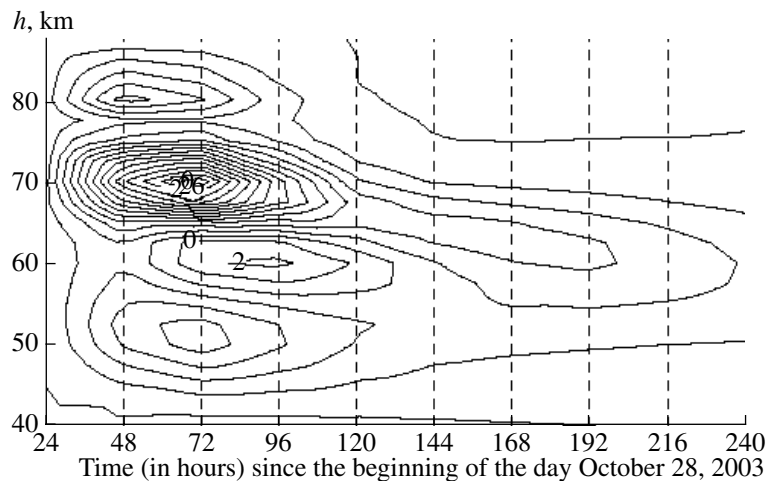


Fig. 52. Variations (%) of ozone content after the flare on October 28, 2003 at 70° N (results of a photochemical modeling).

the magnetospheric magnetic field, which manifested itself both in a strong compression of the magnetosphere and in the approach of the frontal edge of the current sheet to the Earth. During magnetic storms the penetration boundary usually moves smoothly following the dynamics of D_{st} variation. However, in the events under consideration we observed a rapid impulsive shift of the boundary to the Earth three times, in all cases it coincided with a large southward component of the interplanetary magnetic field in the disturbed solar wind and with extremely strong magnetospheric substorms.

(7) It is demonstrated that the penetration boundary of solar cosmic rays is in permanent motion not only during magnetic storms, but during substorm activity as

well. It moves from 68° (quiet level) to 58° in disturbed periods.

(8) The beginning of recovery of D_{st} both on October 29, 2003 and on October 30 coincided with a turn of the IMF to the north, which is typical for weak storms too. It is known that such a turn frequently initiates the beginning of the active phase of a substorm, therefore, substorms should be frequently observed at statistical analysis near the beginning of the drop of D_{st} variation. We see no grounds to abandon earlier made conclusions about an important role played by substorms in development of the asymmetric part of the ring current on the main phase of storms. At the same time, for definite conclusions about the contributions of particular current systems to the development of the

main phase of magnetic storms one needs the complete information about the spatial distribution and dynamics of possible carriers of current and about the magnetic field structure. Since at the moment this information is not available, essentially different interpretations are allowable and even unavoidable.

(9) The ring of active auroras at the main phase of the storm becomes broader and is displaced to the equator. The southern boundary traces the motion of the SCR penetration boundary, while the northern boundary (the polar cap boundary) moves to the pole and to the equator in the rhythm of substorm activity, only for short period being displaced below 60° of corrected latitude.

(10) In the beginning of the active phase of the second magnetic storm on October 29, 2003 two optical observatories (at ICRA and Irkutsk) recorded a substorm in mid-latitude auroras in great detail. The maximum intensity of OI844.6 nm emission reached 12 kRa at Maymaga station on October 29. These unique observations have shown that all elements of classical auroral substorm were present in this substorm. Though there are many descriptions of mid-latitude auroras in popular literature, this is nearly the first case of a scientific description based on observatory observations.

(11) The excitation in the daytime of October 29 and 31 of Pc5 geomagnetic pulsations is one of bright manifestations of the strong magnetic storm in October 2003. These pulsations were characterized by unusually large (up to 600 nT) amplitude with a spectral maximum in the frequency band 2.5–5.0 mHz (periods of order of 3–6 min). The maps of distribution of the integral intensity of pulsations are constructed, and their longitude asymmetry is discovered, as well as structuring of the zones of pulsations in latitude. Geomagnetic pulsations Pi2 and Pi3 were detected in the night sector during the most intensive substorms at the main phase of the magnetic storm on October 30 (18–22 UT). These pulsations were analyzed, and the maps of isolines have been plotted for their amplitudes.

(12) The analysis of the data of an IZMIRAN ionosonde at Troitsk indicates to extremely high level of disturbance of the mid-latitude ionosphere during extremely strong magnetic storms, with specific features typical for high-latitude ionosphere. At middle latitudes such disturbances of the upper atmosphere and ionosphere were observed that are usually detected only in the auroral zone of Arctic and Antarctica.

(13) Investigations of ULF emissions based on the data of the Yakutsk station (ICRA) reveal their complex dynamical structure, more typical for auroral rather than for mid-latitude zone. It is found that there is a relation of ULF emission to geomagnetic pulsations in the dayside sector of the magnetosphere.

(14) An analysis of the radiation conditions onboard the *International Space Station* is performed. In the period under investigation a substantial increase of the absorbed dose was observed, caused by the

arrival of energetic solar protons from the flare of October 28, 2003. It is emphasized that in the period, when the flux of protons was maximum and D_{st} variation was positive, the station executed its flight along the orbits most protected by the Earth's magnetic field. Because of this, the contribution to the absorbed dose was much smaller than during the storm of October 20, 1989.

(15) The paraboloidal model of the magnetosphere applied for description of the processes during October magnetic storms has shown a good agreement of the results of modeling with observations.

This preliminary analysis of the state of near-Earth space in October–November 2003 and characteristic features of dynamic processes observed in the magnetosphere, ionosphere, and atmosphere after extraordinary solar activity at the end of October 2003 give evidence that the response of near-Earth space to extremely strong and long external disturbance was extremely complicated. Perhaps, we deal with the action of new regularities. Coordinated investigation of these processes requires joint efforts and collaboration because of their importance both for fundamental science and for solving the applied problems.

ACKNOWLEDGMENTS

The analysis of magnetospheric disturbances would be impossible without using reference data about the solar wind parameters and geomagnetic indices. These data are available for scientific community via publication of free-access databases on the following Internet websites: <http://swdcbd.kugi.kyoto-u.ac.jp>, <http://www.sel.noaa.gov/>, <http://www-pi.physics.uiowa.edu/cpi-data/survey/sw/2003/>, and others. We thank the experimental groups having presented these data. The magnetic field measurements on many satellites were made by the instruments designed by C. Singer.

The authors are grateful to those teams of Russian observatories who produced and processed the data of ground-based observations which made this publication possible.

The possibility of getting prompt information from the global network of ground observatories INTERMAGNET, Scandinavian profile IMAGE, European network SAMNET, project CPMN, and Australian network of stations was very valuable for us.

The work was supported by a president grant for leading scientific schools NSh-2046.2003.2 and by the grant "Universities of Russia" no. UR.02.03.035.

The work on section 3 was carried out with support of Russian Foundation for Basic Research (grants 01-05-65003, 00-15-96623, 01-07-90117, and 02-05-74643) and a grant of Swedish Academy of sciences.

The works on sections 3.1.1 and 3.1.2 were partially supported by RFBR grant 03-05-39011. Irkutsk team was supported by RFBR grant 03-05-64744 and grant

NSh-272.2003.5 of State support for leading scientific schools of Russian Federation.

The work on section 3.1.3 was supported by the Program of fundamental research of Division of physical sciences of Russian Academy of sciences "Solar wind: generation and interaction with the Earth and other planets (OFN-18)" and by the RFBR grant 02-05-64386.

The team from Central Aerological Observatory was supported by RFBR grant 03-05-64675.

REFERENCES

1. Veselovsky, I.S., Panasyuk, M.I., Avdyushin, S.I., *et al.*, Solar and Heliospheric Phenomena in October–November 2003: Causes and Effects, Present Issue.
2. Petrukovich, A.A. and Rusanov, A.A., AL Index Dependence on the Solar Wind Input Revisited, *Adv. Space Res.*, 2004 (in press).
3. Pudovkin, M.I., Zaitseva, S.A., and Sizova, L.Z., Growth Rate and Decay of Magnetospheric Ring Current, *Planet. Space Sci.*, 1985, vol. 33, pp. 1097–1102.
4. Kamide, Y., Is Substorm Occurrence a Necessary Condition for a Magnetic Storm?, *J. Geomagn. Geoelectr.*, 1992, vol. 44, p. 109.
5. Sharma, A.S., Valdivia, J.A., and Kamide, Y., Dynamic Relationship between Storms and Substorms, in *Substorms-4*, Kokubun, S. and Kamide, Y., Eds., Tokyo: Terra Sci., 1998, pp. 737–741.
6. Iyemori, T., Substorms as a Dissipation Process in Geomagnetic Storms, in *Substorms-4*, Kokubun, S. and Kamide, Y., Eds., Tokyo: Terra Sci., 1998, pp. 99–101.
7. Maltsev, Y.P., Non-substorm Mechanism for Magnetic Storms, *Proc. 6th Int. Conf. on Substorms, March 25–29, 2002*, Winglee, R.M., Ed., Seattle: University of Washington, 2002, pp. 484–489.
8. Ammosov, P.P. and Gavril'eva, G.A., An Infrared Digital Spectrograph to Measure Rotational Temperature of Hydroxyl, *Prib. Tekh. Eksp.*, 2000, no. 6, pp. 792–797.
9. Isaev, S.I., *Morfologiya polyarnykh siyaniy* (Morphology of Auroras), Leningrad: Nauka, 1968.
10. Mikhalev, A.V., Some Features of Observing Mid-Latitude Auroras and Disturbances in Emissions of the upper Atmosphere during Magnetic Storms in Eastern Siberia Region, *Opt. Atmosph. Okeana*, 2001, vol. 14, no. 10, pp. 970–973.
11. Feldshtein, Ya.I. and Galperin, Yu.I., Structure of the Auroral Precipitations in the Nightside Sector of the Magnetosphere, *Kosm. Issled.*, 1996, vol. 34, no. 3, pp. 227–247.
12. *Rukovodstvo URSI po interpretatsii i obrabotke ionogramov* (URSI Manual for Interpreting and Processing Ionograms), Mednikova, N.V., Ed., Moscow: Nauka, 1977.
13. *Atlas of Ionograms*, Report UAG-10, Shapley, A.H., Ed., 1970.
14. Sugiura, M., Hourly Values of Equatorial D_{st} for IGY, *Annals IGY*, 1964, vol. 35, p. 1.
15. Afonin, V.V., Kolomiitsev, O.P., and Mizun, Yu.G., Satellite Measurements of the Electron Temperature and Features of Its Behavior in the Region of Main Ionospheric Trough, *Geomagn. Aeron.*, 1978, vol. 18, no. 3, pp. 432–435.
16. Meng, C.-I., Dynamic Variation of the Auroral Oval during Intense Magnetic Storms, *J. Geophys. Res.*, 1984, vol. 89, pp. 227–235.
17. Tverskaya, L.V., Tel'tsov, M.V., and Shkol'nikova, S.I., Dynamics of the Night Sector of the Auroral Oval Related to Substorm Activity during Magnetic Storms, *Geomagn. Aeron.*, 1989, vol. 29, no. 2, pp. 321–323.
18. Samson, J.S., Harrold, B.G., Ruohoniemi, J.M., and Walker, A.D.M., Field Line Resonances Associated with MHD Waveguides in the Magnetosphere, *Geophys. Res. Lett.*, 1992, vol. 19, pp. 441–444.
19. Kleimenova, N.G., Kozyreva, O.V., Zaitsev, A.N., and Odintsov, V.I., Geomagnetic Pulsations Pc5 Observed by the Global Network of Observatories during Magnetic Storm on March 24, 1991, *Geomagn. Aeron.*, 1996, vol. 36, no. 1, pp. 52–62.
20. Kleimenova, N.G., Kozyreva, O.V., Bitterli, M., and Shott, Zh. -Zh, Long-Periodic (1–6 mHz) Geomagnetic Pulsations at the Initial Phase of a Strong Magnetic Storm on February 21, 1994, *Geomagn. Aeron.*, 2000, vol. 40, no. 4, pp. 16–25.
21. Kleimenova, N.G., Kozyreva, O.V., Bitterli, Zh., and Bitterli, M., Long-Period ($T = 8–10$ min) Geomagnetic Pulsations at High Latitudes), *Geomagn. Aeron.*, 1998, vol. 38, no. 4, pp. 38–48.
22. Pilipenko, V., Kleimenova, N., Kozyreva, O., *et al.*, Long-Period Magnetic Activity during the May 15, 1997 Storm, *J. Atmos. Solar-Terr. Phys.*, 2001, vol. 63, no. 5, pp. 489–501.
23. Alexeev, I.I., Belenkaya, E.S., Bobrovnikov, S.Yu., and Kalegaev, V.V., Modeling of the Electromagnetic Field in the Interplanetary Space and in the Earth's Magnetosphere, *Space Sci. Rev.*, 2003, vol. 107, nos. 1–2, pp. 7–26.
24. Shue, J.-H., Song, P., Russell, C.T., *et al.*, Magnetopause Location under Extreme Solar Wind Condition, *J. Geophys. Res.*, 1998, vol. 103, p. 17, 691.
25. Starkov, G.V., Global Morphology of Auroras, in *Fizika magnitosfery i ionosfery* (Physics of Magnetosphere and Ionosphere), St. Petersburg: Nauka, 1993, pp. 85–90.
26. Burton, R.K., McPherron, R.L., and Russell, C.T., An Empirical Relationship between Interplanetary Conditions and D_{st} , *J. Geophys. Res.*, 1975, vol. 80, p. 4204.
27. Skoug, R.M., Thomsen, M.F., Henderson, M.G., *et al.*, Tail-Dominated Storm Main Phase: 31 March 2001, *J. Geophys. Res.*, 2003, vol. 108(A6).
28. Alexeev, I.I., Belenkaya, E.S., Kalegaev, V.V., *et al.*, Magnetic Storms and Magnetotail Currents, *J. Geophys. Res.*, 1996, vol. 101(4), pp. 7737–7747.
29. Arykov, A.A. and Maltsev, Yu.P., Direct-Driven Mechanism for Geomagnetic Storms, *Geophys. Res. Lett.*, 1996, vol. 23, p. 1689.
30. Darchieva, L.A., Ivanova, T.A., Sosnovets, E.N., and Tverskaya, L.V., Structural and Dynamic Peculiarities of Penetration of Solar Cosmic Rays into the Polar Caps, *Izv. Akad. Nauk SSSR, Ser. Fiz.*, 1973, vol. 37, no. 6, pp. 1313–1317.
31. Ivanova, T.A., Sosnovets, E.N., and Tverskaya, L.V., The Effect of North-South Asymmetry of Solar Cosmic Rays and Dynamics of the Plasma Sheet and Dayside Polar

- Cusp, *Geomagn. Aeron.*, 1976, vol. 16, no. 1, pp. 159–163.
32. Darchieva, L.A., Dronov, A.V., Ivanova, T.A., *et al.*, Studying Magnetosphere Processes Using Solar Cosmic Rays, *Izv. Akad. Nauk SSSR, Ser. Fiz.*, 1983, vol. 47, no. 9, pp. 1838–1841.
 33. Sosnovets, E.N. and Tverskaya, L.V., Ring Current Dynamics from the Data of Direct Measurements and Data on Solar Cosmic Rays in the Magnetosphere, *Geomagn. Aeron.*, 1986, vol. 36, no. 1, pp. 107–113.
 34. Darchieva, L.A., Ivanova, T.A., Sosnovets, E.N., and Tverskaya, L.V., Dynamics of Equatorial and Polar Boundaries of Penetration of Solar Protons with Energies > 1 MeV into the Magnetosphere during a Strong Magnetic Storm, *Geomagn. Aeron.*, 1990, vol. 30, no. 5, pp. 856–858.
 35. Ivanova, T.A., Kuznetsov, S.N., Sosnovets, E.N., and Tverskaya, L.V., Dynamics of the Low-Latitude Boundary of Penetration into the Magnetosphere of Low-Energy Solar Protons, *Geomagn. Aeron.*, 1985, vol. 25, no. 1, pp. 7–12.
 36. Leske, R.A., Mewaldt, R.A., Stone, E.C., and von Rosenwinge, T.T., Observations of Geomagnetic Cutoff Variations during Solar Energetic Particle Events and Implications for the Radiation Environment at the Space Station, *J. Geophys. Res.*, 2001, vol. 106, pp. 3011–3022.
 37. Kuznetsov, S.N., Bogomolov, A.V., Gordeev, Yu.P., *et al.*, Preliminary Results of an Experiment Carried Out with the SKL Instrumentation onboard the *CORONAS-I* Satellite, *Izv. Akad. Nauk, Ser. Fiz.*, 1995, vol. 59, pp. 2–6.
 38. Vlasova, N.A., Gorchakov, E.V., Ivanova, T.A., *et al.*, Monitoring System of Radiation Conditions in the Earth's Magnetosphere aboard Russian Communication, Navigation, and Television Satellites, *Kosm. Issled.*, 1999, vol. 37, no. 3, pp. 245–255.
 39. Balashov, S.V., Ivanov, V.V., Maksimov, I.A., *et al.*, Radiation Environment Control at High-Apogee Spacecraft, *Kosmonavtika i raketostroenie*, 2003, no. 1(30), pp. 95–101.
 40. Kuznetsov, S.N., Suvorova, A.V., and Dmitriev, A.V., Shape and Dimensions of the Magnetopause: Relationship with Interplanetary Medium Parameters, *Geomagn. Aeron.*, 1998, vol. 38, no. 6, pp. 7–16.
 41. Kuznetsov, S.N., Yushkov, B.Yu., Kudela, K., *et al.*, Penetration of Solar Energetic Particles (SEP) into the Magnetosphere, *ISEC 2003 Radiation Belt Science, September 2–3, 2003, Toulouse, France*, Abstracts, p. 51.
 42. Williams, D.J., Arens, J.F., and Lanzerotti, L.J., Observations of Trapped Electrons at Low and High Altitudes, *J. Geophys. Res.*, 1968, vol. 73, pp. 5673–5696.
 43. Vakulov, P.V., Kovrygina, L.M., Mineev, Yu.V., and Tverskaya, L.V., Variation in Intensity and Spectrum of Energetic Electrons in Earth's Radiation Belts during Strong Magnetic Disturbances, *Space Res.*, 1976, vol. 16, p. 529.
 44. Emel'yanenko, S.P., Kuznetsov, S.N., and Stolpovskii, V.G., The Outer Radiation Belt during a Strong Magnetic Storm, *Kosm. Issled.*, 1978, vol. 16, no. 4, pp. 529–543.
 45. Li, X. and Temerin, M.A., The Electron Radiation Belt, *Space Sci. Rev.*, 2001, vol. 95, pp. 569–580.
 46. Tverskaya, L.V., Ginzburg, E.A., Pavlov, N.N., and Svidsky, P.M., Injection of Relativistic Electrons during the Giant SSC and the Greatest Magnetic Storm of the Space Era, *Adv. Space Res.*, 2003, vol. 31, no. 4, pp. 1033–1038.
 47. Tverskaya, L.V., The Boundary of Electron Injection in the Earth's Magnetosphere, *Geomagn. Aeron.*, 1986, vol. 26, pp. 864–865.
 48. Antonova, A.E., Gubar', Yu.I., and Kropotkin, A.P., Towards the Model of Relativistic Electron Fluxes: Acceleration in the Field of Strong Alfvénic Disturbances, *Radiation Measurements*, 1999, vol. 30, no. 5, pp. 515–521.
 49. Tverskaya, L.V., Tel'tsov, M.V., and Shumshurov, V.I., Radiation Dose Measurements onboard the *Mir* Station during Solar Proton Events in September–October 1989, *Geomagn. Aeron.*, 1991, vol. 31, p. 928.
 50. Tverskaya, L.V., Panasyuk, M.I., Reizman, S.Ya., *et al.*, The Features of Radiation Dose Variations onboard ISS and *Mir* Space Station: Comparative Study, *Adv. Space Res.*, 2004 (in press).
 51. Bondarenko, V.A., Mitrikas, V.G., and Tsetlin, V.V., Strong Proton Disturbances in Orbit: 14 Years Later, *Kosm. Issled.*, 2004, vol. 42, no. 6 (in press).
 52. Mitrikas, V.G., A Model of Protectability of Habitable Compartments of the Service Unit on the International Space Station, *Aviakosmicheskaya i ekologicheskaya meditsina*, 2004 (in press).
 53. Mitrikas V.G. and Martynova A.N., A Model of Protectability of Habitable Compartments of the *Mir* Station Docking Unit, *Kosm. Issled.*, 1994, vol. 3, no. 3, pp. 115–123.
 54. Benghin, V.V., Petrov, V.M., Teltsov, M.V., *et al.*, Dosimetric Control onboard the *MIR* Space Station during the Solar Proton Events of September–October 1989, *Nucl. Tracks Radiation Meas.*, 1992, vol. 20, no. 1, pp. 21–23.
 55. Krivolutsky, A.A., Kuznetsov, S.N., and Myagkova, I.N., Changes in the Earth's Ozonosphere Caused by Ionization of the High-Latitude Atmosphere by Solar Protons in October 2003, *Kosm. Issled.*, 2004, vol. 42, no. 6 (in press).